USING MEAN POLARIZATION PROFILES TO STUDY STELLAR MAGNETIC FIELDS

(Spine title: Using Mean Polarization Profiles to Study Magnetic Fields)

(Thesis format: Monograph)

by

Stephen L. S. Shorlin

Graduate Program
in
Astronomy

A thesis submitted in partial fulfillment
of the requirements for the degree of
Doctor of Philosophy

Faculty of Graduate Studies
The University of Western Ontario
London, Ontario, Canada

Your file Votre référence
ISBN: 0-612-96913-4
Our file Notre référence
ISBN: 0-612-96913-4

UWO Licenses

And

Certificate of Examinations

are kept on file at

The University of Western Ontario

In

The Faculty of Graduate Studies

Abstract

Approximately 10-20% of moderate mass main sequence stars show marked chemical peculiarities. Characteristic chemical over- and underabundance patterns are well correlated with several physical attributes; most notably the existence or non-existence of large-scale ordered magnetic fields. The details of the origins of both the fields and abundance patterns are topics of continuing study, as are detailed descriptions of field structures in magnetic stars and the possible existence of magnetic fields in the canonically "non-magnetic" stars. We expect that mean spectral line profiles, calculated from entire stellar spectra in polarized and unpolarized light, will be useful in studying these topics.

Circular spectropolarimetric observations of 74 survey stars were obtained using the MuSiCoS spectropolarimeter in an attempt to detect magnetic fields. The sample observed includes normal B, A and F stars, emission-line B and A stars, Am stars, HgMn stars, λ Boo stars and magnetic Ap stars. Using the multi-line analysis technique known as "Least-Squares Deconvolution" (LSD) to extract mean unpolarized (Stokes I) and circularly polarized (Stokes V) signatures from each spectrum, we find absolutely no evidence for magnetic fields in the normal, Am and HgMn stars, with considerably smaller upper limits on longitudinal field measurements than previously obtained for these objects. We conclude that if any magnetic fields exist in the photospheres of these stars, these fields are not ordered as in the magnetic Ap stars, nor do they resemble the fields of active late-type stars.

We also detect for the first time a field in the A2pSr star HD 108945 and make new precise measurements of longitudinal fields in five previously known magnetic Ap stars, but do not detect fields in five other stars classified as Ap SrCrEu.

Also presented is the first ever exploratory investigation into both the applicability of the LSD technique in analyzing stellar spectra, as well as an examination of how LSD implements the scaling in amplitude of both circularly and linearly polarized line profiles with line depth, Landé factor and magnetic field. The influence of rotation velocity on profile amplitude was also explored. This study shows that circularly polarized spectra are well suited to analysis by the LSD technique over a wide range

of rotation velocities and magnetic fields and the scaling relations assumed in LSD theory are approximately correct. For linearly polarized profiles, the assumptions inherent in the LSD averaging procedures are only a good approximation for stars within limited regimes of rotation velocity and magnetic field and the scalings which arise from the LSD theory *do not* apply over much of parameter space.

Keywords: Stellar astronomy, spectropolarimetry, chemically peculiar stars, magnetic fields, Zeeman effect, spectral line profiles, data reduction,

Strange and beautiful are the stars tonight
"Lost Together"
Blue Rodeo

This thesis is dedicated to my family

Co-Authorship

Chapter 6 of this thesis contains material previously published with the co-authors: G.A. Wade, J.-F. Donati, J.D. Landstreet, P. Petit, T.A.A. Sigut and S. Strasser. Wade was responsible for the initiation of the project and acquiring some of the observational data. Donati was responsible for contributing the data reduction package and the Least-Squares Deconvolution procedure used to analyze the data, as well as acquiring some of the observational data. Landstreet participated in the planning of the project, acquired some of the observational data and discussed the paper as it was being written. Petit and Sigut acquired some of the observational data. Strasser was responsible for some of the data reduction.

Acknowledgments

Thanks go to my supervisor, John Landstreet, for getting this out of me, for patience and for being a great supervisor. John, if any of your students has ever said, "If it wasn't for you ..." and meant it, it's me! Thanks are also necessary to Gregg Wade, who got me started in most of this, and to Jean-Francois Donati, who wrote the ESpRIT and LSD code and who often translated *my* French into real French. Thanks to my additional co-authours: Aaron Sigut, Pascal Petit and Simon Strasser, for their nights of observation and/or days of data reduction.

Thanks go to all past and present astronomy graduate students and post-docs at Western and beyond who made my time here educational and enjoyable. Especially I'd like to thank Gregg (again), Aaron (again), Eric, Todd and Carol.

How can I thank my wife, Kelly Shorlin? She knows what she has meant to me, and to my work, and may I one day (soon) be able to do as much for her.

Parts of this thesis are based on data obtained at l'Observatoire du Pic du Midi, thanks to a generous allotment of observing time and the world-wide collaboration of MuSiCoS spectropolarimeter users. Extensive use has been made of the SIMBAD database, operated at CDS, Strasbourg, France and the Vienna Atomic Line Database, operated at Institut für Astronomie, Vienna, Austria.

Table of Contents

List of Tables

List of Figures

Chapter 1

Introduction

Of all the possible stages of evolution for a star, the main sequence may be considered the easiest to understand. Stars on the main sequence are those that have contracted from protostellar cores and now have sufficiently high internal temperatures to initiate core hydrogen fusion as their sole energy source. They are in hydrostatic equilibrium as pressure and gravitational forces balance to regulate core energy production. This simple equilibrium state allows a star's mass alone to prescribe its internal pressure and temperature structure, which will in turn determine the star's rate of fusion, luminosity, and ultimately, its life expectancy. In fact, it is one of the few points in a star's lifetime where its current state is essentially independent of its previous history. An average star spends 90% of its luminous lifetime on the main sequence, so this stage is where one observes most stars, including the Sun. Main sequence stellar masses range from about one hundred solar masses to one-tenth the mass of the Sun ($M_{\odot}$). Corresponding luminosities range over eight orders of magnitude, and the effective temperatures (temperature of an equivalent blackbody, $T_{\rm eff}$) range from 50000 K for the most massive stars to perhaps lower than 3000 K for the least massive.

If the main sequence is the simplest evolutionary stage, then it is the group of main sequence stars of moderate mass ($8 > M/M_{\odot} > 1.5$, $20000K > T_{\rm eff} > 7000K$) that would seem to be the simplest to understand physically. These stars have cores that are convective, but energy transport is provided by radiation in the region outside the core, known as the envelope. Hydrogen is the most important chemical species that affects the transfer of radiation through the star, and rotation rates are moderate (Abt

& Morrell 1995). The atmospheric physics is not dominated by winds, which carry off significant mass as in hotter stars (Cassinelli et al. 1981), or convective envelopes with magnetic activity, as in cooler stars (Kippenhahn & Weigert 1990). Stellar radiation is well described by models which assume local thermodynamic equilibrium (LTE), wherein the radiation locally follows the laws of the black body radiator. One does not usually observe emission lines or irregular variability for these stars, which would imply that LTE does not apply. Yet the spectra of these moderate mass main sequence stars have been of particular interest for nearly a century because ten to twenty per cent of them contain spectral lines of unexpected strength, implying anomalous chemical abundances, which are in some instances quite extreme. Abundances of chemicals in the Sun have been found to be reasonably representative of the general stellar population, yet compared to the Sun, a small fraction of moderate mass stars show enhancements for elements such as silicon, chromium, manganese and strontium, as well as rare earths including europium (e.g. Baxandall 1913). Some chemicals have been found to be up to six orders of magnitude more abundant than in the Sun. Many anomalous abundances are visible in low-resolution classification spectra (Cowley et al. 1969) and even more are visible at higher resolution. In fact, it is difficult to state exactly what is "normal" for the stars of the middle main sequence, given the wide variation of chemical abundances one observes in them (Hill 1993). The suspected origins of the anomalous line strengths will be discussed later in this introduction, but it is certainly likely that it is the lack of winds or envelope convection in these stars that makes possible the development of observed photospheric chemical peculiarities, and which allows one to observe stars that are chemically peculiar (CP).

Several different families of abundance anomalies are observed for the middle main sequence stars. While the specific anomalies will be discussed later when peculiarity classes are defined, it should be noted that there is a definite relationship between stellar effective temperature and peculiarity in that certain peculiarities are observed only for stars in specific effective temperature ranges. Also, certain peculiarities exclude others (e.g. overabundances of Mn and rare earths are not observed in the same star).

In order to readily compare and discuss different stars, one places them on a diagram showing luminosity vs. effective temperature which is known as a Herzsprung-Russell (HR) Diagram. In an HR diagram the main sequence traces a relatively narrow band with the most massive main sequence stars being the hottest and brightest and the least massive stars the coolest and faintest. Stars are often referred to by their spectral types, which in practical terms rank stars in order of effective temper-

ature. Spectral types under the OBAFGKM scheme are used, where O stars are the hottest and M stars the coolest. Each letter spectral type is further differentiated by numbers ranging from 0 to 9, such that one may speak of a B5 star for example. Stars with lower numbers are hotter than those with higher numbers. Table 1.1 shows representative values of $T_{\rm eff}$ and mass for the range of main sequence spectral types applicable to this thesis. Finally, stars are also described as having early and late spectral types such that hotter stars are regarded as earlier and cooler stars referred to as having later spectral types.

Sp. Type	$T_{\rm eff}$ (K)	M ($M_{\odot}$)
B2	25000	8.7
B5	16000	4.6
B8	13000	2.9
A0	10000	2.4
A2	9000	2.2
A5	8000	1.9
A8	7300	1.7
F0	7000	1.5
F5	6500	1.3

Table 1.1: Representative parameters for middle main sequence stars. Adopted from Gray (1992).

It is important to note that moderate mass main sequence stars which are found to have essentially the same mass, and thus temperature and luminosity, may be observed to be nearly normal or to fall into one of two or three peculiarity classes. It is evident that the stellar physics is being influenced by something other than a star's mass. Insight into what the "something other" may be came with the discovery of a magnetic field in the peculiar A-type (Ap) star 78 Vir by Babcock (1947), which has led to the study of the CP stars by methods sensitive to fields, and to theoretical studies of the influence of magnetic fields on photospheric chemical abundances. Details of field detection methods and results will be outlined later in this thesis, but the essential result of a half-century of observation is that the stars of each peculiarity class of CP stars are either magnetic or non-magnetic. The magnetic

stars have fields which are highly ordered over their entire surfaces, and which are be approximately described as dipoles. The other peculiar stars have fields which, averaged along the line-of-sight, are so close to zero that they have long been considered non-magnetic, although this has been called into question repeatedly, for example, by Mathys, Hubrig, Lanz and others (see Section 6.1). In any case, at the least the structure of fields in the magnetic and "non-magnetic" stars is very different.

Thus the study of the chemically peculiar stars, and perhaps of the entire mid to upper main sequence, is intimately tied to the study of stellar magnetic fields. To explain the observed chemical peculiarities, it is necessary to explore chemical segregation processes in the presence of varied field strengths and configurations *and* in the absence of magnetic fields. In order to compare theory to observation, it is beneficial to have detailed field models for many CP stars as input for theory so that theoretical models may be tested against stellar observations.

1.1 The classes of CP stars

The CP stars fall in the range of main sequence spectral types B2 to F0. They are grouped into the fairly broad classes listed in Table 1.2, based upon identifiable chemical anomalies associated with each. Each group has anomalous abundances for species other than those in the group's name, and representative abundance peculiarities which have been compiled by Wolff (1983) are summarized in Table 1.2. It must be noted that a CP star does not usually exhibit all the abundance anomalies associated with its peculiarity class, and that elements may have varying degrees of over- or underabundance in each class. The classes are loosely related to stellar effective temperature, as indicated in Table 1.2, which is evidence that the chemical peculiarities are due to physical processes in the stars, and do not reflect bulk abundances.

1.1.1 The magnetic chemically peculiar stars

Although the Ap SrCrEu and Si stars make up separate classes of peculiar stars, with the Si stars being consistently hotter, there is some overlap between the two (stars sometimes referred to as "SiCr") and it is thought that they form a continuum of chemically peculiar stars, usually referred to as the "magnetic Ap stars" since they have magnetic fields (which will be introduced in Section 1.2). As a group, they share several characteristics. They rotate more slowly than similar normal A stars, when one compares their apparent rotation velocities, $v \sin i$: the product of the equatorial

$T_{\rm eff}$ (10^3K)	Class name	Underabundant	Overabundant
Magnetic Peculiar Stars			
7–10	Ap SrCrEu	O	Si,Ca,V,Cr,Fe,Sr,RE
9–14	Ap Si	He	Si, Fe group, RE
13–18	He-weak Si, SrTi	He	Si, Ti, Sr, Fe group
18–22	He-strong		He, O, Ne
Non-magnetic Peculiar Stars			
7–10	Am	Ca, Sc	Fe group, Sr
7–10	λ Boo	Si, Ca, Mg, Fe	
9–14	Ap HgMn	He	Fe group, Hg, Mn
13–18	He-weak PGa	He	P, Ga, Hg, Mn

Table 1.2: The classes of chemically peculiar stars. "RE" is rare earth elements. Elements listed are representative, and stars do not typically show all the abundance anomalies associated with their peculiarity class. From Wolff (1983)

rotation velocity with the sine of the angle the rotation axis makes with the plane of the sky. Mean $v \sin i$ values of 30 to 40 $\mathrm{km\,s^{-1}}$ are observed for peculiar A stars compared to 100 to 150 $\mathrm{km\,s^{-1}}$ for normal main sequence A stars (Abt & Morrell 1995). The magnetic Ap stars are found in binary systems about half as often as normal stars (Abt & Snowden 1973) and almost never in those close binaries which may be detected only by observing periodic Doppler shifts in spectral lines (known as spectroscopic binaries, denoted SB), with orbital periods of days or weeks.

Most magnetic Ap stars are detectable as regular brightness variables, with photometric variations as well as variations in colours at the level of a few per cent occurring with a single, constant period for a given star. A light curve of the Ap SrEuCr star 53 Cam is seen in Fig. 1.1 as an example (Musielok et al. 1980). Many magnetic Ap stars are also spectrum variables (e.g. Morgan 1932), with variations ranging from mild profile changes of some spectral lines, to large changes in line depth over a period. Observations of the 4915-4925 Å region of spectrum for the Ap SrEuCr star 53 Cam over time are shown in Fig. 1.2 as an example (Wade et al. 2000a). Often, variations in line strength of several elements are quite well anti-correlated, while in

other stars all elements vary in the same way at the same time (e.g. Kuschnig et al. 1999). It must be noted that all aspects of a magnetic Ap star's variable nature occur with the same period, which is an indication that the variability is caused by rotation. A strong piece of evidence in favour of rotation being the cause of observed variations is that magnetic Ap stars show a wide range of measured periods, P, ranging from days to years for stars which are very similar. Other explanations for variability, such as pulsation, could not provide such a range of period for essentially identical objects. The strongest evidence is the fact that measured values of $v \sin i$ are always anti-correlated with P as one would expect for a rotating star. If one assumes a reasonable value for a Ap star's radius ($R \approx 3R_{\odot}$) then its measured $v \sin i$ value is always less than or equal to the equatorial rotation velocity implied by its period.

The association of variability with rotation immediately implies inhomogeneity across a stellar surface. Spectral variations may be attributed to patchy chemical distributions on the stellar surface which are brought into and out of sight by stellar rotation. Light and colour variations may be then attributed to changes in the flux distribution caused by the patchiness.

The He-weak Si and SrTi stars display many of the characteristics of the cooler magnetic Ap stars, including photometric and spectrum variability (Catalano & Leone 1996) explainable by rotation, as well as abundance anomalies similar to the cooler stars. The still more massive He-strong stars are the hottest CP stars known and thus the tasks of calculating chemical abundances, and even effective temperatures, are difficult for these objects with sparse spectra. Similar photometric and line profile variability (e.g. Wade et al. 1997) for these stars leads one to conclude that the He-strong stars are the hottest part of the continuum of magnetic peculiar stars.

1.1.2 The non-magnetic chemically peculiar stars

The Am, HgMn and He-weak PGa stars are very nearly the analogues of the magnetic chemically peculiar stars that fall in the same temperature ranges, as seen in Table 1.2, although there are some distinct differences. This family of stars does not form a smooth continuum of peculiarities from coolest to hottest. While He-weak PGa stars are seen as a hotter extension of the HgMn stars, since there are overlaps in abundance

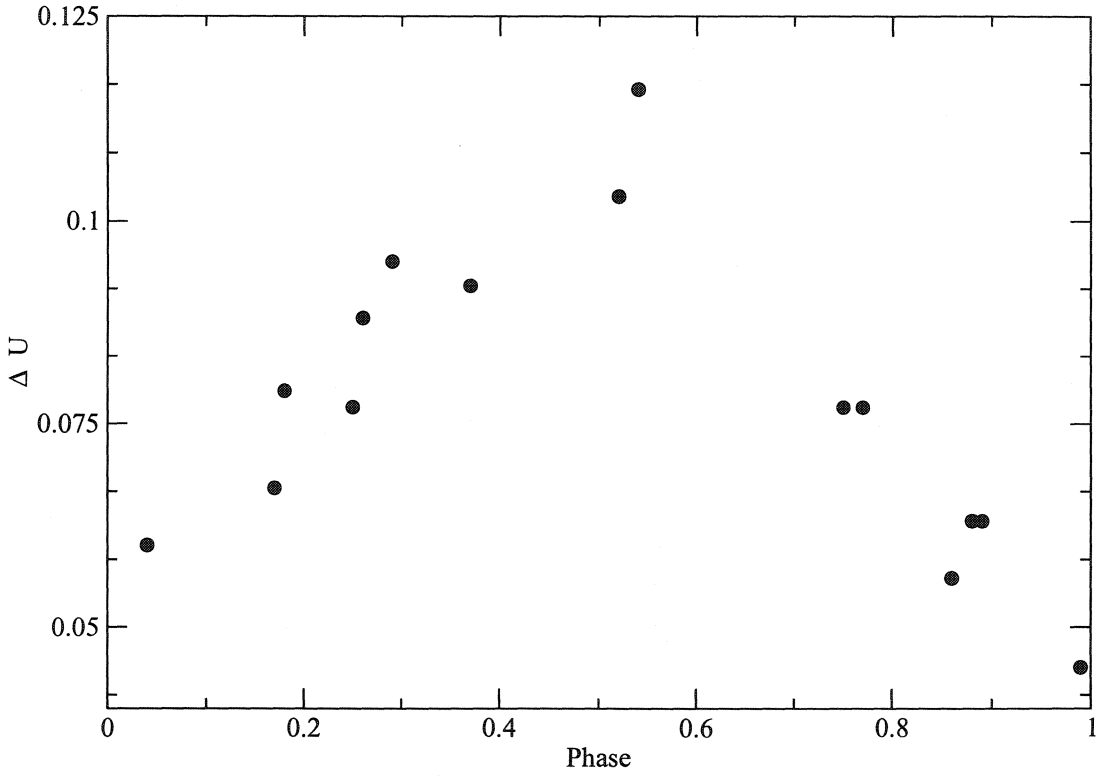

Figure 1.1: Light curve of the Ap SrEuCr star 53 Cam from data by Musielok et al. (1980). The U magnitude is that defined by Musielok et al., with an effective wavelength of 3450 Å. Shown here are ΔU values which are measured with respect to a standard non-variable star, and phased according to the ephemeris of Musielok et al.

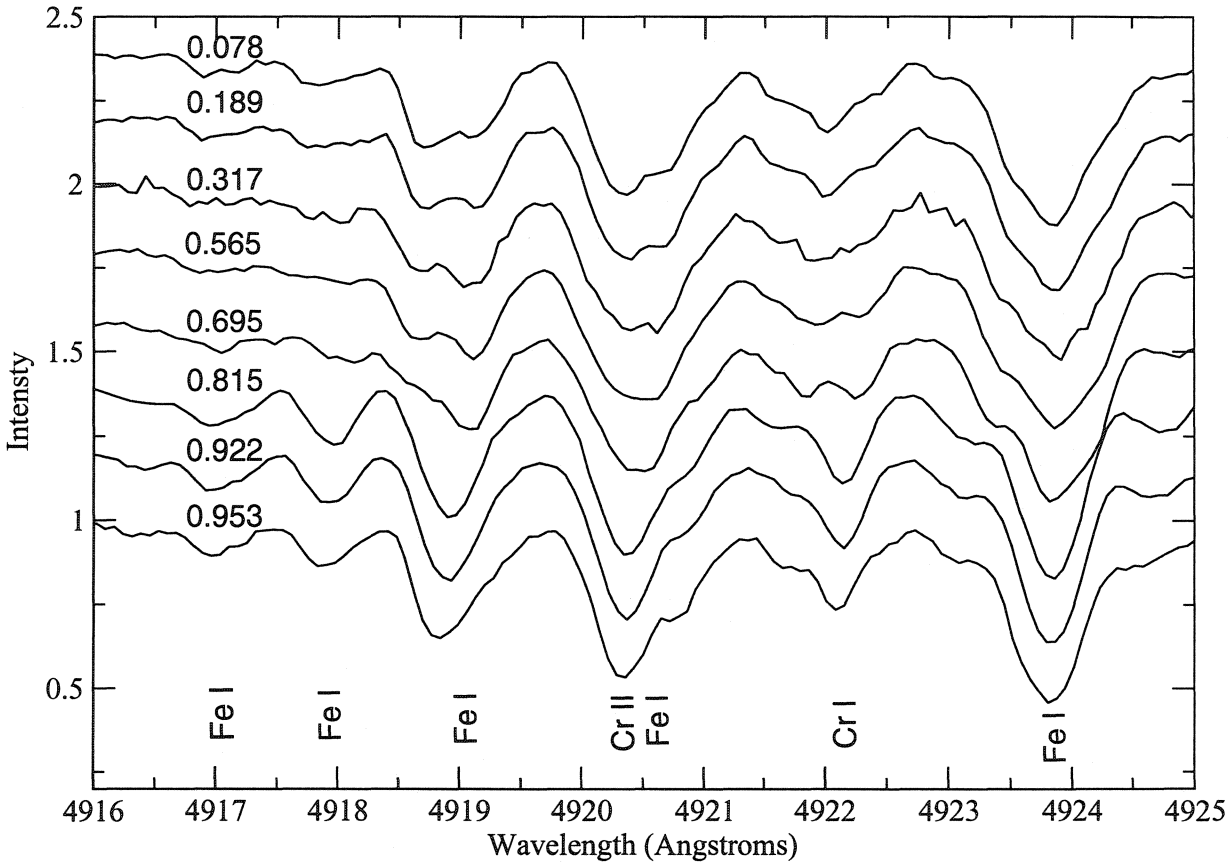

Figure 1.2: Variations with rotation of the 4915-4925 Å region of spectrum for 53 Cam. Each spectrum was obtained at a different rotational phase, given as the number above the spectrum, by Wade et al. (2000a). Identifications of some of the strongest and/or most isolated lines are taken from Wade (2002). Some lines in this region have never been identified as to chemical species.

peculiarities between the two classes, there is a lack of "transition" stars between the Am and HgMn classes, i.e. stars with both Am and HgMn characteristics. It is not certain, then, that the Am stars are merely cool HgMn stars, while a continuum of peculiarities is well-established in the magnetic CP stars. There is some speculation (Adelman et al. 2003) that HgMn stars of a certain mass may evolve into Am stars as they cool during main sequence evolution, although a mechanism for this has not been given.

Like their magnetic counterparts, the Am and HgMn stars are slow rotators compared to normal A and B stars. Unlike magnetic CP stars, Am stars are found in close binary systems much more often than normal stars. The metallic-line phenomenon *does* appear in single stars, so it is not thought that interactions between companions are necessary for the production of an Am star, although it seems that binarity has some influence. The HgMn stars exhibit binarity at about the frequency which is normal for stars of their spectral type, thus differing from both the magnetic peculiar stars and the Am stars.

One striking characteristic of the non-magnetic family of chemically peculiar stars is the lack of variations – photometric, spectral or otherwise – which distinguishes them from the previously discussed group of magnetic CP stars. The lack of variations is a clear indication that the non-magnetic peculiar stars are homogeneous over their surfaces, at least to the extent that their rotation does not reveal any inhomogeneities. Since the magnetic peculiar stars do typically have variations, with fields apparently creating or at least influencing the creation of dark "starspots" and chemical patchiness, then the decided lack of variability in the non-magnetic stars is an argument against their having magnetic fields.

The λ Boo stars are seen as a separate class of stars from the Am, HgMn and PGa stars, as well as the magnetic CP stars. They are characterized by marked underabundances in many elements, the origins of which are still quite uncertain. Current theories are that a λ Boo star's abundances are influenced by its local environment, perhaps by the accretion of material onto the star (Heiter et al. 2001). They differ in another important way from other chemically peculiar stars; their rotation rates are the same as other normal A stars of similar spectral types. While slow rotation seems to be either a partial cause or result of the peculiarities seen for all other CP stars, the λ Boo stars are not affected in this way. Therefore, one may think of them as certainly a separate group of peculiar stars.

1.2 Observing magnetic fields

1.2.1 Longitudinal fields

The Ap SrCrEu, Ap Si, He-weak Si, SrTi and He-strong stars are referred to as the *magnetic* Ap stars because magnetic fields have been detected in many examples of stars with those peculiarities. The most commonly available measure of a star's magnetic field is the line-of-sight component of the field, averaged over the visible hemisphere of the star, termed the longitudinal field, B_z. The details of the measurement of stellar longitudinal fields are reserved for Section 2.2.2, but it is important to note here that fields have been measured for many magnetic Ap stars. When observed over time, magnetic Ap stars show periodic variations in their longitudinal fields. As an example, the variation of mean longitudinal field measurements of 53 Cam is shown in Fig. 1.3. The periods of such variations are the same as those of other variations introduced in Section 1.1.1 (e.g. photometric, spectral line) and thus may be explained by the *oblique rotator* model as originally discussed by Deutsch (1956). In the oblique rotator model the magnetic field is "frozen" into the star and, with the star's rotation, different aspects of the field are presented on the visible hemisphere. To the simplest approximation, longitudinal field measurement variations are sinusoidal for most magnetic Ap stars and may be explained by a frozen-in dipolar field, inclined at some angle to the rotation axis of the star. Yet the simplest dipolar model often does not explain the variations of other quantities that describe magnetic fields. Other observational methods allow for the measurement of the modulus, $\langle B \rangle$, of the vector magnetic field, averaged over the visible disk of the star. Measurements may also be made of the degree and angle of linear polarization averaged over the stellar disk, which are determined by the field strength and direction. Longitudinal field measurements also sometimes show departure from simple sinusoidal variations. When considered together, the field observations for the magnetic Ap stars indicate that fields are often primarily dipolar, with a magnetic axis at an angle to the rotation axis, with additional field structure necessary to explain the details of all variations.

In order to characterize "typical" field strengths in stars whose fields vary over time, and to compare them, one may use the RMS (root-mean-square) longitudinal field strength of a star over a number of observations, $\langle B_z^2 \rangle^{\frac{1}{2}}$. RMS magnetic fields of magnetic Ap stars range from 16 kG for the strongest Ap field known to near 100 G, which is at the detectability limit for classical techniques. A preliminary survey using a particularly sensitive technique to study stars with magnetic Ap-like peculiarities,

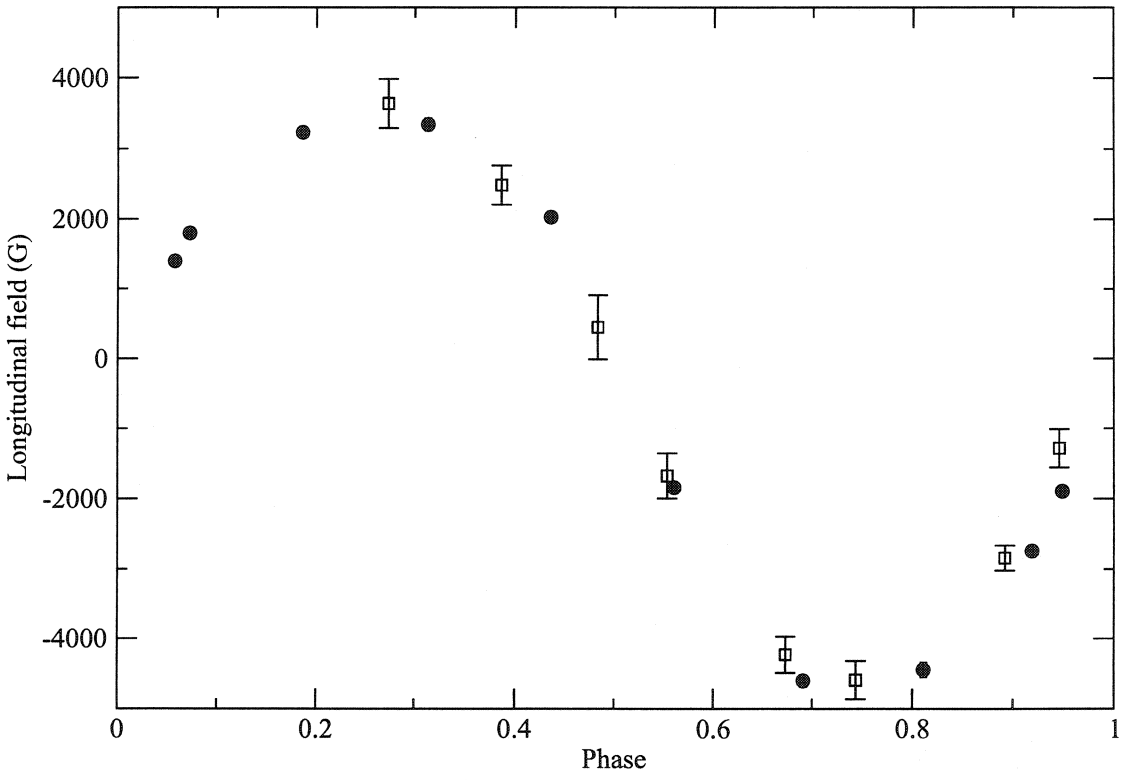

Figure 1.3: Mean longitudinal field curve of 53 Cam: Filled circles are from LSD mean V profiles by Wade et al. (2000b), open squares are some of the Balmer-line measurements by Hill et al. (1998). 1σ error-bars for measurements by Wade et al. are smaller than the point-size.

but in which no fields have previously been detected, has been largely successful in finding weak fields, and lends support to the idea that all of the "magnetic Ap stars" do indeed have magnetic fields (Aurière et al. 2003). The distribution of field strengths for the magnetic stars with $T_{\rm eff} < 15000$ K has a median value of approximately 300 G, and is skewed to low values of $\langle B_z^2 \rangle^{\frac{1}{2}}$ (Bohlender & Landstreet 1990). Magnetic fields are also found in the He-weak Si and SrTi stars, and He-strong stars, the presence of which further suggests that they are the extension of the magnetic Ap stars into the middle to early B-type main sequence. The median RMS longitudinal fields for the magnetic He-weak stars is greater than that for the cooler magnetic stars (Bohlender et al. 1987, Thompson et al. 1987), while the fields for the hottest magnetic Ap stars, the He-strong stars, are stronger still.

The non-magnetic CP stars have been so labelled because many spectropolarimetric studies have been unable to detect any effects attributable to magnetic fields (e.g. Borra & Landstreet 1980, Landstreet 1982, Borra et al. 1983, Bohlender & Landstreet 1990). These studies were attempts to detect longitudinal fields, and found no convincing evidence that they exist. Typical values of standard error σ for measurements of the longitudinal field were 100 G for the Am and HgMn stars and 200 G for the λ Boo stars. The implication is that these stars do not contain strong, ordered magnetic fields.

Such studies do not rule out even weaker fields, or much more complex fields which could have almost arbitrarily large strength, yet whose average along the line of sight would be near zero due to their complexity. Mathys & Lanz (1990) claimed the first detection of a complex, solar-like field in an Am star, namely *o* Peg, based upon the equivalent widths of two Fe II lines of different magnetic sensitivities. Other studies, to be discussed in Section 6.1, claim to find evidence for similar fields in several other Am stars, as well as two HgMn stars. Chapter 6 of this thesis will consist partly of new spectropolarimetric studies of the "non-magnetic" Ap stars which will provide new upper limits on their longitudinal magnetic fields, and discuss the effects those limits have on their status as "non-magnetic" stars.

1.2.2 Polarized line profiles

A measure such as longitudinal field is a single quantity that is *related* to the shapes and amplitudes of line profiles, both polarized and unpolarized. If one has adequate signal-to-noise ratio (S/N) and spectral resolution in the data to resolve the profiles *themselves* , then one may treat the detailed profiles as observables which represent

the effect of the stellar field, and thus have more information than is available in a single magnetic measurement. For example, if a star's longitudinal field is found to be zero it may be because the star has no magnetic field, or that the star has regions with equal but opposite field vectors which average to zero along the line-of-sight. If the star is rotating, then detailed polarized line profiles would easily distinguish between the two cases. A true non-magnetic star would of course show no polarization. A rotating magnetic star would have light coming from different regions of the star, Doppler shifted redward and blueward of any line center, and thus net polarization may be seen.

One may also see the effects of stellar magnetic fields in , provided one has the necessary to resolve adequately the profiles. Models may then be constructed that match the polarization signatures in detail, with fewer ambiguities than for modelling data which characterize the magnetic field by a single quantity, such as the longitudinal field. Recent work by Donati et al. (1997) has made it possible to extract numerically the polarization signatures from, in theory, all spectral lines in an observed spectrum to construct an average signature that improves the effective signal-to-noise ratio of the data. The technique, known as Least-Squares Deconvolution (LSD), will be discussed in more detail in Section 5.1. Examples of polarization in individual lines and in LSD mean profiles are shown in Figs. 5.1 and 5.2.

One benefit of such high S/N profiles may be seen in the very precise longitudinal field measurements made by Wade et al. (2000b). The LSD technique was used to extract average circular polarization profiles for stellar spectra (discussed in detail in Section 2.2.2), which were then used to calculate longitudinal fields. The mean longitudinal field measurements of 53 Cam by Wade et al. (2000b) using LSD extracted profiles in Fig. 1.3 are an example. The small uncertainty in these measurements ($\sigma(B) < 100$G) is a great improvement over previous measurements such as those of Hill et al. (1998) also seen in Fig. 1.3.

While using high signal-to-noise ratio polarization profiles to compute longitudinal fields leads to much better defined B_z variations, the benefit of using the detailed shapes of the polarization profiles themselves is to be investigated. Since the shapes of profiles will depend on magnetic field strength, geometry and topology, one might expect a large dataset of profiles to provide adequate input for comparison to models. Unfortunately, while a mean profile calculated from all polarized spectral lines will have an increased signal-to-noise ratio compared to individual lines, a degree of error is introduced by averaging profiles which are not identical. Theory, to be discussed in Section 5.1.2, shows how individual line profiles may be scaled by factors that depend

on line-depth, Landé factor and wavelength, in order to compute a useful average. It is not clear yet that this scaling is always applicable, and effects on LSD extraction of such characteristics as $v \sin i$, variable chemical abundances on a stellar surface and the details of how the Zeeman effect splits and polarizes individual lines have to be worked out before LSD-extracted profiles are reliably used as input for field modeling.

The development of LSD to extract polarized line profiles complements the design and construction of the MuSiCoS (Multi-Site Continuous Spectroscopy) spectrograph, available with a polarimetric analyzer at the Pic-du-Midi observatory in France. The MuSiCoS spectropolarimeter allows for the observations of very large spectral windows in four components which describe the polarization state of the light, known as the Stokes components, and is introduced in more detail in Section 2.3.1. The use of MuSiCoS polarized spectra for scientific analysis would not be possible without the development of a data reduction package designed to reduce and extract spectra from complicated raw data frames. This data reduction package, ESpRIT, is discussed in Section 3.1. It is the combination of the MuSiCos spectropolarimeter to make observations, the ESpRIT package to reduce the data, and LSD to extract the polarization information which has made this thesis possible.

1.3 Atmospheric physics of CP stars

1.3.1 Rotation and the origins of chemical peculiarities

The chemical peculiarities evident in both magnetic and non-magnetic CP stars, and to a lesser degree in some "normal" A-type stars (Hill 1993), are believed to be mainly a result of the competition between the downward gravitational diffusion of elements in the predominantly hydrogen atmosphere and envelope and the upward radiative acceleration in spectral lines experienced by many species. Radiative acceleration arises from the absorption of photons by a given chemical species at spectral line wavelengths, by which it preferentially gains momentum in the upward direction. Species with relatively low abundances but rich spectra will be accelerated upwards preferentially while elements with sparse spectra and high abundances will settle downward. This provides a qualitative explanation for the overabundances of rare earth elements and the helium and oxygen underabundances seen in many Ap stars.

Diffusion will also be affected by convection and other large-scale circulation motions (such as possibly turbulent meridional circulation) which tend to mix elements (Charbonnel et al. 1992, Richer et al. 2000). Turbulent velocity fields are expected

to arise in the low-density surface regions of rapidly rotating stars, thus inhibiting element separation. Stars that rotate more slowly may not develop turbulence in their outer regions and this would not become a source of mixing. Since rotation is apparently such an important contributor to the development of chemical peculiarities, a discussion of the rotation of the CP stars is necessary.

In general, as previously stated, both the magnetic and non-magnetic chemically peculiar families of stars rotate more slowly than normal stars of similar spectral types, (neglecting the λ Boo stars). In the case of the magnetic stars, the slow rotation is likely due to a phenomenon known as "magnetic braking": the interaction of the star's magnetic field with its own stellar wind (if one exists), or with accreting material, causes the star to lose angular momentum, particularly during the pre-main sequence evolutionary phase. The characteristics of the peculiar stars found in binary systems are different for stars of differing peculiarities. Magnetic Ap stars are found to be spectroscopic binaries less often than normal A-type stars, while the frequency of visual, or very wide, binary systems is the same for Ap and normal A-type stars. The Am stars, on the other hand, are almost always found to be spectroscopic binaries (Wolff 1983). Of those spectroscopic binaries, stars with both very close and wide separations show no peculiarities, while it is those with intermediate separations which are peculiar. These facts are in agreement with the picture of slowly rotating chemically peculiar stars, compared to normal rapid rotators. In the case of close binaries, one expects tidal forces to cause the rotation periods to synchronize with the orbital periods (typically hours). Since the orbital periods are short, due to their being close together, the stars will having correspondingly rapid rotation rates. For the distant binaries, tidal synchronization will not be important and the stars will have their original rotation velocities, which reflect those of the general population of A-type stars. But for the spectroscopic binaries of intermediate separation, tidal synchronization will match the rotational periods to the longer orbital periods (typically a few days), creating slowly rotating stars. Since this group is the one which develops chemical peculiarities, the influence of rotation on abundance anomalies is further supported (Mestel 1999).

As slow rotation seems to be crucial for the development of chemical peculiarities, one now asks why the peculiarities are different for stars with and without magnetic fields. The convective outermost regions of a magnetic Ap star may be dominated by the magnetic field energy density, thereby inhibiting mixing in the photosphere. This could allow the development and persistence of patchiness inferred for magnetic stars which is never seen for the non-magnetic stars. Richer et al. (2000) also proposed that

turbulent envelopes affect the observed abundance anomalies in the Am and HgMn stars, perhaps by inhibiting the development of large overabundances. There has also been the suggestion that the fields in magnetic Ap stars tend to stabilize their atmospheres, although the influence this may have on the development of abundance anomalies in far from certain.

Magnetic fields also contribute to the development of peculiarities since the Zeeman broadening of magnetically sensitive lines in magnetic CP stars will tend to provide more radiative acceleration for those species. This would help to explain the extreme overabundances of many rare earth species seen in the magnetic stars. Theoretical studies have shown that horizontal magnetic fields may inhibit the sinking of ionized species and thus cause enhanced abundances in stellar photospheres (Vauclair et al. 1979). Also, Michaud et al. (1981) identified cases where neutral elements would rise vertically due to radiative acceleration, but ionized species would sink along field lines towards a magnetic pole, thus creating a surface inhomogeneity. The current theoretical situation is that the precise physical effect of magnetic fields on abundances and patchiness is unclear.

A stellar wind may lead to the levitation of some or all species in the atmosphere and would alter the case of simple diffusion. If a species becomes concentrated in a layer, due to diffusive processes, a wind may levitate that layer into or out of the line-forming region of a stellar atmosphere. It may also remove some species completely from a star. Babel (1992) introduced an anisotropic wind into models of the Ap star 53 Cam in order to explain the inhomogeneous distributions of elements on its surface, and was successful for some but not all species. There has been no convincing direct observational evidence for such a wind in Ap stars, although efforts are being made to detect one.

The main point to be taken from observational and theoretical investigations into the origins of chemically peculiar stars is that the complete picture is unclear and worthy of continued study.

1.3.2 Field origins and evolution

Magnetic fields in stars may presumably be generated by two mechanisms: the dynamo effect in which the field is supplied with energy by bulk motions within the star, or an external field which threads the material from which the star is formed, creating a stellar magnetic field which is now decaying. Dynamo fields are prevalent in late-type stars, such as the Sun, which have large convective zones in their outer

envelopes. If Ap fields were generated by dynamos, one would expect there to be a positive correlation between field strengths and stellar rotation rates, such as one observes for lower main sequence stars (Solanki 1992). No such correlation is found for upper main sequence stars, however (Borra & Landstreet 1980).

The continued existence of previously created, or fossil, fields in Ap stars would probably not imply any correlation of field strength with rotation rate. The fossil field theory allows stellar fields to have widely varying strengths that depend only on the local conditions at the time of star formation and the field evolution during the main sequence. This theoretical origin for Ap magnetic fields is supported by the decay time for such a field, determined from electromagnetic theory. Assuming the field is purely poloidal and axisymmetric in nature, and that the medium is stationary, then the field may be represented by a vector potential $\vec{A}$ which induces a toroidal electric field, $\vec{E} = (1/c)\,\partial\vec{A}/\partial t$. Using Ohm's law, $\vec{j} = \sigma\vec{E}$, as well as Maxwell's equations, the decay equation is found to be

$$\frac{\partial \vec{A}}{\partial t} = -(c^2/4\pi\sigma)\nabla \times (\nabla \times \vec{A}). \tag{1.1}$$

Using dimensional analysis, the decay time is $\tau = 4\pi(\sigma/c^2)a^2$ where a is the scale of the medium, say the stellar radius (Mestel 1999). The conductivity of the stellar plasma, σ, has been calculated by Cowling (1945) as $\pi^2 c^2 \sigma = 10^{-4}$ E.M.U., which results in a typical decay time of $\sim 10^{10}$ years. This time is on the scale of the age of the universe, and so the theory of primeval fields as the origin of those found in Ap stars is certainly plausible. In addition, Thompson et al. (1987) found that typical fields of Ap stars do not decrease by more than about a factor of two over the course of half a main sequence lifetime.

Although the strength of a star's magnetic field may not change considerably over a main sequence lifetime, assuming it is a fossil field, the orientation and perhaps even the structure of the field certainly may. One reason for such changes comes from the fact that a star is in general a rotating body. In the radiative envelope of an non-rotating early-type star, neglecting any magnetic field, there are no large-scale motions of matter. Rotation, however, introduces a slight non-sphericity in the stellar structure that further causes a pressure gradient between the rotational poles and the equator. This rotationally-induced pressure difference results in large scale currents that travel approximately along meridians passing through the poles. Envelope material forms a circulating cell that travels parallel to the surface from pole to equator, inward to the core parallel to an equatorial radius line, parallel to

the core-envelope boundary back to the rotation axis, where it travels outward to the surface completing a full circulation (Tassoul 2000).

Meridional circulation will also be present in a rotating early-type star with a magnetic field, in which case circulation may affect the field itself through advection; the slow "dragging" of field lines caused by the motion of the plasma. The results of such circulation processes on magnetic fields are not easily generalized, but some important points may be noted. Slowly rotating stars induce weaker meridional currents than fast rotators, such that slow rotation may have little or no effect on a magnetic field. Fast rotators may induce large enough currents to effectively bury magnetic fields below their surfaces (Mestel 1999). The obliquity of the field (the angle between the rotation and magnetic axes) does play a role in how the field evolves, even for fast rotators. As determined by Moss (1984) and illustrated by Mestel (1999), a highly oblique magnetic field, i.e. one at a large angle to the rotation axis, will tend to be compressed toward the rotational equator by meridional circulation. Presumably, there are critical values of rotation period, obliquity and field strength which, in combination, determine whether a field is buried, altered in obliquity (and to what degree) or whether it remains effectively untouched by meridional circulation.

As discussed by Landstreet & Mathys (2000), who found that the typical obliquity angles in magnetic Ap stars differ for fast and slow rotators, the situation is further complicated by the fact that not only does rotation affect the field, but the field affects rotation through the presumed magnetic braking. Thus, the strength and orientation of the magnetic field are interconnected with the rotation rate of a magnetic star as it forms and evolves, and there is no simple cause and effect relationship of one upon the other.

1.4 Questions for this thesis

1.4.1 Do "non-magnetic" stars have magnetic fields?

When the magnetic and non-magnetic families of peculiar A-type stars are compared to each other and to the nominally normal A-type stars, the question of the existence of magnetic fields arises. As stated earlier, the data for the magnetic Ap stars are very often well-explained by the oblique rotator model: a highly ordered, topologically poloidal field which is fixed at an angle to the rotation axis in a rotating star. Periodic variations of chemical abundance, brightness, colour and magnetic field then arise from the star's rotation. "Magnetic" Ap stars for which chemical peculiarities

and/or periodic variations exist, but for which no magnetic fields have been observed, have been assumed to have field strengths less than the detection limits of current techniques, or at least the limits of available observations.

The Am, HgMn, PGa family of peculiar stars, in not showing periodic variations or detectable longitudinal magnetic fields, have been labelled the non-magnetic peculiar stars. Obviously, the development of completely different peculiarity characteristics does imply that this group is different from the family of magnetic Ap stars, and the existence or non-existence of magnetic fields could be a vital component of the explanation. However, this does not explain why normal middle main sequence stars, also having no detectable magnetic fields, do not develop the peculiarities of similar Am and HgMn stars, except perhaps as a consequence of differences in rotation velocities.

Rotation and binary synchronization, as discussed in Section 1.3.1, are certainly important factors in the development of chemical peculiarities, but as Hill (1993) has found, A-type stars may be found with a range of $v \sin i$ values, yet having essentially normal abundances. This fact, as well as the apparent detections of strong fields in the "non-magnetic" middle main sequence stars, as discussed in Section 1.2.1, lead to the first questions in this thesis: Can a highly sensitive magnetic field detection technique make measurements of fields in the "non-magnetic" mid to upper main sequence, namely in Am, HgMn and normal stars? Do stars with magnetic Ap peculiarities, but no previously detected fields, actually have fields measurable by more sensitive methods? And, if fields can or cannot be detected in these groups of stars, what does this tell us about the mid to upper main sequence as a whole? The use of LSD-extracted circular polarization profiles for a survey group of mid to upper main sequence stars is the author's attempt to answer these questions, and is the focus of Chapter 6.

1.4.2 Can average linear polarization profiles be used to study stellar fields?

The averaging of circular polarization profiles in many individual spectral lines by means of the LSD extraction routines has been shown to be a valid procedure, providing average profiles with shapes and amplitudes as expected. The calculation of longitudinal field strengths using the LSD-extracted profiles has not only provided measures consistent with previous work, but ones which have greatly reduced uncertainties. The extension of the averaging procedure to *linear* polarization profiles,

however, has not been rigorously tested and remains a contentious point.

As will be discussed further, the ability to use linear polarization profiles in concert with circular polarization profiles allows for much more certainty in the modelling of a stellar magnetic field over a star's surface. Using circular polarization profiles only, created by the line-of-sight component of the field, does make it possible to map a star's field as it rotates, and some modelling has been done in this way. If one has the additional observable of linear polarization, however, which is created by the component of the vector field in the plane of the sky, then one has a very large constraint on what the stellar field must look like.

The problem with using linear polarization profiles is that the polarization amplitude is very small. These signatures are weaker than those for circular polarization, and are often not detected (at moderate S/N and resolution) in individual lines, except for some strongly magnetic stars and even then only in strong, sensitive lines. The LSD process was developed to allow for the averaging of many similar lines to "deconvolve" the *average* line profile (in unpolarized or polarized light) which would be then used as the observable in modelling (see Section 5.1 for more details). Unfortunately, the averaging of linear polarization profiles is complicated by the fact that they are often not similar. Preliminary synthetic line profiles have shown that the assumption of the similarity of all profiles is simply not true. The author will address this issue by determining the acceptable range of parameters for which it *is* true. In particular, there will be an examination of the range of magnetic field strengths and stellar rotation velocities for which the averaging process may be validly followed, as well as the lines for which it be be done, concentrating on the depth and magnetic sensitivity of the lines involved. This examination, as well as a more detailed discussion of the assumptions which make up the formalism for the LSD averaging process, will comprise Chapter 7.

1.4.3 This thesis

In order to answer the preceding questions, one requires a discussion of the new datasets and techniques which make this thesis possible. The theory of polarimetric and spectropolarimetric observations, as they pertain to this thesis, are outlined in Chapter 2 as a pre-requisite for the discussion of the spectropolarimetric instrument, MuSiCoS. The specialized data reduction package, ESpRIT, which makes the data from MuSiCoS possible to use, is introduced in Chapter 3. The observational program is laid out in Chapter 4, including the details of star selection, the observations

themselves, and the collaboration entered into by the author. The interpretation of the data is outlined in Chapter 5, which includes an introduction to LSD and the details of its use, as well as longitudinal field measurements. Chapter 6 is comprised of the survey of middle to upper main sequence stars to make new or improved detections of magnetic fields, and a discussion of the implications of non-detections and new upper limits. Chapter 7 outlines the examination of the use of LSD-averaging to find average linear polarization profiles. In particular, the stellar and line parameters for which such averaging is valid will be determined. Finally, a summary is presented, as well as a direction for the future use of spectropolarimetry using the LSD technique.

References

Adelman, S. J., Adelman, A. S., & Pintado, O. I. 2003, A&A, 397, 267

Abt, H. A., & Morrell, N. I. 1995, ApJS, 99, 135

Abt, H. A., & Snowden, M. S. 1973, ApJS, 25, 137

Aurière, M., Silvester, J., Wade, G. A., Bagnulo, S., Donati, J.-F., Johnson, N., Landstreet, J. D., Ligneres, F., Lueftinger, T., Mouillet, D., Paletou, F., Petit, P., & Strasser, S. 2003, "A survey of magnetic Ap/Bp stars for weak longitudinal magnetic fields", A peculiar Newsletter (ApN), 39

Babcock, H. W. 1947, ApJ, 105, 105

Babel, J. 1992, A&A, 258, 449

Baxandall, F. E. 1913, MNRAS, 74, 32

Bohlender, D. A., & Landstreet, J. D. 1990, MNRAS, 247, 606

Bohlender, D. A., Landstreet, J. D., Brown, D. N., & Thompson, I. B. 1987, ApJ, 323, 325

Borra, E. F., & Landstreet, J. D. 1980, ApJS, 42, 421

Borra, E. F., Landstreet, J. D., & Thompson, I. B. 1983, ApJS, 53, 151

Cassinelli, J. P., Waldron, W. L., Sanders, W. T., Harnden, F. R. Jr., Rosner, R., & Vaiana, G. S. 1981, ApJ, 250, 677

Catalano, F. A., & Leone, F. 1996, A&A, 311, 230

Charbonnel, C., Vauclair, S., & Zahn, J.-P. 1992, A&A, 255, 191

Cowley, A., Cowley, C., Jaschek, M, & Jaschek, C. 1969, AJ, 74, 375

Cowling, T. G. 1945, MNRAS, 105, 166

Deutsch, A. J. 1956, PASP, 68, 92

Donati, J.-F., Semel, M., Carter, B. D., Rees, D. E., & Collier Cameron, A. 1997, MNRAS, 291, 658

Gray D.F., 1992, *The Observation and Analysis of Stellar Photospheres*, Second edition, Cambridge University Press

Heiter, U., Weiss, W. W., Paunzen E. 2001, A&A 381, 971

Hill, G. M. 1993, PhD Thesis, The University of Western Ontario

Hill, G. M., Bohlender, D. A., Landstreet, J. D., Wade, G. A., Manset, N., Bastien, P. 1998, MNRAS, 297, 236

Kippenhahn, R. & Weigert, A. 1990, *Stellar Structure and Evolution*, Springer-Verlag

Kuschnig, R., Ryabchikova, T. A., Piskunov, N. E., Weiss, W. W., Gelbmann, M. J. 1999, A&A, 348, 924

Landstreet, J. D. 1982, ApJ, 258, 639

Landstreet, J. D. & Mathys, G. 2000, A&A, 359, 213

Mathys, G., & Lanz, T. 1990, A&A, 230, L21

Mestel, L. 1999, *Stellar Magnetism*, Clarendon Press

Michaud, G., Charland, Y., & Megessier, C. 1981, A&A, 103, 244

Morgan, W. W. 1932, ApJ, 76, 315

Moss, D. 1984, MNRAS, 209, 607

Musielok, B., Lange, D., Schöneich, W., Hildebrandt, G., Želwanowa, E., Hempelman, A., Salmanov, G. 1980, Astron. Nachr., 301, 71

Richer, J., Michaud, G., & Turcotte, S. 2000, ApJ, 529, 338

Solanki, S. K. 1992, in ASP Conf. Ser. 26, *Seventh Cambridge Workshop on Cool Stars, Stellar Systems, and the Sun*, eds. Mark S. Giampapa & Jay A. Bookbinder

Thompson, I. B., Brown, D. N., & Landstreet, J. D. 1987, ApJS, 64, 219

Tassoul, J.-L. 2000, *Stellar Rotation*, Cambridge University Press

Vauclair, S., Hardorp, J., & Peterson, D. M. 1979, ApJ, 227, 526

Wade, G.A. 2002, "Spectral Line Polarisation Atlases for 53 Cam (A4p) and α^2 CVn (A0p)", A peculiar Newsletter (ApN) 38.

Wade, G. A., Bohlender, D. A., Brown, D. N., Elkin, V. G., Landstreet, J. D., Romanyuk, I. I. 1997, A&A, 320, 172

Wade, G. A., Donati, J.-F., Landstreet, J. D., & Shorlin, S. L. S. 2000a, MNRAS, 313, 823

Wade, G. A., Donati, J.-F., Landstreet, J. D., & Shorlin, S. L. S. 2000b, MNRAS, 313, 851

Wolff, S. C. 1983, *The A-type stars: problems and perspectives*, NASA SP-463

Chapter 2

The MuSiCoS spectropolarimeter

2.1 Overview

The design of an astronomical instrument depends on the observations which are to be made, which ultimately depend on the problem to be studied. The study of magnetic fields in stars is made possible by the physics of the Zeeman effect which results in split and polarized spectral lines. An effort to investigate stellar magnetic fields may make use of an instrument which can provide information on how the Zeeman effect acts upon stellar spectra, thus allowing the observer to make inferences as to the field itself.

Methods for investigating magnetic fields may be categorized as one of two types: polarized or unpolarized. Methods that involve the observations of spectra in unpolarized light are possible because the magnetic field splits atomic levels and thus splits, or at least alters the appearance of, spectral lines. This effect can be difficult to detect, however, except at high spectral resolution and high S/N levels, and even then is best suited for slowly rotating stars with very strong fields.

Methods that make use of observations in polarized light are in general applicable to a wider range of field strengths and stellar rotation rates (although they depend on the field not being too complex), but they necessitate the design of new polarimetric instruments that are used instead of or in concert with spectrographic components. The use of such polarimetric components will usually add complexity to the observation process, by requiring multiple observations of differing polarization states, which in turn complicate the process of extracting the useful data from the observational output. The complications in design, observation and data extraction will, however, usually be a fair trade-off given the rich information obtained from polarimetric observations.

2.2 The anomalous Zeeman effect

2.2.1 Introduction

Magnetic fields have been detected in chemically peculiar stars (and in a small number of other stars) through the Zeeman effect, namely through the energy level splitting and polarization of light in spectral lines which is the result of the interaction between an absorbing atom and the stellar magnetic field. In order to design and operate an instrument which allows an observer to detect and study stellar magnetic fields, one must therefore understand the physics of the Zeeman effect.

An atomic level with total angular momentum quantum number J and Landé factor g, in the presence of a magnetic field, B, will be split into $2J+1$ states, characterized by their magnetic quantum number M. The magnetic quantum numbers will take on the values $M = -J, -J+1, ..., J-1, J$. The energies of the split atomic states will have values

$$E(M) = E_o + gM\hbar\omega_L \tag{2.1}$$

where E_o is the energy of the unsplit level, and ω_L is the Larmor frequency

$$\omega_L = eB/(2m_e c), \tag{2.2}$$

Here m_e is the electron mass, e the electronic charge and c the speed of light, in Gaussian cgs units. The scaling factor of the magnetic splitting, g, for atoms with fine structure in pure LS-coupling is found to be

$$g = 1 + \frac{J(J+1) - L(L+1) + S(S+1)}{2J(J+1)}, \tag{2.3}$$

where L is the orbital angular momentum quantum number and S the spin angular momentum quantum number, while other couplings provide other such formulae. In general, experimentally determined Landé factors are preferred to those derived from the above or similar formulae since pure LS coupling often does not accurately describe atomic levels. Landé factors from experiments have been compiled from various sources by the Vienna Atomic Line Database (Kupka et al. 1999, Ryabchikova et al. 1998), which is a freely available source of spectral line data for use in research.

In the absence of a magnetic field, transitions between two levels i and j are characterized by a single frequency $\nu_o = (E_i - E_f)/h$, where E_i and E_f are the energies of the levels involved in the transition. In the presence of a field, the spectral

line that results from the transition is split into a number of lines of frequencies

$$\nu = \nu_o + (g_f M_f - g_i M_i)(eB/4\pi mc) \quad (2.4)$$
$$= \nu_o + [(g_f - g_i)M_f + g_i \Delta M](eB/4\pi mc) \quad (2.5)$$

where $\Delta M = M_f - M_i$. Transitions between split levels obey the quantum selection rule allowing $\Delta M = -1, 0$ or $+1$. Lines resulting from transitions where $\Delta M = 0$ are referred to as π components while transitions where $\Delta M = \pm 1$ result in σ components. The π components are distributed symmetrically around the line of unsplit frequency ν_o while the σ components are distributed above and below the central frequency, usually with $\Delta M = -1$ on one side and $\Delta M = +1$ on the other. The precise pattern of π and σ components that arise from the Zeeman effect is determined by the g and J values of the atomic levels involved in the transition.

The characteristic frequency spacing between π and σ components implies a wavelength spacing of order $\Delta\lambda = B\lambda^2/4\pi mc^2$. The spacing for a given transition is characterized by the effective Landé factor $\bar{g}$, the intensity-weighted mean displacement of the σ components from the centre of the π components, in units of $\Delta\lambda$. Thus the average wavelength displacement of a σ component from the line's wavelength at zero magnetic field is

$$\Delta\lambda_B = \bar{g}B\lambda^2/4\pi mc^2 \quad (2.6)$$
$$= 4.67 \times 10^{-13} \bar{g} B \lambda^2 \quad (2.7)$$

with B in Gauss and wavelengths given in Å.

2.2.2 Polarization and magnetic fields

When the magnetic field is highly ordered, such as in a predominantly dipolar field, the net field along the line of sight (or any direction) is generally non-zero. Thus, one may take advantage of the polarization properties of the Zeeman effect to measure the mean line-of-sight component and transverse components of the magnetic field. If one observes an absorption line affected by a purely longitudinal field, one set of σ components absorbs only right-handed circularly polarized (RCP) light, while the other absorbs only left-handed circularly polarized (LCP) light. The π components vanish. For a purely transverse field, the residual flux in the π components is linearly polarized perpendicular to the field while the flux in both sets of σ components is polarized parallel to the field.

Polarized light may be represented by the Stokes vector which is suited to the description of the intensity and polarization of spectral lines affected by a magnetic field. The components of the Stokes vector, $I = (I, Q, U, V)$, are defined as follows, with a co-ordinate system for astronomical polarimetry chosen such that the x- and y-axes are in the plane of the sky and the z-axis pointed toward the observer. I is the intensity of the light linearly polarized in the x-direction, plus the light linearly polarized in the y-direction. It is equivalent to the emergent intensity measured without a polarizer in place. Q is the intensity of the light linearly polarized in the x-direction minus the light linearly polarized in the y-direction. In the case of a purely transverse field in the y-direction, $Q = (i_\perp - i_\parallel)$, where $i_\perp$ and $i_\parallel$ are the intensities polarized perpendicular and parallel to the field. U is the intensity of the light linearly polarized in the direction rotated positive 45 degrees with respect to the x-direction, minus the light linearly polarized in the direction rotated positive 45 degrees with respect to the y-direction. Thus it gives a measure of the transverse component of the field not aligned with the x- or y-axis. V is the intensity of the light circularly polarized in the right-handed sense, minus the light circularly polarized in the left-handed sense. It is a measurement of V which allows a measure of the mean longitudinal field.

In practice, linear polarization due to the Zeeman effect is much weaker than circular polarization, so most measurements have been made of longitudinal fields, using circularly polarized light. The first measurement of a magnetic field in a star other than the Sun was for the Ap star 78 Vir (Babcock 1947) using what became known as the photographic technique. In this method, the centroid of a spectral line (in practice, of many spectral lines) is measured in LCP and RCP light, and using Equation 2.7 (where B is the longitudinal field and $\Delta\lambda$ the separation of the RCP from the LCP centroid), the longitudinal field may be inferred. A schematic representation of the effect of longitudinal and transverse fields of a stellar absorption line, as well as the resultant Stokes V and Q profiles, may be seen in Fig. 2.1.

Longitudinal field measurements have also been made by measuring stellar line *profiles* in left and right circularly polarized light. Originally, this technique was the basis for Babcock's (1953) solar magnetograph, but its use has been expanded to other stars. The longitudinal magnetic field may be inferred from the shape of the Stokes V line profile, using a technique discussed by Landstreet (1980). In the limit of a weak magnetic field for a slowly rotating star, the line profile in one polarization sense, say right circularly polarized, is approximately equal to the unpolarized profile, $I(\lambda)$. The profile in left circularly polarized light is then $I(\lambda) + (\mathrm{d}I/\mathrm{d}\lambda)\ 2\Delta\lambda$, where

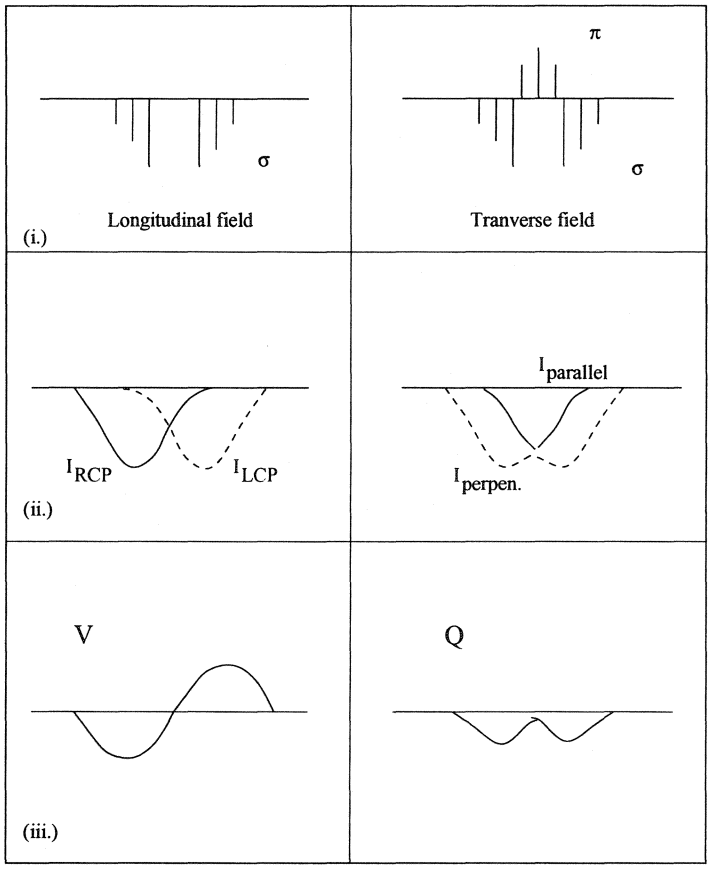

Figure 2.1: A schematic representation of the effect of a longitudinal (left column) and a transverse magnetic field (right column) on an absorption line. Row (i.) shows the π (above the line) and σ (below the line) components. Row (ii.), for the longitudinal field, shows the observed line (stellar line profile convolved with the Zeeman components) in RCP (solid) and LCP (dashed) light. Row (ii.) for the transverse field shows the absorption line in light polarized perpendicular to the field (solid) and parallel to the field (dashed). Row (iii.) shows $i_{RCP} - i_{LCP} = V$ for the longitudinal field, and $i_{\parallel} - i_{\perp} = Q$ for the transverse field.

$\Delta\lambda$ is from Eq. 2.7 with B the longitudinal field. The net circular polarization may be expressed as $V/I = [I_{\rm L} - I_{\rm R}]/[I_{\rm L} + I_{\rm R}]$ so that

$$\begin{aligned} V/I &\approx \frac{I(\lambda) + (\mathrm{d}I/\mathrm{d}\lambda)\ 2\Delta\lambda - I(\lambda)}{I(\lambda) + I(\lambda) + (\mathrm{d}I/\mathrm{d}\lambda)\ 2\Delta\lambda} \\ &\approx \frac{\Delta\lambda}{I}\frac{\mathrm{d}I}{\mathrm{d}\lambda}, \end{aligned} \tag{2.8}$$

because $(\mathrm{d}I/\mathrm{d}\lambda)\Delta\lambda$ is small compared to $I(\lambda)$. The measurable quantities are the shape of the unpolarized line, $\mathrm{d}I/\mathrm{d}\lambda$, and the difference between the intensities of left and right circularly polarized light in the line, V, as functions of wavelength through the line. The longitudinal field, B_z, is then inferred from the calculated value of $\Delta\lambda$. Eq. 2.8 is an accurate approximation only when the rotational velocity is small, so that contributions to the line profile from different parts of the star are not Doppler shifted apart, and the magnetic field is small so that the magnetic splitting is a small perturbation on the natural line profile.

This method has been further expanded to make use of polarization in Balmer lines of hydrogen with the development of the Balmer-line Zeeman analyzer. Although the line profiles in Balmer lines are not as steep as in metal lines ($\mathrm{d}I/\mathrm{d}\lambda$ is small) and thus the measured polarization is smaller, the stellar rotational velocity does not have a large effect on Balmer linewidth. The result is that this method does not have a rapidly decreasing sensitivity with increasing $v \sin i$ and the Balmer-line Zeeman analyzer has proven to be a valuable instrument.

Linear polarization can also be detected in stellar spectra but, as may be seen in Fig. 2.1 it is of smaller amplitude than circular polarization. In the longitudinal field case in Fig. 2.1, the right-handed and left-handed circularly polarized absorption lines may be well-separated in wavelength and thus their difference (Stokes V) is of comparable amplitude to the stellar absorption line. In the transverse field case, the line polarized linearly parallel to the field direction and that polarized perpendicular to the field direction are not separated in wavelength from one another. They are of comparable extent in wavelength and their difference (Stokes Q) is much smaller. In practice, linear polarization levels are 10 to 20 times weaker than circular polarization signals for typical magnetic Ap stars. Therefore, specialized measurements and/or analysis techniques are necessary to extract the weak linear polarization information from stellar spectra.

2.3 Spectropolarimetry

The astronomical technique of obtaining information about how stellar spectral lines are polarized by a magnetic field (or perhaps other atmospheric phenomena) is called spectropolarimetry. It is the combination of the two widely used tools: spectroscopy and polarimetry. Stellar spectroscopy is similar to any other use of spectroscopy in the physical sciences, in that it uses instruments that disperse the light from a source, in this case a star, into a spectrum so that the resultant flux distribution may be analyzed. Polarimetry is somewhat less common in the physical sciences, but is useful when studying the phenomena that polarize light originating from a source, in this case a star. Starlight will generally be polarized in a mixed sense, i.e. light will be comprised of components polarized linearly in different directions as well as circularly in different rotation senses. A polarimeter allows for the measurement of light from a source which is polarized in the senses that define the components of the Stokes vector.

One possible design for a polarimetric instrument to measure linear polarization (Q and U) will contain a retarder (a half-wave plate) which will preferentially retard one component of an orthogonal pair of linearly polarized components followed by a birefringent crystal (a polarizer) which splits the orthogonally polarized components into two separate linearly polarized beams. The half-wave plate may be aligned in different directions which will allow the user of the polarimeter to select which direction of linear polarization one wants to investigate. Normally, the alignment will be such that one of the linear Stokes components, Q or U, may be measured. In order to measure circular polarization, a quarter-wave plate, instead of the half-wave plate, is used as a retarder which transforms circular polarization into linear polarization, which may then be split by the crystal into two separate beams. In either case, the resultant intensity from the two beams can then be measured and the differences may be used to calculate the appropriate Stokes parameter for the observation. Observations made in this way may be used to study the polarization of all wavelengths of light accessible to one's detector, or it may be constrained to a finite spectral window by filters, whether to observe broadband polarization in a relatively wide region of spectrum (Leroy 1962) or concentrate on specific features such as hydrogen lines (Landstreet 1982).

Spectropolarimetry is the result of directing the separate orthogonally polarized beams from the polarimeter into a spectrograph which then provides the observer with polarization information as a function of wavelength. The union of the two

instruments is non-trivial and is discussed further in Section 2.3.1. The reason one wishes to obtain spectropolarimetric measurements is as outlined in Section 2.2.2; the stellar magnetic field will polarize the light in a spectral line in a way that depends on the line itself and the strength and structure of the field. Therefore, a detailed description of how light is polarized across a spectral line, or many spectral lines, should allow one to derive detailed representation of the stellar field, in which the spectral line is produced.

2.3.1 Instrument requirements

The design of a spectropolarimetric instrument is constrained by the nature of the observations being made. Since stellar line polarization, especially linear polarization, may be weak, the polarimeter component must be designed such that very little instrumental polarization is introduced into the starlight, or that the polarization which is introduced varies slowly with wavelength. Also, if one wishes to investigate the spectrum over a wide range in wavelength, then the polarimeter must be largely achromatic in operation. If one is interested in observing only a very small spectral window, containing a single line or, at most, several lines, then a high-resolution spectrograph would serve the purpose very well. Unfortunately, the weak polarization levels could make such observations of a single line not very useful, since the signal to-noise ratio may not allow the polarization to be seen. The development of a technique that makes use of many spectral lines at once to create a representation of the average polarization in those lines (Least-Squares Deconvolution, see Section. 5.1) means that the observation of as wide as possible a spectral region may be the most useful.

The resolution of the spectrograph must be such that spectral lines are reasonably well-resolved, while not dispersing light too much, which would reduce the signal-to-noise ratio in each detector element. Also, increased resolution results in decreased operating spectral window for a given detector size. One spectrograph design that allows for reasonably high resolving power as well as a large spectral window is an échelle spectrograph. An échelle spectrograph uses a cross-dispersing element which "stacks" subsequent regions of the stellar spectrum on a two-dimensional detector (eg. a CCD) such that the dispersion axis runs in one direction for each section, or order, of spectrum, and subsequent orders are recorded such that they are "stacked" in the orthogonal direction. This allows for a very large region of spectrum to be imaged during a single observation. It also generally makes the reduction of the spectral image quite difficult, the specifics of which will be discussed in Section 3.1.

2.4 The MuSiCoS spectropolarimeter

The MuSiCoS spectropolarimeter is an instrument that meets the requirements of stellar spectropolarimetry outlined above. It is an échelle spectrograph equipped with a polarimeter whose detailed specifications are described by Donati et al. (1999). The spectrograph has a resolving power ($\lambda/\Delta\lambda$) of about 35000, which corresponds to approximately 8 $\mathrm{km\,s^{-1}}$ in velocity units. It is possible with MuSiCoS to observe a 2000 Å window in the visible spectrum of a star anywhere between 3900 to 8700 Å, but with the polarimetric module it is used to observe from 4480 to 6620 Å. The detector is a thinned 1024×1024 pixel SITE CCD.

As light enters the polarimeter, it may pass through a quarter-wave plate if one is interested in circular polarization, or not, if one is interested in linear polarization. Light then passes through a Savart-type beam splitter which separates the light into two orthogonally polarized beams, which are then fed into the spectrograph and recorded simultaneously on the CCD. Calibration data are normally obtained and are discussed in Section 3.1. A single stellar observation consists of four sub-exposures during which either the instrument (for linear polarization) or the wave plate (for circular polarization) is rotated by ±90 degrees, in the order 1,2,2,1, where 1 is the initial orientation and 2 is the orientation rotated by +90 degrees. This procedure is followed to switch the positions of the orthogonally polarized spectra as they are recorded on the CCD, and to exchange the beams within the instrument. The aim of the observing procedure is to reduce the amount of spurious polarization seen during an observation, as well as to image orthogonally polarized spectra on exactly the same pixels during an observation, thus reducing the effects of pixel-to-pixel sensitivity differences. The four Stokes spectra may then be calculated from the series of the orthogonally polarized spectra imaged during the subexposures by using the method outlined in Section 3.1.1.

The MuSiCoS spectropolarimeter is one of very few stellar spectropolarimeters available in the world and offers a nearly unique opportunity to obtain polarization information in all four Stokes parameters over a large range in wavelength for stars. MuSiCoS does present some challenges for the scientist, given that its échelle spectrograph output is quite complex, and the reduction techniques necessary to extract the data are non-trivial. The details of the data reduction procedures are outlined in Section 3.1.

References

Babcock, H. W. 1947, ApJ, 105, 105

Babcock, H. W. 1953, ApJ, 118, 387 N1

Donati, J.-F., Catala, C., Wade, G. A., Gallou, G., Delaigue, G., & Rabou, P. 1999, A&AS, 134, 149

Kupka, F., Piskunov, N. E., Ryabchikova, T. A., Stempels, H. C., & Weiss, W. W. 1999, A&AS, 138, 119

Landstreet, J. D. 1980, AJ, 85, 611

Landstreet, J. D. 1982, ApJ, 258, 639

Leroy, J.-L. 1962, Ann. Astrophys., 25, 127

Mathys, G. 1988, in Elemental Abundance Analyses, (Inst. Astr. Univ. Lausanne, Chavennes-des-Bois), 82

Ryabchikova, T. A., Piskunov, N. E., Stempels, H.,C., Kupka, F., & Weiss, W. W. 1998, *Proc. of the 6th International Colloquium on Atomic Spectra and Oscillator Strengths*, Victoria BC, Canada , Physica Scripta, T83, 162

Chapter 3

Data Reduction

3.1 ESpRIT

Data reduction is the term for the series of steps one performs in order to transform raw observational output into a form which may be used for astronomical research. In the case of CCD spectroscopy, the raw data are in the form of a digital image of a spectrum, recorded on a two-dimensional pixel array. It is stored in a data file and must be converted into a one-dimensional spectrum of intensity as a function of wavelength. In CCD spectroscopy, the detector is normally aligned in the spectrograph so that the dispersion direction is parallel to one axis on the CCD chip, designated as the X-axis. The spectrograph slit forms an image in the Y-direction at each point along the X-axis, thus forming the spectrum. The data reduction process must optimally extract the intensity data at each point along the dispersion axis, and calibrate the spectrum in terms of wavelength, while eliminating or at least reducing instrumental effects (such as sensitivity variations between pixels) introduced by the spectrograph and the detector. In the case of CCD spectropolarimetry, the simplest possible case would be very similar to spectroscopy, with the difference that two orthogonally polarized spectra need to be imaged, sequentially or simultaneously, so that one may determine the values of two Stokes components (one intensity and one polarization) as a function of wavelength.

For output from an échelle spectrograph, the data reduction routine must account for the fact that the spectrum is divided into orders, recorded in separate sections "stacked" on the image. The CCD image is formed from a spectrum which runs in the X-direction, but which is longer than may be imaged on a single frame. A cross-dispersing element causes subsequent orders of the spectrum to be imaged on the CCD detector such that a number of orders are recorded on the same frame.

In the case of MuSiCoS spectra, the orders do not run *exactly* horizontally but are curved, as may be seen in Fig. 3.1, a portion of a raw MuSiCoS spectrum frame. The amount of curvature varies smoothly from order to order. The illuminated intensity also varies smoothly from order to order and across each order. Available data reduction software packages were not optimized for such complex data or for data where orthogonally polarized spectra are imaged on the same frames. Thus, in order to extract one-dimensional polarized spectra from MuSiCoS output, the development of a new package was desirable. The Echelle Spectra Reduction: an Interactive Tool (ESpRIT) software package was developed by Donati et al. (1997) specifically for the output of instruments like MuSiCoS and was used in the completion of this thesis.

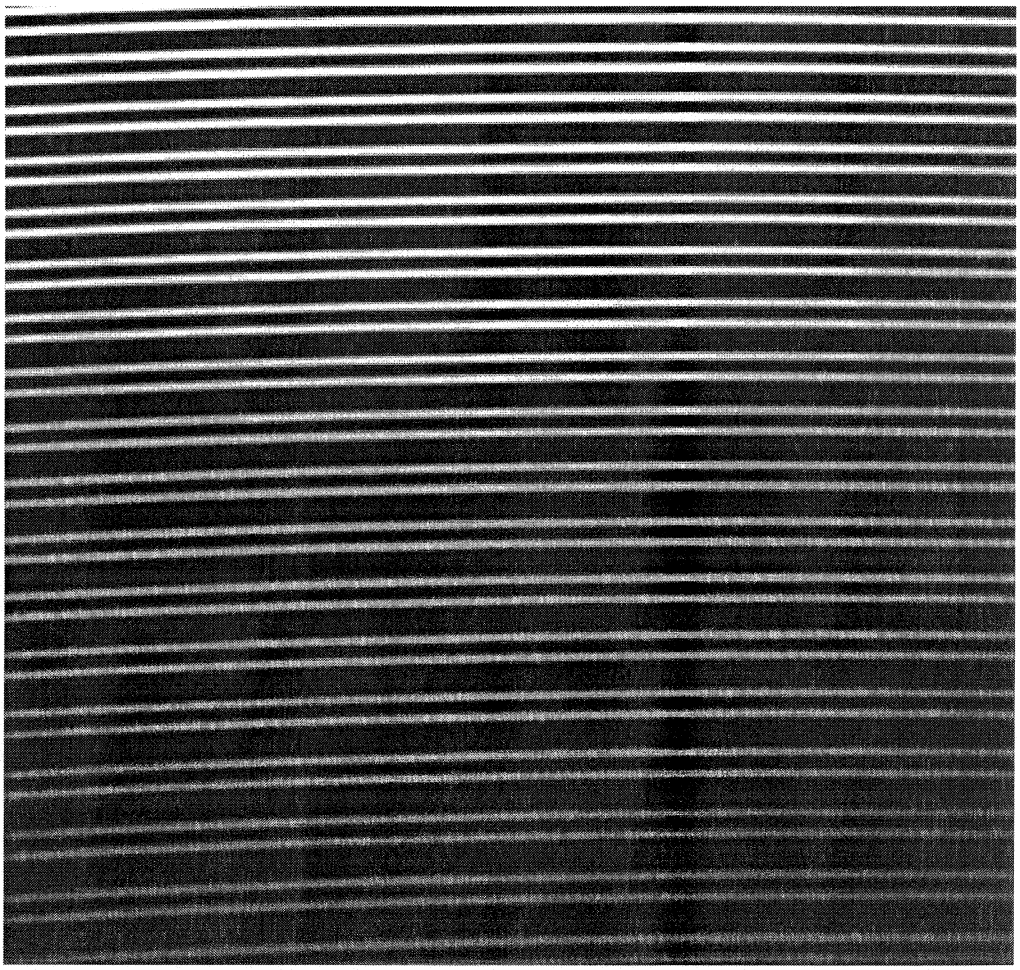

Figure 3.1: The central region of a typical MuSiCoS flat-field frame, showing the curvature of the orders.

The general purpose of ESpRIT is to perform the basic steps of CCD data reduction and extraction of spectral information, while accounting for the fact that the data are in échelle format and that the orders may be curved and tilted on the CCD. It is also necessary to extract the polarization information from a set of subexposures so that the Stokes spectra may be computed, and ESpRIT is designed to perform this task as well.

3.1.1 Operation

Image processing

The steps performed by ESpRIT for the reduction of MuSiCoS CCD data into polarized spectra are discussed in extensive detail by Donati et al. (1997). The discussion here will be limited to the use of the package by the author, with details provided as necessary to provide a clear explanation. In order to produce a reduced MuSiCoS spectrum, one requires a number of CCD data frames to be taken on a given night. An image, known as the bias image, is taken with an exposure time of zero in order to measure the baseline response of the CCD. During this exposure a constant voltage is applied to the CCD so that the average baseline level will be non-zero. If the baseline level was left at zero, then random noise would cause some of the pixels' intensities to be negative. In general, the electronics in CCDs are unsigned (not designed to differentiate between negative and positive numbers), so the negative value could either be stored as zero or some positive number, which is a loss of the information either way. Therefore, a positive bias level is applied to all pixels, and removed later. In the case of the CCD used at the Telescope Bernard-Lyot to record MuSiCoS frames, the bias level is found to be a smooth function of pixel location and is fit by a two-dimensional (X and Y position of the frame) second-order polynomial. This level is then subtracted automatically from all subsequent MuSiCoS frames on the given night.

The spectrograph is then used to take images, known as flat-field images, of a standard lamp having no spectral lines. Light from the flat-field lamp is passed through the same optical path as light which emerges from the telescope focus. The flat-field is later used by ESpRIT to correct for any pixel to pixel sensitivity differences in the data images, and it is also used to determine the geometry of the orders in the spectra. A single image may be contaminated in a random way by pixels that return larger than normal intensity values due to cosmic ray impacts. Furthermore,

each CCD pixel has a finite reservoir of electrons which can be excited by incoming photons, so that there is a maximum intensity of light that may be measured by any one pixel before it is said to be saturated. CCD chips are more sensitive to light at red wavelengths and so the pixels that capture the red orders of the spectrum will saturate more quickly than those that record the blue orders. Combining multiple spectra allow one to increase the signal-to-noise ratio at blue wavelengths without saturating anywhere. Therefore a large number, usually fifteen, flat-field images are taken and they are median-combined to provide a useful flat-field that is free from any image to image differences. The final flat-field will also have reasonable S/N at all wavelengths without saturating pixels at more sensitive red wavelengths.

The geometry of the curved orders on the échelle spectra must be known in order to convert data images into one-dimensional spectra. The user provides the location of the central pixel, and the width, of the first order of the combined flat-field frame, and ESpRIT automatically traces each order. The trace of the orders is determined, as well as the change in the curvature with increasing order. This information about order geometry is stored as a set of polynomial coefficients, which allows ESpRIT to locate all the orders on the CCD. Once the geometry of the orders is found, a comparison échelle spectrum of a thorium argon (ThAr) hollow cathode lamp, also taken each night during the observing run, is used in order to determine the slit shape as well as the slit direction in all orders. The mean slit shape and the set of polynomial coefficients that describe how the slit direction changes across the CCD are stored in another file. The ThAr échelle spectrum is then collapsed along the slit for each order, meaning that the intensity is added along the direction of the slit at each pixel location, and the 2D spectrum is reduced to a 1D file of intensity versus pixel for each order.

The ThAr spectrum is then used to determine the absolute wavelength of each pixel, known as the dispersion relation. An initial approximate dispersion relation is provided by the user for one order and, given the wavelengths of known lines in the ThAr spectrum, ESpRIT uses that relation to identify the lines in the observed ThAr spectrum for that order, thus better determining the dispersion relation. As a consequence of the grating equation which governs spectrograph optics, the first dispersion relation may be scaled by the ratio of order numbers and used for each order. Note that this is still just an approximate relation and is used simply to identify all the lines in the ThAr spectrum. Once identified, all lines are used simultaneously to determine the exact dispersion relation across each order, and how it varies with increasing order, as a two-dimensional polynomial. The coefficients of this polynomial

are stored in another file and are used for the wavelength calibration of all spectrum images.

The essential elements for ESpRIT reduction of stellar spectra are then assembled: the bias level, the flat-field frame and the files that contain the information about the geometry of the orders, the slit direction and shape across the CCD and wavelength calibration. The bias level is subtracted from each stellar and flat-field frame. Since count levels at the edges of orders are very small compared to those at center (a consequence of using an échelle spectrograph) each flat-field is "flattened down" by dividing it by the mean horizontal profile of the flat-field. Each stellar frame is then divided pixel-by-pixel by the flat-field frame. An additional step of background subtraction is done by measuring the levels between the orders in each stellar frames, where the intensity should ideally be zero but in practice is non-zero due to scattered light. A two-dimensional polynomial fit to these background levels is subtracted from each frame. One-dimensional spectra are extracted from each frame using the geometrical and slit information and are finally wavelength calibrated using the dispersion relation.

The process of removing the large-scale background shape of the spectrum, known as continuum normalization, is also automated using ESpRIT. This normalization is done because we are not interested in the shape of the overall spectral energy distribution, or continuum, but in the spectral lines that are usually studied relative to the continuum. Each spectrum is normalized by ESpRIT by dividing it by a function defined by points considered to be part of the continuum, or outside of spectral lines. The code identifies continuum points throughout the entire spectrum and first fits a high degree 1D polynomial to them, using it for an initial normalization. A different, lower degree 2D polynomial is then fit to the continuum points to remove any remaining trends in continuum shape from one order to the next, with one dimension tracing the continuum shape in an order and the other dimension indicating the variation of continuum shape with order. The user has the choice of how continuum normalization is performed by altering the size of the interval at which ESpRIT chooses continuum points and the degree of polynomials in the 2D normalization fit. This continuum fitting routine minimizes the error introduced by attempting to normalize a spectrum near the very wide Balmer lines, given that the normalization polynomials are fit over the entire spectrum and would not be permitted to vary widely enough to "normalize out" the Balmer lines. Still, the normalization will not be perfect near the Balmer lines, but the effect on our data is minimized by neglecting those lines, as well as lines near them in our analysis. Finally, the wavelength calibration of the spectra is

transformed to the heliocentric reference frame by using information about exposure times and dates and observatory location found in image header files.

Calculation of polarized spectra

The above steps would be largely sufficient for the reduction of a single, unpolarized stellar spectrum. The reduction of MuSiCoS polarization spectra is more complex because an observation normally consists of four subexposures, and because orthogonally polarized spectra are recorded simultaneously on the same CCD frame. Each frame is processed as outlined above, with each polarization state extracted independently, so that the four subexposures result in eight independent spectra. The Stokes I spectrum, which is simply the mean intensity spectrum, is derived by adding them all together. While the other Stokes spectra (V, Q and U) are defined in terms of the differences of orthogonally polarized spectra, their calculation is not done this way in practice. In order to reduce spurious effects and systematic errors that would arise from this simple approach, ESpRIT calculates the ratios of orthogonally polarized spectra, instead of the differences, the calculation of which is explained below. Errors are further reduced by the procedure of making four subexposures for each final spectrum. Of the four sequential subexposures, the first and fourth are made with the polarimeter oriented in the same way. The second and third subexposures are also taken identically, but with the polarimeter or waveplate in an orientation rotated by 90° compared to that of the first and fourth subexposures. This sequence of subexposures is made for two reasons. First, it results in orthogonally polarized spectra being captured on the same pixels during the sequence. This reduces potential systematic errors such as those caused by inhomogeneous CCD pixel sensitivities. The bracketing of exposures taken with one orientation by two which are rotated reduces the error caused by changes in the polarization spectrum with time, either due to instrumental drift or the rotation of the Earth or changes observed in the spectra themselves, such as those caused by rotation and spectral variability.

A polarization spectrum (V, Q or U), referred to here generally as P, is defined as $P = i_\perp - i_\parallel$, the difference of two orthogonally polarized spectra ($i_\perp$ and $i_\parallel$) whose states (circular or linear) and orientations define the Stokes spectrum being calculated. The unpolarized spectrum, I, is the sum of the two orthogonally polarized spectra, so that

$$\frac{P}{I} = \frac{i_\perp - i_\parallel}{i_\perp + i_\parallel} = \frac{R-1}{R+1}. \tag{3.1}$$

where $R = i_\perp / i_\parallel$. When an observation consists of four subexposures, one may

calculate R as the fourth root of

$$R^4 = \frac{i_{1,\perp}/i_{1,\parallel}}{i_{2,\perp}/i_{2,\parallel}} \frac{i_{4,\perp}/i_{4,\parallel}}{i_{3,\perp}/i_{3,\parallel}}, \tag{3.2}$$

where $i_{k,\parallel}$ and $i_{k,\perp}$ are the two orthogonally polarized spectra obtained in subexposure k. If there were no systematic errors or spectrum changes, each of $i_{1,\perp}, i_{2,\parallel}, i_{3,\parallel}$ and $i_{4,\perp}$ for example would be equivalent (since subexposures 2 and 3 were taken with the instrument rotated) and the validity of using Eq. 3.2 to find R is obvious. When systematic errors are present, the rotation of the instrument to make the subexposures will have reduced them. Since changes in a spectrum with time are also likely to be present, the calculation of R using four subexposures provides a good measure of the polarization at the mid-point of the entire observation. When calculated, the value of R is then used to find the general polarized spectrum. For example, the net polarization spectra in circularly polarized light, V/I, would be found using Eq. 3.1 where R is determined from Eq. 3.2 using subexposures imaging right and left circularly polarized light.

3.1.2 Installation

ESpRIT was installed in 1999 on the Sun 248 MHz UltraSparc-II running SunOS 5.6 in the Department of Physics and Astronomy at the University of Western Ontario. The precompiled version which was transferred to the UltraSparc had been compiled on a DEC Alpha computer, and so all programs and subroutines had to be reinstalled and compiled locally. The installation took a great deal of effort to perform properly, mainly because the author was attempting it with little or no supporting documentation. An additional complication was that ESpRIT is primarily written in C, of which the author needed to acquire a basic knowledge in order to perform some steps in the installation.

ESpRIT uses routines that are provided by the set of graphics subroutine libraries known as PGPLOT. PGPLOT is freely available, non-commercial software copyrighted by the California Institute of Technology, and downloads were made from their website. Necessary libraries included the PGPLOT C language interface library called CPGPLOT. Although PGPLOT was present on the UltraSparc used by the author, the package had to be reinstalled in order to include the CPGPLOT library. ESpRIT also uses display drivers in PGPLOT that are not selected in the set of default drivers provided during an automatic installation of PGPLOT, and the installation of PGPLOT had to be performed several times before the correct drivers

were identified and installed.

Since ESpRIT is a modular package, there are many subroutines and functions located in individual files making up the ESpRIT function libraries. These files all had to be located and recompiled under the Sun operating system. Several ESpRIT scripts that had references to directory structures on other computer systems were edited to reflect local directories and filenames. A number of subroutines made use of mathematical functions that are defined system-wide in library files, but the names of the libraries and/or the locations of the functions were not the same on the machine where ESpRIT was previously installed as on the Sun. In order to properly select local libraries for inclusion during the compilation, ESpRIT subroutines were compiled, missing or unknown functions were noted, and local mathematical libraries were searched for references to the functions. If a likely candidate was found, the library was included in the compilation, and the subroutines recompiled while noting any additional missing or unknown functions. This procedure was repeated until all of ESpRIT could be compiled completely.

Initial tests of the ESpRIT package after the installation did not return proper results and it was discovered that one sub-program, one script and several command line functions must indicate whether or not byte-swapping is to be enabled. A multi-byte integer may be stored in a computer's memory such that it is read most significant byte first, or least significant byte first. The convention used depends on the computer. Byte-swapping is the process of converting the order of how information is stored in bytes from one format to another. Running ESpRIT on the Sun requires that byte-swapping be disabled, so all references to byte-swapping in ESpRIT were found and edited to ensure that it was disabled.

Since the installation of ESpRIT was done by the author without much specific external assistance, and since it was found to be a sometimes difficult task, an installation manual was written so that in future its installation will be facilitated. This manual has been used as a reference by a student at the University of Western Ontario (who assisted in the reduction of some data), as well as a group in the Netherlands. The manual is included as Appendix A.

References

Donati, J.-F., Semel, M., Carter, B. D., Rees, D. E., & Collier Cameron, A. 1997, MNRAS, 291, 658

Howell, S. B., 2000, *Handbook of CCD Astronomy*, Cambridge University Press

Chapter 4

Observations

4.1 Collaboration

The observations of stars studied in this thesis were not made solely by the author, but by a group of observers in a collaborative effort. This effort was necessary given the nature of the observations being made. The principal observational projects are studies of magnetic stars, both magnetic Ap and magnetic cool stars, for each of which a number of repeated observations was necessary. Magnetic stars, like all stars, rotate so that observations over time permit one to see the most complete view possible of the surface of the star. Repeated observations ultimately allow for the study of a star's magnetic field as it rotates, which is necessary for a re-construction of the global field. In order to be efficient, the observations were scheduled so that identical rotational phases were not duplicated. The ideal phase coverage for a single star would be approximately ten observations spaced evenly in phase so that the entire observable surface is spectropolarimetrically imaged. The scheduling of such repeated observations would then depend on the rotation period of the stars being observed, as well as the phases that have already been observed.

An additional project consisted of a small number (one to three) of observations of individual stars in order to detect or confirm magnetic fields. These did not have to be scheduled at specific times or dates, and so were completed in between scheduled observations of magnetic stars. Typical total exposure times for a single observation were 24–40 minutes, with one observation (Stokes V) for each survey star and each cool magnetic star and three observations (Stokes V, Q and U) necessary for almost all of the magnetic Ap stars. Thus, the typical number of stars which may be observed on a single winter night at an observatory at mid-northern latitude is around ten, assuming no loss of time because of equipment or weather difficulties.

Given the large number of observations necessary to adequately provide phase coverage for the magnetic Ap stars and to make a reasonable survey, long duration runs (up to five weeks) were necessary and observing time was required in several successive years. Since a large number of nights were needed, observing was performed by a group of observers. Some members of this collaboration were primarily interested in the magnetic fields of other types of stars (solar-type stars, hot stars) and the schedule of each observing run was designed to permit observations of stars from a number of programs. Thus, the author did not personally make all the observations of stars included in this thesis. Conversely, some observations made by the author do not appear in this thesis, but have been included in other studies. Studies for which observations were contributed include magnetic field structure and differential rotation investigations of solar-type stars (Petit et al. 2004). Observations were made, and the data reduced and analyzed for a study of the magnetic field of the hot star β Cep (Henrichs et al. 2000) as well as the pulsating variable star RR Lyr (Chadid et al. 2004). Observations and analyses made by the author have also contributed to studies of magnetic Ap stars other than those found in this thesis (Bagnulo et al. 2001, Wade et al. 2000a, Wade et al. 2000b).

In order to obtain time for such long and repeated runs, especially at a French telescope, an international collaboration including French astronomers was formed. Members of the collaboration included several astronomers from the University of Western Ontario: J.D. Landstreet, T.A.A. Sigut, G.A. Wade (now at Royal Military College, Kingston), and S. Strasser (now at University of Minnesota). French astronomers included J.-F. Donati and P. Petit of Observatoire Midi-Pyrenées, Toulouse.

4.2 Star selection

Stars were chosen for observation in order to complete our projects based on several criteria and constrained by some limitations. All stars needed to be observable from the site at Pic-du-Midi, so only stars with declinations greater than about $-20°$ could be selected, while declinations greater than zero were preferred. Telescope time in the winter months was requested in order to make continued observations of a list of both solar-type and magnetic Ap stars which are favourably located for observation then. Repeatedly requesting and being granted winter observing time allowed for excellent phase coverage of a large sample of magnetic stars, as well as long nights for scheduling observations, but it limited the number of stars which were available

for survey purposes.

For the primary magnetic star program, stars were selected for the ongoing study into the detailed magnetic field structure of well-established magnetic chemically peculiar (Ap SrCrEu, Si) stars in order to measure longitudinal fields and obtain high signal-to-noise polarization signatures for modelling. It was necessary that the stars selected be favourable to observation with a 2m telescope, so only bright stars ($V_{\rm mag} < 7$) were chosen. Stars were chosen with reasonably short periods (less than two weeks) to allow for rotational phase coverage, but with relatively low rotation velocities. Stars with low rotation velocities are desirable because spectral lines are increasingly "Doppler broadened" as $v \sin i$ increases, making them shallower and thus increasing the uncertainty in longitudinal field measurement, as will be shown in Section 6.5. Well-studied examples of Ap stars with strong magnetic fields, such as 53 Cam and β CrB, were chosen along with less well-studied examples, or stars with weaker fields, such as ϵ UMa and θ Aur. Multiple observations were planned and made in order to provide rotational phase coverage of many stars, with 0.1 of a rotational cycle as the desired gap between observations.

Stars were selected for the cool star project by Donati and his collaborators. They included active late G and K type stars which have fairly large rotation velocities for late-type stars ($v \sin i > 20$ km s^{-1}) as well as being reasonably bright ($V_{\rm mag} \leq 7.4$). The specific stars selected are all RS CVn type binaries, which are thought to be highly magnetic active due to increased dynamo processes, caused by high rotation rates which are ultimately a result of tidal coupling between the binary pair. The stars selected have been previously diagnosed as magnetic, and the project was designed for continued observation to study the structure and evolution of the fields of these cool stars.

The third study is a survey project to search for and possibly measure fields in stars for which no fields had previously been conclusively found. This is the project which forms a major part of this thesis. The survey was designed to investigate the magnetic fields of stars in the complete range of spectral types from early B to late F, while concentrating on the canonically non-magnetic chemically peculiar stars. Again, the most favourable targets for study are the brightest stars with relatively low rotation velocities, and such stars were chosen whenever possible. Stars selected for the survey project were divided into six categories: Am, HgMn, λ Boo, normal, Ap SrCrEu and Ap Si, and emission-line stars. Am and HgMn stars were identified based primarily on peculiarities listed in their Bright Star Catalog spectral types as well as classifications by Abt & Morrell (1995), and selected so as to be bright ($V_{\rm mag} \leq 7.7$)

with relatively low rotation velocities ($v \sin i \leq 60$ km s^{-1}). Some specific Am and HgMn stars were particularly included because they have been featured in previous studies indicating that they possess strong surface fields. These stars are discussed in detail in Section 6.3.1.

Normal and emission-line targets included main sequence stars with spectral types from B0.5 to F9, plus several giant stars (moderate to high mass stars which have evolved off the main sequence) with spectral types from B6 to F5, as well as two supergiants (high mass stars which have evolved well off the main sequence). All stars had $V_{\rm mag} < 6$, and the sample of normal stars predominately has rotation velocities less than approximately 50 km s^{-1}. In order to survey the emission-line stars and some hotter stars, we had to include stars which have rotation velocities up to $v \sin i = 230$ km s^{-1}, although field measurements of such targets will have large uncertainties. Two λ Boo stars were chosen to test the applicability of the LSD to the study of high rotation velocity, low line density spectrum stars. Multiple observations of a number of Am, HgMn and normal stars were made in order to detect any temporal variability of possible signatures.

The survey was also designed to include stars which have chemical peculiarity classes corresponding to the existence of magnetic fields (Ap SrCr Eu, Ap Si) but for which no conclusive field detections had been made, or for which improvements to the precision of field measurements were intended to be made. The stars were chosen from a number of previous magnetic field investigations in order to be bright ($V_{\rm mag} < 6$) and to have relatively low rotation velocity ($v \sin i < 65$ km s^{-1}), although one star with $v \sin i = 90$ km s^{-1} was also observed.

4.3 Observing run

4.3.1 The Bernard-Lyot telescope

The Bernard-Lyot telescope (TBL) was used for all observations in this thesis. It is a 2 meter telescope located at the Pic-du-Midi Observatory in France at the geographical co-ordinates: 0°8′.7 east, 42°56′.2 north, at an altitude of 2861 meters. It is operated by the French Centre National de la Recherche Scientifique (CNRS), the Université Paul Sabatier (Toulouse) and the Observatoire Midi Pyrenées.

4.3.2 Operation

Observations were made over a period of 14 nights in January 1999 either by the author alone, or by the author together with G.A. Wade or J.-F. Donati as the schedule dictated. A log of the observations is given in Appendix B. Each night's observing program included stars from each of the three main areas of study. The additional observations made by other observers of the collaboration, not including the author, have not been included in the appendix.

Each night's observing procedure was very similar, differing only in the objects being observed. Bias (zero second) exposures and ThAr comparison spectra were taken at the beginning and end of each night. Bias frames were checked to ensure that the level and standard deviation of counts were within the acceptable working range as dictated by the MuSiCoS observing procedures manual. ThAr spectra were checked occasionally to ensure that the detector was aligned correctly and that the instrument was in focus. A series of fifteen flat field exposures of fifteen seconds duration each was captured at the beginning of each night using the standard flat field lamp for MuSiCoS at the TBL.

The list of stars which was planned to be observed was given to the night assistants and they carried out the telescope pointing and general operation as each observation was requested. A television display, in the scientist's portion of the control room, showing the telescope's view, allowed the observers to see that each target was located, and allowed for a selection among nearby targets in several cases where stars were located in crowded fields.

An early attempt at automatic guiding by the telescope operators was not successful, so guiding was performed by hand by the observers with the aid of an exposure meter showing the intensity of light passing through the slit. The telescope was pointed such that the intensity was maximized on the exposure meter, but unfortunately the meter did not perform consistently during the observing run. Guiding was then done by hand such that the apparent centre of the stellar disk, as seen on the television display of the observed star, was kept within the crosshairs, indicating the optimal telescope pointing.

The keeping of a detailed observation log was especially important during the run. The reduction package, ESpRIT, has the ability to read in pertinent data about each observation that are stored as keywords in the header of each datafile. These data include star name and co-ordinates, time and date of observation, observatory location and other data that are necessary for proper data reduction. In the case of

MuSiCoS spectra, the data acquisition software did not automatically write all these keywords, or did not write them in a standard format. Thus, the detailed log allowed for the later header editing without which the data reduction would have been much more difficult.

After each set of four sub-exposures was taken, preliminary data reductions were performed by the observer using ESpRIT and LSD (see Sections 3.1 and 5.1 for details). Such preliminary reductions had several purposes, depending on the object being observed. In all cases, data reduction which returned only an error message would be an indication that perhaps there was a problem with the spectrograph, the data transfer, or perhaps one or more of the calibration frames. It was during one such set of preliminary reductions that a problem was discovered regarding the alignment of the spectrograph, which was then resolved before more observing time was wasted.

Preliminary reductions also allowed for some degree of confirmation of the identification of the stars being observed. The absence of a polarization profile or an unfamiliar unpolarized line profile for a known magnetic star, for instance, would be an indicator that there was a mis-identification, although this did not happen. The detection, or marginal detection, of a polarization signal in a star for which none had been previously detected would allow the observer to alter the night's observing program in order to make additional observations of that star. This did happen in the case of a survey observation of the Be star γ Cas (HD 5394), although the observed polarization signature turned out to be of instrumental and not stellar origin. Preliminary reductions could also allow one to determine whether repeated observations might be necessary in order to combine multiple observations to improve the S/N to a useful level.

4.3.3 Observing efficiency

Making efficient use of scheduled time during the run in January 1999 was complicated by several factors including weather and technical issues. Weather conditions caused observers to end observations early on several nights, and did not permit observations at all on several others. Problems with the computer hardware responsible for transferring and storing data caused time to be lost. An error by the author caused the dewar holding the CCD detector to be displaced from its position in the light path and part of an evening was lost in diagnosing and correcting the problem. Intermittent problems experienced by night assistants in getting the telescope

to point correctly cost some time, as did a problem in actually locating the night assistants after the weather cleared one evening.

Total time lost during the January 1999 observing run was approximately 50%, with almost all of that due to the weather. Only 4% was lost due to problems with either the telescope, the telescope operators, the instrument or the computer system. This level of efficiency is fairly typical of the overall efficiency of all observing runs at Pic-du-Midi from 1997 to 2000 involving our collaborators.

4.4 Header editing

As mentioned in Section 4.3.2, the raw spectra and calibration frames from the MuSiCoS spectropolarimeter were stored in files with headers that allow for the storage of pertinent information about the observation being made. The file structure is known as FITS (Flexible Image Transport System), and is the standard data format used for astronomy. Each data file contains the spectrum data itself, plus the header where information is assigned to keywords such as `DATE-OBS = 1999/01/14` which would indicate that the date of observation was January 14, 1999. The ESpRIT data reduction package uses the information stored in keywords to perform certain tasks. For example, it is necessary to remove the contribution of radial velocity due to the Earth's motion from the spectra, thus correcting the data to a standard heliocentric reference frame. The program therefore requires information about the location of the observatory, plus the stellar co-ordinates and the date and time of observations. These pieces of information need to be stored in the correct keywords and in the proper format for ESpRIT to read them.

Unfortunately, the software used to capture and store the data at Pic-du-Midi did not properly write many of the FITS keywords, including the observatory latitude, the stellar co-ordinates and the dates and times of observations. An undergraduate student, S. Strasser, was employed to edit the headers to add or correct the necessary keywords under the supervision of the author. Strasser made use of the widely available astronomical data reduction and analysis software package, IRAF (Image Reduction and Analysis Facility), to edit some of the keywords. Other keywords were corrected by using IRAF to save FITS headers as separate text files, which were then edited using shell scripts and re-inserted as FITS headers with IRAF. When completed, the observational data were reduced using ESpRIT as outlined in Section 3.1.

References

Abt, H. A., & Morrell, N. I. 1995, ApJS, 99, 135

Bagnulo, S., Wade, G. A., Donati, J.-F., Landstreet, J. D., Leone, F., Monin, D. N. & Stift, M. J. 2001, A&A. 369, 889

Chadid, M., Wade, G. A., Shorlin, S. L. S., & Landstreet, J. D. 2004, A&A, 413, 1087

Henrichs, H. F., de Jong, J. A., Donati, J.-F., et al. 2000, *The Be Phenomenon in Early-Type Stars*, ASP Conference Proceedings, eds. Myron A. Smith & Huib F. Henrichs. Astronomical Society of the Pacific, 214, 324

Petit, P., Donati, J.-F., Wade, G. A., Landstreet, J. D., Bagnulo, S., Lũftinger, T., Sigut, T. AȦ., Shorlin, S. L. S., Strasser, S., Aurière, M. & Oliveira, J. M. 2004, MNRAS, 348, 1175

Wade, G. A., Donati, J.-F., Landstreet, J. D., & Shorlin, S. L. S. 2000a, MNRAS, 313, 823

Wade, G. A., Donati, J.-F., Landstreet, J. D., & Shorlin, S. L. S. 2000b, MNRAS, 313, 851

Chapter 5

Interpretation

5.1 Least-squares deconvolution

5.1.1 Overview

The use of the Least-Squares Deconvolution (LSD) technique to analyze polarization spectra is made necessary by the fact that polarization signals, especially for linear polarization, are inherently weak. A circular polarization profile corresponding to a strong, magnetically sensitive spectral line in a magnetic Ap star with a field of several kG has a peak amplitude relative to the unpolarized continuum (I_c) of $|V/I_c| \approx 0.1$, while for weaker lines or stars with weaker magnetic fields, the amplitudes are much lower. In order to detect such a profile, say at a $n\sigma$ level, one requires a signal-to-noise ratio (S/N) level in the spectra of the order of $n/0.1$. This is the very minimum S/N required for the strongest polarization profiles. In our experience, linear polarization profiles (Q/I_c and U/I_c) will be at most approximately one-tenth as strong as circular polarization for the same line, requiring still ten times larger the signal-to-noise ratio (and one hundred times more photons) to detect. Therefore, observations of linear polarization profiles associated with single lines usually do not provide an adequate signal-to-noise ratio to detect polarization. Linear polarization profiles may be detected in individual lines for very high signal-to-noise observations, implying the observation of bright stars, long integration times or large telescopes. Linear polarization will also be more readily detected for stars with strong fields and strong lines, particularly in the most magnetically sensitive lines. In general, however, linear polarization profiles may be hidden in the noise. An example of a polarimetric observation of individual lines may be seen in Fig. 5.1. The region surrounding the strong Fe II line at 5018 Å is shown in all four Stokes parameters at a single rotational

phase for the magnetic Ap star 49 Cam. The observations have a signal-to-noise ratio of approximately 200 to 300. While marginal evidence for circular polarization is seen in Stokes V for the line at 5018 Å there is no significant polarization in this line in Stokes Q and U.

The LSD technique was developed as a solution to this problem, with the thought that although no signal may be evident above the noise level in the polarization profile associated with any single line, profiles for *many* lines could be used to compute a coherent average, while greatly increasing the signal-to-noise ratio. The main assumption in LSD is that all of the polarization profiles in a stellar spectrum, for a single Stokes parameter, are similar. That is, we assume at a given phase, an individual Stokes profile corresponding to a spectral line may be described by a single mean Stokes profile, located at the wavelength of the line and scaled by a factor which depends on the properties of the line. The mean Stokes profile depends on the properties of the star (e.g. magnetic field, $v \sin i$) and the scaling factor depends, as will be shown, on the Landé factor, the wavelength and the depth of the line.

It follows then that an entire polarized spectrum is approximately a convolution of the mean Stokes profile with a function that describes the location and the scaling factor associated with each line. The task of the LSD technique is to extract the mean Stokes profile, since it contains the information about the properties of the star. The mean Stokes profile is deconvolved from the stellar spectrum by searching for the least-squares solution which satisfies the stellar spectrum.

To illustrate the usefulness of the LSD technique, average LSD extracted profiles for 49 Cam, in all four Stokes parameters, are shown in Fig. 5.2. The improvement in signal-to-noise ratio, as well as detectability of linear polarization, is apparent when Fig. 5.2 is compared to Fig. 5.1.

5.1.2 Theory

Following Donati et al (1997) and Wade et al. (2000a), the principles of the Least-Squares Deconvolution theory are as follows. A star is assumed to have any arbitrary magnetic field distribution on its surface. The typical magnetic $(\pi - \sigma)$ splitting of an individual spectral line is Eq. (2.7)

$$\Delta\lambda_B = 4.67 \times 10^{-13} \bar{g} B \lambda^2 \tag{5.1}$$

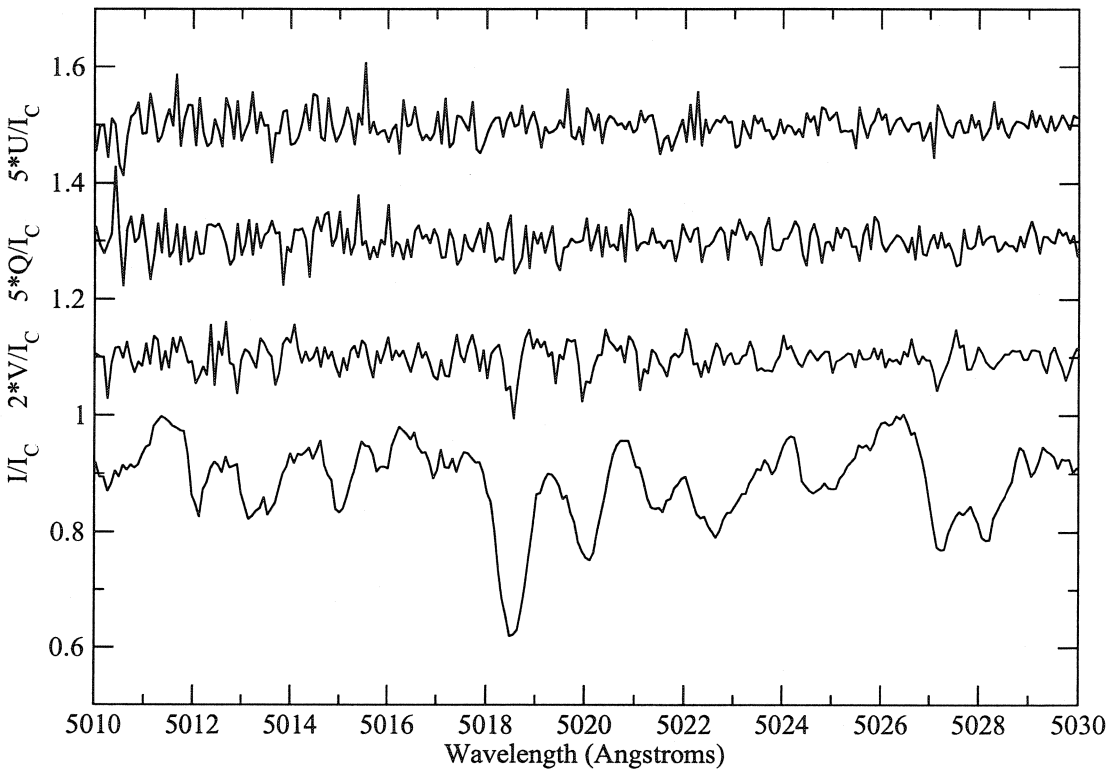

Figure 5.1: Observations of the spectral region surrounding the Fe II 5018 Å for the magnetic Ap star, 49 Cam, in all four Stokes parameters. V, Q and U have been shifted upward respectively by 1.1, 1.3 and 1.5. V has been expanded by a factor of 2 and Q and U have been expanded by a factor of 5. Observations were made with the MuSiCoS spectropolarimeter on Feb 4, 1998.

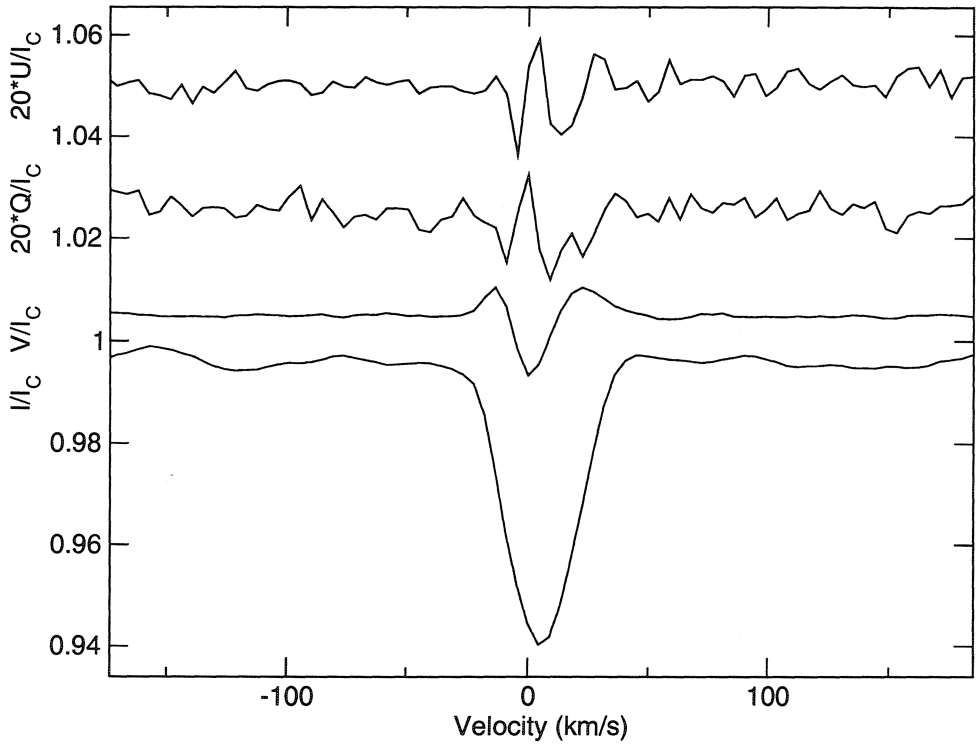

Figure 5.2: LSD-extracted polarization profiles for the magnetic Ap star 49 Cam, in all four Stokes parameters. V, Q and U have been shifted upward respectively by 1.005, 1.03 and 1.05, and Q and U have been multiplied by a factor of 20. Observations were made with the MuSiCoS spectropolarimeter on Feb 4, 1998.

where B is in gauss and wavelength in Å. The thermal motion of absorbers in the stellar photosphere contribute to the Doppler width of the line which is

$$\Delta v_D = \left(\frac{2kT}{m}\right)^{\frac{1}{2}}, \tag{5.2}$$

where k is the Boltzmann constant, T is the photospheric temperature and m is the mass of the atom. For iron-peak elements at typical photospheric temperatures for Ap stars, $\Delta v_D = 2 - 3$ km s^{-1}. When the magnetic splitting is much smaller than the Doppler width one is working in the weak-field regime which is satisfied at optical wavelengths for magnetic field strengths $B \leq 1$ kG and is the regime for which we introduce the LSD theory. Please note that the formalism below is only completely valid in the weak-field regime and becomes an approximation as local field strengths increase. This means that the choice of using LSD circular polarization profiles to search for *weak* fields in stars, as will be done in Chapter 6, is a reasonable one. It also means that using LSD profiles to model fields in *strongly* magnetic stars, as will be discussed in Chapter 7, means that the formalism may break down.

In the weak-field regime, the Stokes V profile in the local spectrum emitted from a point on the stellar disk may be determined by examining Fig. 5.3. The difference in intensity between the profile in left circularly polarized light and that in right circularly polarized light, as shown in the figure, is $2\Delta\lambda\ \partial I/\partial\lambda$. This allows one to determine the previous result from Eq. (2.8)

$$V/I = \frac{I_L - I_R}{I_L + I_R} = \frac{I(\lambda) + 2\Delta\lambda\ \partial I/\partial\lambda - I(\lambda)}{I(\lambda) + 2\Delta\lambda\ \partial I/\partial\lambda + I(\lambda)}. \tag{5.3}$$

Since $\Delta\lambda\ \partial I/\partial\lambda$ is small compared to $I(\lambda)$, Eq. (5.3) reduces to

$$V/I \cong \Delta\lambda \frac{1}{I}\frac{\partial I}{\partial\lambda}. \tag{5.4}$$

The local V profile may be re-written in velocity units using Eqs. (5.1) and (5.4), where the velocity unit v is defined as $c(\lambda - \lambda_\circ)/\lambda$, where $\lambda_\circ$ is the reference wavelength, usually the spectral line's laboratory wavelength. The resulting approximate profile (valid since $\lambda - \lambda_\circ$ is very small compared to λ) is

$$V_{\rm loc} \approx 1.4 \times 10^{-7} g\lambda B_z \frac{\partial I_{\rm loc}(v)}{\partial v} \tag{5.5}$$

where B_z is the longitudinal component of the local magnetic field in gauss, v is in km s^{-1}, and $I_{\rm loc}$ is the local Stokes I, or unpolarized, line profile. Assuming all line profiles have similar shapes in the local spectrum and that each profile is simply scaled

by the local line central depth, d, then the dependence on the partial derivative of $I_{\rm loc}$ may be simplified to a linear dependence on d (i.e. $\partial I_{\rm loc}/\partial\lambda \sim d/v_D$). Eq. (5.5) can be re-written as

$$V_{\rm loc} = k_B(v) g \lambda d \tag{5.6}$$

where the factor $k_B(v) = 1.4 \times 10^{-7} B_z$, multiplied by a factor ($\sim 1/v_D$) which accounts for the approximate shape and width of the local line profile in velocity units. Because the lines are assumed to be similar, $k_B(v)$ contains no information about the specific line.

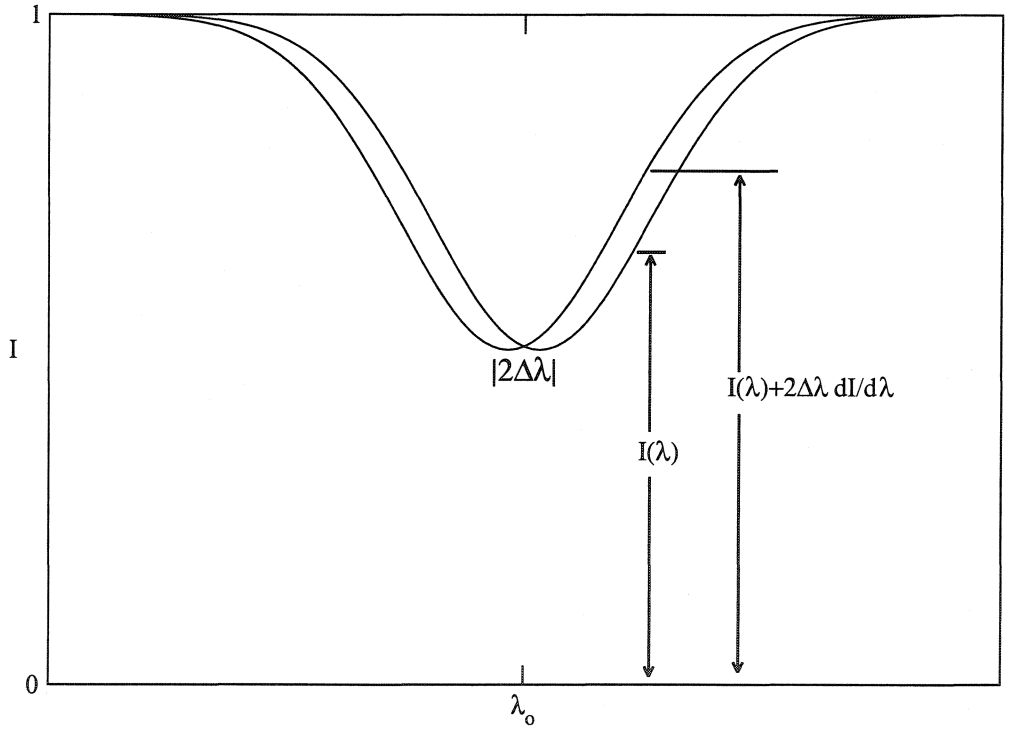

Figure 5.3: Change in depth of an absorption line when viewed in right and left circularly polarized light. From Landstreet (1980).

In order to compute the Stokes V profile observed from the entire stellar disk, one must integrate over the visible portion of the rotating star. This is done be integrating

over all points M of brightness b_M (since the disk is not of uniform brightness, due to limb-darkening) and radial velocity v_M (since the star is rotating) to obtain,

$$V(v) = \int\int b_M V_{\rm loc}(v - v_M) {\rm d}S \tag{5.7}$$

$$= g\lambda d \int\int b_M k_B(v - v_M) {\rm d}S \tag{5.8}$$

$$= w_V Z_V(v). \tag{5.9}$$

Assuming that the limb-darkening is not dependent on wavelength, then the integral, $Z_V(v)$ is constant for all lines, and can be referred to as the mean Stokes V Zeeman signature or LSD profile. Any Stokes V line profile is then the mean Zeeman signature scaled by $w_V = g\lambda d$. A example of $Z_V(v)$ for a magnetic Ap star, 49 Cam, may be seen in Fig. 5.2.

The above formalism may be extended to linear (Stokes Q and U) polarization profiles in a similar fashion. Using a second-order Taylor expansion of an expression for Stokes Q, as shown by Wade et al. (2000a), one obtains

$$Q_{\rm loc}(v) \simeq \Delta v_B^2 \frac{\partial^2 I_{\rm loc}(v)}{\partial v^2} \propto g^2\lambda^2 \; B_{\rm T}^2 \frac{\partial^2 I_{\rm loc}(v)}{\partial v^2} \tag{5.10}$$

where $B_{\rm T}$ is the transverse component of local field. Eq. (5.10) is analogous to Eq. (5.5) which describes $V_{\rm loc}$, and the same analysis and disk integration as above results in

$$Q(v) = w_Q Z_Q(v) \tag{5.11}$$

where $Z_Q(v)$ is the mean Stokes Q Zeeman signature and $w_Q = g^2\lambda^2 d$. The result may be extended to Stokes U profiles, which have the same weighting factor, $w_U = g^2\lambda^2 d$. The validity of this procedure, as well as testing of the assumptions made here, will be discussed further in Chapter 7.

In order to determine the mean Zeeman signature from a polarized spectrum, we first define a line pattern or line mask function $M(v)$

$$M(v) = \sum_i w_i \delta(v - v_i), \tag{5.12}$$

where w_i and v_i are the weight and position in velocity space of spectral line i, and δ is the Dirac delta function. A polarized spectrum (e.g., Stokes V) is then the convolution of the mean Zeeman signature with the line mask function ($V = M * Z$), and the least-squares deconvolution process (see Donati et al. (1997) for details) returns the best-fit mean polarization profile, Z.

The operation of LSD on a reduced polarized stellar spectrum is essentially an automated task performed by the user after running ESpRIT to reduce a series of spectra (see Chapter 3). The user inputs the spectrum name, the LSD line mask to be used, and an output file name as command line arguments of the LSD **add** function. The LSD program (also written by J.-F. Donati and installed at UWO by the authour as described in Section 3.1.2) then performs the deconvolution and returns the mean Zeeman signature for the spectrum.

5.1.3 LSD error bars

Each CCD pixel in a data frame has an error bar associated with it, calculated by ESpRIT from photon counting statistics. The error bars are propagated through the data reduction steps so that each point in a reduced polarization spectrum has a unique error estimate. In the LSD averaging process, these error bars are then used to assign uncertainties to each point in the final polarization profiles. Once an average profile is determined, it may be used to determine the "calculated" polarization spectrum, by simply reversing the steps and multiplying the LSD profile by the line mask function, M. When this is done, the difference between "observed" and "calculated" spectra, or $O - C$ residuals, may show that the error bars determined from propagating photon errors are not appropriate. In other words, the size of the $O - C$ residuals may be larger than the error-bars in the spectra. In practice, this occurs when polarization signatures in individual lines greatly exceed the local photon noise, which allows one to detect the fact that the weak line and weak field assumptions inherent in LSD are only approximations, and that the convolution description of the model spectrum is poor.

To compensate for this inappropriate description of the uncertainty, the LSD error bars are scaled by a factor equal to the square root of the $O - C$ reduced χ^2, when the reduced χ^2 is greater than one. This usually occurs in Stokes V profiles for magnetic stars where polarization signatures are large, and not for linear polarization signatures or for non-magnetic stars. The final error bars are propagated through the calculation of longitudinal fields from LSD Stokes V profiles to provide field measurement uncertainties, as discussed in Section 5.3.

5.2 Customizing LSD

5.2.1 Generating LSD line masks

The line mask function, $M(v)$ in Eq. (5.12), is the sum of a set of delta functions, located at the wavelengths of the lines in the spectrum, scaled by the appropriate weight for each line. In practice, this function is calculated from a text file that includes the wavelength, Landé factor and depth of all the lines in the stellar spectrum. The weights are calculated automatically from g, λ, and d as appropriate for either circular or linear polarization profiles.

The line masks were created using line lists from the Vienna Atomic Line Database (VALD) (Kupka et al. 1999, Ryabchikova et al. 1998), which is an online database containing data for atomic spectral lines of astronomical interest. The catalogued data include wavelengths, excitation potentials, $\log(gf)$ values, damping parameters, Landé factors, atomic level term information and upper and lower quantum numbers J for lines of interest. VALD's *extract stellar* interface allows one to submit upper and lower wavelength limits, stellar effective temperature and surface gravity and abundances for elements in the star, and the database returns the atomic data for all lines that occur between the wavelength limits and satisfy a minimum central depth criterion, where depth is calculated at zero rotation velocity. In generating the linelist, VALD makes a calculation of the central depth of each line using an appropriate stellar atmosphere model from the set of models available from the Kurucz CDROM, June 23, 1993 edition. The depth criterion in the line request is expressed as a percentage of the continuum, so that selecting 5% as a criterion will cause VALD to return all lines whose central depths are as deep as 5% of the continuum and deeper. The listing of λ, g and d allows the LSD program to calculate the weights and positions for all the lines in a spectrum, which *is* the line mask, and one need only ensure that the stellar parameters are correct and that the line data are extracted correctly from the VALD lists.

The abundance analyses of Adelman et al. (1997) and Adelman (1996) were examined to provide abundance tables for the Am stars as a function of effective temperature. Two characteristic abundance tables for Am stars were used; one for the hot Am stars (9000K – 10000K) and one for the cooler Am stars ($T_{\rm eff} \leq$ 8500K). The abundance tables reported by Adelman (1992) were used to provide average HgMn star abundances as a function of effective temperature, since almost all of the HgMn stars observed in our survey have been studied by Adelman. Characteristic

abundance tables for HgMn stars having effective temperatures of 10000K, 11000K, 12000K, 13000K and 14000K were taken from that work. A characteristic λ Boo type abundance table was adopted from Stürenburg (1993). An Ap SrCrEu abundance table was created by increasing the abundance of metals to 10$\times$ solar, except for chromium which was increased to 100$\times$ solar. The Ap SrCrEu abundance table was chosen to match that adopted in LSD linemasks used in previous magnetic field studies (Wade et al. 2000a, 2000b). All other line atlases were computed with solar abundances which are the default for the VALD database. The actual abundance used for each line mask is given in Appendix C.

The line mask used for the analysis of an individual observation is given in Table 6.1, where the prefix (Am, HgMn, λ Boo, slr [= solar], or Ap) denotes the abundance table used, the numerical portion indicates the effective temperature used in thousands of degrees, and the suffix Ib indicates that the surface gravity used was appropriate for a supergiant star.

In the cases where Landé factors, g, were available from VALD for spectral lines, they were adopted for line masks. Otherwise, except for the case of neon, values of g were calculated in LS coupling from the quantum numbers S and L as determined from the term information corresponding to each transition as provided in the VALD linelists, and J given explicitly in the VALD linelists. The extraction of the S and L quantum numbers from VALD linelists was complicated by the fact that the term information is not given in a consistent format. A VALD list includes two text lines for any single spectral line. The relevant parts of the first line of text are the chemical species, wavelength, J quantum numbers, and Landé factors. The second line of text contains the term information for each transition (e.g. ^2D - ^2F), from which the quantum numbers S and L may be calculated in LS coupling, but the format of this line of text may change from element to element, from ionization state to ionization state for a given element, and occasionally just for some lines. For example, the term information describing the transition which forms the Ti II line at 4636Å is in a different format in VALD linelists than for any other titanium line.

A FORTRAN program, written by G. Wade for converting VALD line lists to input files for another purpose, was customized by the author for using VALD lists to create LSD line masks. The program needed to explicitly include different formats for reading in the term information based on the chemical species, and even then the output line masks were examined individually and edited to account for the occasional differences in data formats which would result in S and L quantum numbers being improperly determined and thus incorrect Landé factors being assigned. Landé factors

Table 5.1: Details of the LSD line masks created by the author. The temperature is given as the numerical portion of the line mask name, in thousands of degrees. Abundance references: 1. Adelman et al. (1997) and Adelman (1996), 2. Adelman (1992), 3. Stürenburg (1993), 4. metals 10× solar, Cr 100× solar, 5. VALD solar

LSD Line mask	$\log g$	Number of lines	Abund. Ref.	LSD Line mask	$\log g$	Number of lines	Abund. Ref.
Am10.0	4.0	570	1	slr26	4.0	214	5
Am9.5	4.0	754		slr20	4.0	189	
Am9.0	4.0	1054		slr17	4.0	210	
Am8.5	4.0	1561		slr16	4.0	187	
Am8.0	4.0	2202		slr15	4.0	268	
Am7.5	4.0	2793		slr12.5	3.5	360	
Am7.0	4.0	3000		slr10	4.0	402	
HgMn14	4.0	390	2	slr10Ib	2.0	603	
HgMn13	4.0	429		slr9.0	4.0	768	
HgMn12	4.0	267		slr8.5	4.0	1076	
HgMn11	4.0	429		slr8.0	4.0	1525	
HgMn10	4.0	390		slr7.5	4.0	1967	
λ Boo9	4.0	168	3	slr7.0	4.0	2084	
Ap9	4.0	2996	4	slr6.5	4.0	2834	
Ap10	4.0	1957		slr6.25Ib	2.0	3156	
Ap11	4.0	1585		slr6.0	4.0	3114	

$g \geq 3$ (which would be unusual) were noted and re-calculated by hand to ensure that they were correct. In doing so, a number of lines were found that were not being read properly from VALD lists, which therefore did not have correct Landé factors, such as the Ti II line at 4636Å, so a list of recurring problem lines was compiled. This list, with Landé factors calculated by hand, was used to edit each LSD line mask as it was generated. Problem lines included some lines of C I, N II , O I, O II, S I, S II, and Fe I.

Landé factors for neon energy levels, for which LS coupling is a poor approximation, were taken from Moore (1949) where available, and the rest were calculated in pair coupling according to a procedure described by Sigut (1999). While the departure from LS coupling may be important for some individual lines, we do not expect this to significantly degrade our linelists for LSD profile extraction. Most lines in our linelists (85-90%) have experimentally determined Landé factors, or factors calculated from detailed wave-functions, in the VALD database and the inclusion of hundreds of lines in each linelist diminishes the effect which departures from LS coupling in a few lines may have.

5.2.2 Depth tests

VALD linelists were requested to include all lines in the MuSiCoS spectral range with depths greater than 5% of the continuum. Several linelists were then tested to ascertain the cut-off in line depth that optimizes the S/N of the LSD extracted profiles. Initially, it was assumed that including weak lines would serve to dilute the profiles, since the average would then be computed by including many extremely noisy lines. Using LSD linelists with cut-off depths of 5%, 10%, 20%, 30% and 40%, we extracted LSD Stokes V profiles for a number of the Am and HgMn stars. When compared, it was seen that the LSD Stokes V profiles did not differ greatly as the depth cut-off criterion was changed. Since the contribution of each line to the average line profile is weighted by line depth, the shape of the profiles examined were essentially determined by the strongest lines. The noise outside the lines, however, did decrease as more weak lines were used to extract the average, i.e. the linelist was cut off at a smaller depth. In some cases, the noise reached a minimum when linelists cut off at 10% were used, while for others, using lines down to 5% seemed to reduce the noise even farther. In all cases, the decrease in noise level between 10% and 5% was minimal. An example is shown in Fig. 5.4, which is a section of the Stokes V profile of the A2m star HD 60178. The figure shows part of the profile which is outside the

extent of the spectral line, and thus is a reflection of the noise level. The colours of the lines indicate the depth cut-off in the the line masks used to calculate the LSD profiles. As may be seen in Fig. 5.4, the yellow, green and blue profiles, corresponding to depth cut-offs of 40%, 30% and 20%, generally decrease in amplitude while the red and black lines (10% and 5%) are smaller still in amplitude, but quite similar to one another. This behaviour is typical for LSD profiles of the stars tested. Because of this behaviours, all linelists were cut off to include lines deeper that 10% of the continuum.

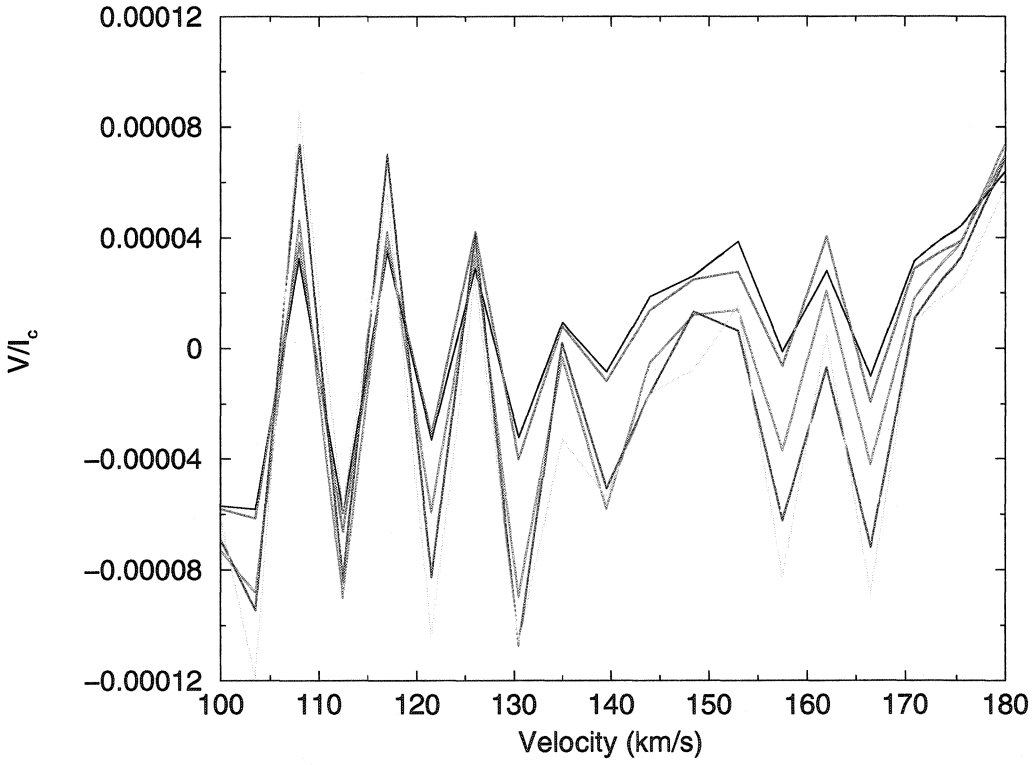

Figure 5.4: Noise levels in Stokes V profiles of HD 60178 generated using line masks with different depth criterion cut-offs. Key is: Black–5%, Red–10%, Green–20%, Blue–30%, Yellow–40%.

5.3 Field measurements

In order to use LSD extracted Stokes profiles to measure the longitudinal field, Wade et al. (2000b) employed a useful form of Eq. (5.4), following Mathys (1989) and

Donati et al. (1997). They changed from wavelength units to velocity units, used the expression for $\Delta\lambda$ from Eq. (5.1), then inverted and integrated over v to solve for B_z in gauss as

$$B_z = -2.14 \times 10^{11} \frac{\int vV(v)\mathrm{d}v}{g\lambda c \int [I_c - I(v)]\mathrm{d}v}. \tag{5.13}$$

Since this value for B_z is based upon the LSD mean Stokes profile, g and λ in Eq. (5.13) are the mean Landé factor and mean wavelength of the lines in the line mask used to calculate the mean profile.

The limits of integration in Eq. (5.13) are chosen visually such that they just include the entire extent of the spectral line in the Stokes I (unpolarized) LSD profile. The integration and calculation is performed by a program written by Donati. The user is responsible for supplying the values of g and λ (the mean Landé factor and wavelength of the lines used in the average) which are output from the LSD extraction process. The calculation of B_z provides both the value of and the uncertainty in the field measurement, which is obtained by propagating the photon counting errors in each original CCD pixel through the reduction of the spectra, the LSD averaging and the field calculation.

References

Adelman, S. J. 1992, MNRAS, 258, 167

Adelman, S. J. 1996, MNRAS, 280, 130

Adelman, S. J., Caliskan, H., Kocer, D., & Bolcal, C. 1997, MNRAS, 288, 470

Donati, J.-F., Semel, M., Carter, B. D., Rees, D. E., & Collier Cameron, A. 1997, MNRAS, 291, 658

Kupka, F., Piskunov, N. E., Ryabchikova, T. A., Stempels, H. C., & Weiss, W. W. 1999, A&AS, 138, 119

Mathys, G. 1989, Fund. Cosmic Phys. 13, 143

Moore, C. E. 1949, Atomic Energy Levels, Vol. 1 (NBS Circ. 467; Washington DC: GPO)

Ryabchikova, T. A., Piskunov, N. E., Stempels, H.,C., Kupka, F., & Weiss, W. W. 1998, Proc. of the 6th International Colloquium on Atomic Spectra and Oscillator Strengths, Victoria BC, Canada , Physica Scripta, T83, 162

Sigut, T. A. A. 1999, ApJ, 519, 303

Stürenburg, S. 1993, A&A, 277, 139

Wade, G. A., Donati, J.-F., Landstreet, J. D., & Shorlin, S. L. S. 2000a, MNRAS, 313, 823

Wade, G. A., Donati, J.-F., Landstreet, J. D., & Shorlin, S. L. S. 2000b, MNRAS, 313, 851

Chapter 6

Field survey [1]

6.1 Introduction

Preston's (1974) classification of the chemically peculiar A and B type stars into magnetic and non-magnetic subtypes has generally been found to be valid. The existence of strong, ordered magnetic fields in many Ap SrCrEu, Ap Si, He-weak Si and SrTi, and He-strong stars, and the lack of detectable fields among the Ap HgMn, Am, He-weak PGa and λ Boo stars (Conti 1969; Borra & Landstreet 1980; Landstreet 1982; Borra et al. 1983; Bohlender & Landstreet 1990) appears to be a real (and important) physical property distinguishing the two classes. This is strongly supported by the fact that neither the Am stars, the Ap HgMn stars, nor the He-weak PGa exhibit *any* of the phenomenology associated with magnetic stars on the upper (or the lower) main sequence. As mentioned in Section 1.1.2, they do not show the photometric or line profile variability common among the magnetic upper main sequence stars (although isolated reports of such behaviour do exist; see for example Rao et al. 1990, Adelman et al. 2002) , nor do they exhibit resonance line emission, X-ray emission, or photometric variability (attributed to spottedness) accepted as indicators of magnetism among the late-type stars.

However, a number of studies published within the past decade indicate that perhaps the situation is not quite so clear-cut as was originally suggested. In particular, apparently significant detections of strong, complex magnetic fields in the Am stars o Peg (HD 214994) (Mathys 1988; Mathys & Lanz 1990) and 15 Vul (HD 189849) (Bikmaev et al. 1998), and in the Ap HgMn stars χ Lup (HD 141556) and 74 Aqr (HD 214694) (Mathys & Hubrig 1995) have been made using an effect that depends on

[1] A version of this chapter has been published as "A highly sensitive search for magnetic fields in B, A and F stars", Astronomy & Astrophysics, 392, 637

the star's magnetic field modulus and not, for example, the line-of-sight component of the field. In the presence of a magnetic field, a strong line may have its intrinsic line profile broadened in a way that depends on its Zeeman pattern, thereby increasing its equivalent width. Differences in magnetic sensitivity between otherwise identical lines provide the diagnostic which allows for a detection of a field. Such detections suggest that magnetic fields may exist in at least *some* classical non-magnetic stars and are perhaps more like those of active FGKM stars than those of the well-known magnetic A and B stars. Furthermore, reported probable detections of magnetic fields in two of three Am stars studied by Lanz & Mathys (1993; HD 29173 and HD 195479A) may indicate that similar magnetic fields exist in *most* classical non-magnetic stars, or at least in the Am stars. Confirmation of this possibility would profoundly modify our understanding of stellar atmosphere physics in this area of the HR diagram. It would provide important new constraints on the mechanisms responsible for magnetism in the early-type stars, as well as on the physical processes responsible for the chemical peculiarities observed to some degree in almost *all* A-type stars.

Finally, in order to solve the problem of the origins of magnetic fields in the mid to upper-main sequence, one must understand what the problem really is. Do 5% of A stars have large-scale ordered fields, as we have assumed in the past, while the others are non-magnetic, or do some or all of the others have magnetic fields, but magnetic fields that are of a different nature than those in the classical magnetic Ap stars? The two cases are very different, and one cannot expect to address the problem of field origins and evolution without determining which best describes the true situation. For all these reasons we have carried out a large programme to search for magnetic fields in all kinds of B, A, and F stars.

6.2 Detection of stellar magnetic fields

The classical method for detecting stellar magnetic fields in the mid to upper main sequence, as outlined in Section 2.2.2, has been the detection of circular polarization in spectral lines due to the line-of-sight component of a star's magnetic field. The quantity inferred from the spectropolarimetric observations is the line-intensity weighted average over the stellar disk of the line-of-sight component of the magnetic field, the longitudinal field or effective field discussed in Section 2.2.2. Stars that have detectable longitudinal magnetic fields exhibit the chemical peculiarities we now associate with magnetic Ap stars, and they nearly always exhibit photometric and/or line

profile variation with the same period as the variation in longitudinal field. Stars that show chemical peculiarities typical of magnetic Ap stars and/or periodic photometric and line profile variations, but for which no longitudinal fields have been detected, are usually assumed to have fields smaller than the current observational errors.

Conversely, no longitudinal magnetic fields have been convincingly detected for the "non-magnetic" chemically peculiar stars, or normal middle main sequence stars. The upper limits on longitudinal field strengths have typically been of the order of 100 G (Borra & Landstreet 1980). If recent observations of non-magnetic peculiar stars, which have implied mean field moduli of several kilogauss, are correct, then longitudinal field measurements with precisions better than 100 G do put some constraint on the complexity of the stars' global field structures. Improving the precision of longitudinal field measurement, however, could perhaps make possible the detection of a weak net longitudinal component, or more tightly constrain the topology of a possible complex field.

Since the complex magnetic fields reported may be similar to those observed in cool active stars, the use of a field detection method that works well for active stars is appropriate. To this end, we have employed the cross-correlation technique Least-Squares Deconvolution (LSD; Donati et al. 1997, see Section 5.1) to analyze circularly polarized spectra of non-magnetic stars mostly having significant rotation velocity. LSD takes advantage of the similar shapes of spectral lines and their associated polarization features in order to obtain large improvements in the signal-to-noise ratios (S/N) of Stokes V profiles by using the information contained in all of the lines in the stellar spectrum. Donati et al. (1997) have employed LSD to detect the very weak circularly polarized (Stokes V) signatures in the spectral lines of a number of active late-type stars. The disk-integrated magnetic field strength reported for o Peg is of the order of that deduced by Donati (1999) for the cool active star HR 1099. We expect that this technique should therefore be very effective for detecting such complex fields. In Fig. 6.1 we show illustrative LSD mean Stokes I) and V signatures for the RS CVn binary HR 1099 (Donati 1999). The peak-to-peak amplitude of the LSD Stokes V signal is about 0.1%, and this signal is clearly detected in the LSD spectrum which has a S/N of 9100:1. Zeeman-Doppler imaging of the parent magnetic field configuration (Donati 1999) shows that the Stokes V morphology and modulation of HR 1099 imply a very complex surface magnetic field with a brightness-weighted unsigned averaged longitudinal field strength over the surface of about 200 G.

Wade et al. (2000) used LSD extracted Stokes V profiles to measure longitudinal fields of magnetic Ap stars, and typically improved the standard errors of field

measurements by a factor of five to ten over previous work. This improvement in precision is expected to allow us to greatly improve on upper limits for longitudinal fields of the non-magnetic stars.

A strong motivation for this study is our concern that the methods that have been used recently to detect magnetic fields in the canonically non-magnetic chemically peculiar stars are ambiguous, since they employ the subtle effects of magnetic intensification in spectral lines (often a single pair of lines) as their magnetic diagnostic. As pointed out by Hubrig & Castelli (2001), uncertainties in atomic physics, as well as possible unrecognized blends, cause these methods of detection to be somewhat uncertain themselves. Although we are unable to use our observations to make similar measurements of mean field moduli for B, A, and F stars, because of the limited resolution of our spectra, we are able to provide very precise circular polarization profiles.

Another motivation for this study is as a test of the performance of the LSD technique at detecting magnetic fields in a varied population of stars. Previously, work with LSD has been concentrated on relatively well-studied magnetic Ap stars and on cool active stars. Our use of LSD for the study of magnetic fields in stars with a range of chemical peculiarities, rotation velocities, temperatures and gravities allows us to determine where our technique is most applicable, as well as where it may be limited.

6.3 Observations

Stokes V and Stokes I spectra of 25 Am stars, 10 HgMn stars, two λ Boo stars, 22 normal stars, 11 stars of "magnetic" Ap peculiarities (Ap SrCrEu, Ap Si), and four emission-line stars were obtained using the MuSiCoS échelle spectropolarimeter attached the 2 m Bernard Lyot telescope at l'Observatoire du Pic du Midi, during four runs between Feb. 1997 and March 2000. The specifications of the MuSiCoS spectropolarimeter and observing procedures are detailed in Sections 2.3.1 and 4.3. The échelle polarization spectra were reduced and extracted using the ESPRIT reduction package (see Section 3.1) (Donati et al. 1997).

6.3.1 Survey candidates

Details of the criteria for selecting survey candidates are discussed in Section 4.2. Am, HgMn, λ Boo, normal, Ap SrCrEu Si and emission-line stars were chosen covering

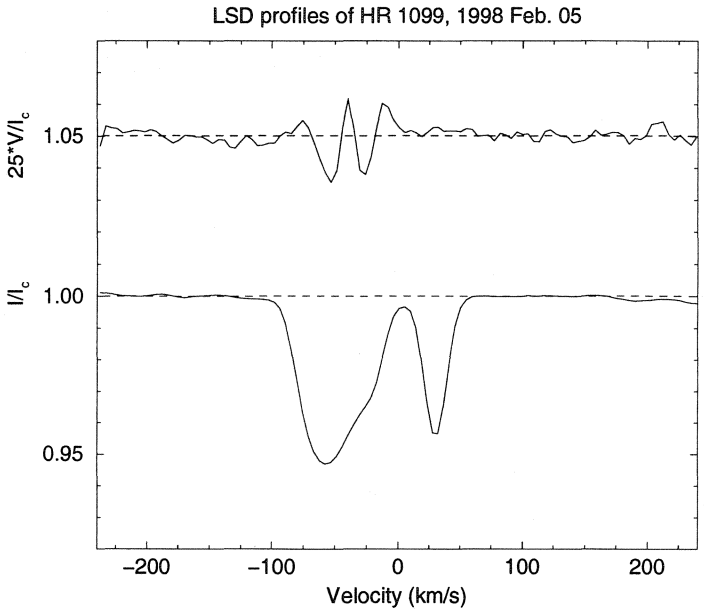

Figure 6.1: LSD mean Stokes I (bottom) and V (top) profiles of the active RS CVn binary HR 1099. A strong ($\sim 0.1\%$ peak-to-peak amplitude) Stokes V signature is clearly detected, associated with the more rapidly rotating component. Note that, for display purposes, the Stokes V profile has been expanded by a factor of 25 and shifted upward by 1.05.

the main sequence from early B to late F spectral types, and also including giant and supergiant stars. Specifically included in the survey were HD 29173, HD 27295, HD 112412 (α^1 CVn), HD 195479, and HD 214994 (o Peg). HD 112412 is an Am star reported by Babcock (1967) to be probably magnetic. The Am stars HD 29173 and HD 195479A (the primary component of the spectroscopic binary HD 195479) are reported by Lanz & Mathys (1993) as "...likely to possess...a magnetic field of about the same strength (as that of o Peg)". The Am star HD 214994 was reported by Mathys and Lanz (1990) to be compatible with a 2 kG magnetic field. Hubrig & Castelli (2001) include HD 27295 in a list of HgMn stars likely to be magnetic.

We obtained multiple observations for several stars. HD 48915 (Sirius), HD 77350, HD 78362, HD 108642, and HD 110951 were each observed twice, with observations a year apart, while HD 126661 was observed twice in two years. HD 141795 was observed three times over a period of 12 days in 1998, while HD 73709, HD 87737, HD 110379, HD 116656, and HD 129174 were each observed twice in the same year, with observations anywhere from five to thirty-three days apart. These multiple observations were made to allow for a simple search for any temporal variability (perhaps due to rotational modulation) of a magnetic signal. The journal of the stellar observations is presented in Table 6.1.

Table 6.1: Journal of observations. See notes at end.

HD No.	Spectral Type	m_V	$T_{\rm eff}$ (K)	$\log g$	$v \sin i$ (km s^{-1})	$v_{\rm rad}$ (km s^{-1})	HJD 2,440,000+	Exp (s)	S/N	LSD mask
					Am stars					
29173	A1m	6.7	9070	4.22	14 ± 1	15	11198.355	1440	170	Am9.0
48915	A1m;SB1	−1.5	9970	4.32	16.2 ± 0.6	−4	10502.371	120	1650	Am10.0
							10864.322	$240^{2\times}$	2090	
60178	A2Vm	2.9	9000	4.25	20 ± 1	2	11584.536	2400	1410	Am9.0
73709	F2III	7.7	8080	4.02	21.9 ± 0.5	25	11586.450	2400	90	Am8.0
							11611.476	2400	120	
78209	F3m	4.5	7690	4.25	38 ± 1	3	10854.447	1440	620	Am7.5
78362	F3m;SB1	4.7	7390	4.17	11.3 ± 0.5	−10	10858.601	1440	460	Am7.5
							11202.550	1600	490	
89021	A2IV	3.4	8980	3.67	50 ± 2	10	11579.681	2400	910	Am9.0
90277	F2m	4.7	7480	3.50	36 ± 2	18	10854.474	1440	440	Am7.5
95418	A1V	2.3	9630	3.87	45 ± 1	13	11577.692	2400	1460	Am9.5
95608	A3m	4.4	8840	4.11	18.3 ± 0.6	−11	11192.561	1440	350	Am9.0
97633	A2V	3.3	9290	3.64	23.5 ± 1.0	8 ± 2	11580.611	2400	1000	Am9.0
108642	A7m;SB2	6.5	8100	4.11	$< 10, < 10$	$34, -69^{\dagger}$	10851.636	2400	240	Am8.0
						$-15, +22^{\dagger}$	11197.710	2400	190	
108651	F2m	6.6	8100	4.36	23 ± 1	5	11204.684	1600	100	Am8.0
109485	A0IV	5.4	9430	3.72	18.6 ± 0.5	5	11601.637	2400	410	Am9.5
110380	F0V	3.6	7830	4.57	27 ± 1	−22	11587.639	2400	540	Am7.5
110951	F2m;SB2	5.2	7290	3.85	$19 \pm 3, 80 \pm 10$	$+15^{\dagger}$	10856.595	1440	380	Am7.0
							11201.674	1600	360	
112412	F3m	5.6	7010	4.36	18 ± 3		10859.724	1600	330	Am7.0
116657	A1m	4.0	9760	4.04	51*		11587.712	2400	210	Am8.5
125337	A2m:SB2	4.5	9560	3.90	< 10	$0^{\dagger}$	11603.675	2400	350	Am8.5
126661	F1m	5.4	7840	3.74	36 ± 2	−28	10856.680	1440	370	Am8.0
							11606.591	2400	220	

Table 6.1: **Continued.** Journal of observations. See notes at end.

HD number	Spectral Type	m_V	$T_{\rm eff}$ (K)	$\log g$	$v \sin i$ (km s^{-1})	$v_{\rm rad}$ (km s^{-1})	HJD 2,440,000+	Exp. (s)	S/N	LSD mask
					Am stars, continued					
141675	F3m;SB1	5.9	7910	4.11	33 ± 2	-3	10857.725	1440	250	Am7.5
141795	A7m	3.7	8450	4.20	33.5 ± 0.5	-11	10851.738	1200	590	Am8.5
							10861.723	$1200^{2\times}$	650	
							10862.726	$1200^{2\times}$	580	
159560	F0m;SB1	4.9	7460	4.15	42 ± 1	-23 ± 2	10859.695	1200	310	Am7.5
195479	F2m;SB1	6.2	8480	4.08	18.0 ± 0.6	-44	10860.738	1440	110	Am8.5
214994	A1III	4.8	9600	3.62	< 10	9	11193.291	1440	370	Am9.5
					Ap HgMn stars					
27295	B9HgMn	5.5	11970	4.23	< 10	4	11202.347	1440	320	HgMn12
63975	B8HgMn	5.1	13470	3.30	28 ± 3	32	11203.501	1600	250	HgMn13
75333	B9HgMn	5.3	12320	3.76	36 ± 3	30 ± 2	11202.516	2400	310	HgMn12
77350	B9SrCrHg	5.5	10320	3.61	19.0 ± 0.3	-15	11201.627	2000	250	HgMn10
							11602.601	2400	340	
78316	B8MnHg	5.2	13700	3.76	< 10	61	11192.609	1440	260	HgMn14
106625	B8gMn	2.6	12070	3.34	37 ± 4	-3	11578.678	2400	1000	HgMn12
129174	B9HgMn	4.9	13060	3.94	16.4 ± 0.8	-1	11193.712	1440	300	HgMn13
							11198.756	1440	430	
143807	A0pHg	5.0	10780	3.99	< 10	-23	11603.714	2400	370	HgMn11
144206	B9HgMn	4.7	12070	3.79	10.5 ± 0.5	3	11203.732	1440	350	HgMn12
145389	B9p:Mn	4.2	11090	4.01	10.9 ± 0.2	-19	11601.712	2400	450	HgMn11
					λ Boo stars					
110411	A0	4.9	8830	4.36	140*		11192.642	1440	280	λ Boo9
125162	A0p	4.2	8610	4.24	110*		11608.650	2400	680	λ Boo9

Table 6.1: **Continued.** Journal of observations. See notes at end.

HD number	Spectral Type	m_V	$T_{\rm eff}$ (K)	$\log g$	$v \sin i$ (km s^{-1})	$v_{\rm rad}$ (km s^{-1})	HJD 2,440,000+	Exp. (s)	S/N	LSD mask
					Normal stars					
20902	F5Ib	1.8	6250	2.10	20‡	$-1^{\dagger}$	11587.411	1600	1360	slr6.25Ib
24760	B0.5V	2.9	25700	3.75	155‡		11194.306	1200	630	slr26
41753	B3V	4.4	17180	3.76	40‡		11612.380	2400	250	slr17
61421	F5IV-V	0.3	6570	4.02	< 10	-3	11604.416	$480^{2\times}$	500	slr6.5
82328	F6IV	3.2	6360	4.08	10.5 ± 0.5	12	11600.577	2400	940	slr6.5
87737	A0Ib	3.5	10470	2.18	15 ± 2	1	11579.623	2400	880	slr10Ib
							11612.748	2400	960	
95382	A5III	5.0	8180	3.98	71*	-3	11608.537	2400	460	slr8.0
98353	A2Va:	4.8	8620	4.24	50‡		11586.488	2400	260	slr9.0
99028	F4IV	4.0	6670	3.82	17 ± 1	-12	11599.584	1440	510	slr6.5
104321	A5V	4.6	8080	3.51	61*		11608.572	2400	500	slr8.0
110379	F0V	3.6	6810	4.36	35 ± 1	-16	11587.608	2400	570	slr7.0
							11600.620	2400	850	
114710	F9.5V	4.3	6080	4.38	< 10	2	11599.608	1440	530	slr6.0
118216	F2IV	4.9	6540	3.46	16.4 ± 1.0	4	11599.633	1440	340	slr7.0
123299	A0IIISiCr	3.6	9950	3.62	28 ± 2	12	11599.706	1440	700	slr10
123999	F9IV	4.8	6220	3.99	$14 \pm 3, 12 \pm 3$	$54, -36^{\dagger}$	11603.640	2400	340	slr6.0
124850	F6III	4.1	6130	3.86	33 ± 1	12	11602.647	2400	700	slr6.0
126660	F7V	4.1	6370	4.35	30 ± 3	-10 ± 2	11580.691	2400	760	slr6.0
128167	F2V	4.5	6680	4.44	10 ± 1	2	11600.694	2400	540	slr7.0
144284	F8IV	4.0	6290	3.99	30‡	$17^{\dagger}$	11584.756	2400	670	slr6.0
147394	B5IV	3.9	14940	3.84	30‡		11579.726	2400	640	slr15
155763	B6III	3.2	12500	3.50	43 ± 2	-14 ± 2	11580.733	2400	930	slr12.5
160762	B3IV	3.8	17730	3.74	10‡	$-23^{\dagger}$	11606.673	2400	360	slr16

Table 6.1: **Continued.** Journal of observations. See notes at end.

HD number	Spectral Type	m_V	$T_{\rm eff}$ (K)	$\log g$	$v \sin i$ (km s^{-1})	$v_{\rm rad}$ (km s^{-1})	HJD 2,440,000+	Exp. (s)	S/N	LSD mask
Ap SrCrEu, Si stars										
60179	A1VSrEu	1.6	10000	4.0*	19 ± 1	1	11612.445	1200	1380	Ap10
74521	A1pEuCr	5.6	11720	3.47	10*	25†	11612.414	2400	370	Ap11
108662	A0pSrCrEu	5.2	11000	4.21	10*	-2†	11612.536	2400	430	Ap10
108945	A2pSr	5.4	8590	3.89	65*		11612.571	2400	390	Ap9
115735	A0VHewk.	5.2	10750	3.99	90*	10 ± 3	11600.658	2400	410	Ap10
116656	A1VpSrSi	2.3	9430	4.22	25*	24†, -18†	11578.717	2400	1460	Ap9
						-9†	11587.679	2400	1160	
120198	B9pEuCr	5.7	10460	3.81	45*	0†	11601.673	2400	210	Ap10
125248	A0pCrEu	5.8	10750	4.36	10*	-16†	11599.671	$1440^{2\times}$	200	Ap11
						-16†	11612.680	1440	240	
140160	A0	5.3	9220	4.16	65*		11606.630	2400	180	Ap9
148112	B9pCr	4.6	9440	3.69	35*		11602.688	2400	370	Ap9
148330	A2SiSr	5.7	9510	3.75	10.5 ± 0.5	-7	11599.730	1440	270	Ap9
Emission-line stars										
103287	A0Ve	2.4	9330	3.87	165*		11580.647	2400	1430	slr9.0
108844	A5δDel	5.4	7960	3.76	78*		11586.665	2400	360	Am8.0
109387	B6IIIpe	3.9	13920	1.76	230‡		11608.610	2400	880	
163472	B2IV-V	5.8	20350	3.65	120‡		11586.712	2400	170	slr20

Table 6.1 Notes: Am spectral types are the metallic-line spectral types by Abt & Morrell (1995). $T_{\rm eff}$ and $\log g$ are determined from Strömgren photometry. The projected rotation velocities in column 6 are measured here, except as noted by $*$ which are from Abt & Morrell (1995) and by ‡ which are from Uesugi & Fukuda (1985). The heliocentric radial velocities in column 7 are measured here and are ± 1 km s^{-1} except where noted. A second rotation or radial velocity corresponds to that of a secondary star. Radial velocities marked with † are estimated from LSD profiles. The peak S/N obtained in each échelle spectrum is listed in column 10. The superscript $2\times$ in "Exp." indicates that two identical observations were made in succession.

6.3.2 LSD linemasks

LSD mean signatures were computed using the technique described in Chapter 5. The linemask used during the least-squares deconvolution for each individual star was generated as outlined in Section 5.2.1, is described in Table 5.1 and is listed in Table 6.1 in column 11. The name of each linemask (e.g. Am10.0) has a prefix which

indicates the abundance table used to generate it and a numerical suffix which gives the temperature in multiples of 1000 K. See Section 5.2.1 for more details.

6.3.3 Stellar parameters

Stellar effective temperatures and surface gravities were determined primarily from Strömgren ($uvby\beta$) photometric data as compiled by Hauck & Mermilliod (1998). Photometry in the Strömgren system consists of measuring stellar magnitudes through filters at differing wavelengths (e.g. the u filter is centered at 3500 Å and is 300 Å wide). The differences between magnitudes are used to calculate colours (e.g. $(v-b)$, $(u-v)$) and several colour indices are defined (e.g. $c_o = (u-v)-(v-b)$). The β index is defined as the difference in two magnitudes measured in passbands centered on the Hβ Balmer line. The c_o and β indices are, respectively, sensitive to temperature and surface gravity to stars earlier than A0, and to surface gravity and temperature for those later than A0. Additional indices are calculated which resolve the ambiguity of the sensitivity of each index around spectral type A0. The calibration of Moon & Dworetsky (1985), which relates a grid of Strömgren indices to the temperatures and surface gravities of normal stars, was used to find the stellar parameters used here, with the following exceptions. The parameters for the hot star HD 41753 were taken from analysis by Castelli (1991) which uses an extension of the Moon & Dworetsky (1985) grid. HD 60178 and HD 60179 (α Gem A & B) did not have Strömgren photometry available individually, so estimates of their temperatures and surface gravities were taken from the analysis by Smith (1974). For the B6III star HD 155763, for which Strömgren photometry is unavailable, $(T_{\rm eff}, \log g)$ parameters were adopted from Adelman (1996).

As noted, the calibration of Moon & Dworetsky (1985) was determined for normal stars and its use for determining temperatures and surface gravities for chemically peculiar stars will introduce some error. But, even an error in temperature of 1000 K (which is large) would only change the LSD averaged profiles inasmuch as the line list used for the LSD averaging would be changed. Tests were performed on several stars in order to quantify the effect of using line lists corresponding to varying temperature, and the effect is minimal. In the Am star HD 29173, LSD averaged profiles were calculated using line masks for stars both 1000 K hotter and cooler that the 9000 K inferred from Strömgren photometry. Using the hotter and cooler line masks

resulted in profiles noisier by a factor of approximately 20%, but with no significant polarization in any profiles. The calculated longitudinal fields were non-detections with uncertainties in B_z differing by approximately 20%. In a magnetic star case, HD 74521, line masks 1000 K hotter and cooler than the 11000 K found for this star were used. The results were that the hotter and cooler masks resulted in profiles noisier by less than 10%, and the inferred longitudinal fields differed by less than 5% with uncertainties ranging from 17 to 21 G. Our conclusions are that temperatures should be determined as accurately as possible, but that errors in temperature do not preclude the use of LSD profiles for field detection or even accurate measurement in magnetic stars.

Values of $v \sin i$ and radial velocity were obtained where possible for stars in this study using the technique of comparison with synthesized spectral regions as outlined by Landstreet (1998). The details of the technique are found in that reference, and the spectrum synthesis code, ZEEMAN, is described by Landstreet (1988) and Landstreet et al. (1989). The code searches automatically for a synthesized spectrum that best fits the observed spectrum, by varying chemical abundance, $v \sin i$ and radial velocity. The code was run using the values of $T_{\rm eff}$ and $\log g$ given in Table 6.1, and at a constant microturbulent velocity, ξ. Microturbulence is a component of the total line-broadening caused by the non-thermal motion of absorbers in the atmosphere, and is characterized by the velocity, ξ, which accounts for Doppler-broadening of the line . The code was re-run while varying ξ, and the resulting best-fit abundances were plotted versus ξ in "Blackwell diagrams" for different lines of the same chemical species, namely for the Fe II $\lambda\lambda$ 4620, 4625, 4629 and 4635 lines and separately for the Cr II $\lambda\lambda$ 4616, 4618 and 4634 lines. In all cases for which $v \sin i$ and radial velocity have been obtained, the variation of determined abundance with microturbulent velocity for a given species converged at a common value of ξ. Values of $v \sin i$ and radial velocity from the best-fit synthesized spectra at that value of ξ were averaged to provide us with the values given in Table 6.1. An example of $v \sin i$ determination is shown in Appendix D.

Several stars have not had their rotation and radial velocities measured in this way, most often due to composite spectra or too high a rotation velocity, giving lines that are too broad for the small synthesis window used for the comparisons. In the cases of the magnetic Ap stars, it is necessary to model each star's magnetic field, as well as possible abundance variations across the stellar surface, in order to provide accurate

Table 6.2: Estimates of $v \sin i$ for some stars in this survey determined using the FWHM of Gaussian fits to their LSD line profiles and Equation (1).

Star	$v \sin i$ ($\mathrm{km\,s^{-1}}$)
HD 106625	37 ± 4
HD 108642 (secondary)	< 10
HD 110951	19 ± 3
HD 112412	18 ± 3
HD 123999 (primary)	14 ± 3
HD 123999 (secondary)	12 ± 3

estimates of $v \sin i$, since the abundance and field variations will shape the spectral lines. Since rotation velocity determinations were intended as a useful and quick side project, attempts were not made at such detailed modelling for the magnetic survey stars. In cases where stars had lines that could not be measured using the spectral synthesis comparison technique, radial velocities have been estimated from their position in LSD profiles. This is done mainly for spectroscopic binaries for which the primary was modelled by the synthesis code but the secondary was not.

Values of $v \sin i$ have also been estimated from a few LSD profiles using an approximate linear relationship between stellar rotation velocities and the full-width at half-maximum (FWHM) of Gaussian fits to their LSD Stokes I profiles. This relationship is shown in Fig. 6.2 and the linear regression solution is

$$v \sin i = (0.617 \pm 0.020) \times \mathrm{FWHM} + (0.86 \pm 0.61). \tag{6.1}$$

Using this relationship, we have obtained estimates of rotation velocities for several stars from their LSD profiles, as listed in Table 6.2. Uncertainties are estimated from the scatter of $v \sin i$ about the regression relation. Note that this relationship is not to be used to estimate low rotation velocities ($v \sin i < 10\ \mathrm{km\,s^{-1}}$), given the resolving power of the spectropolarimeter.

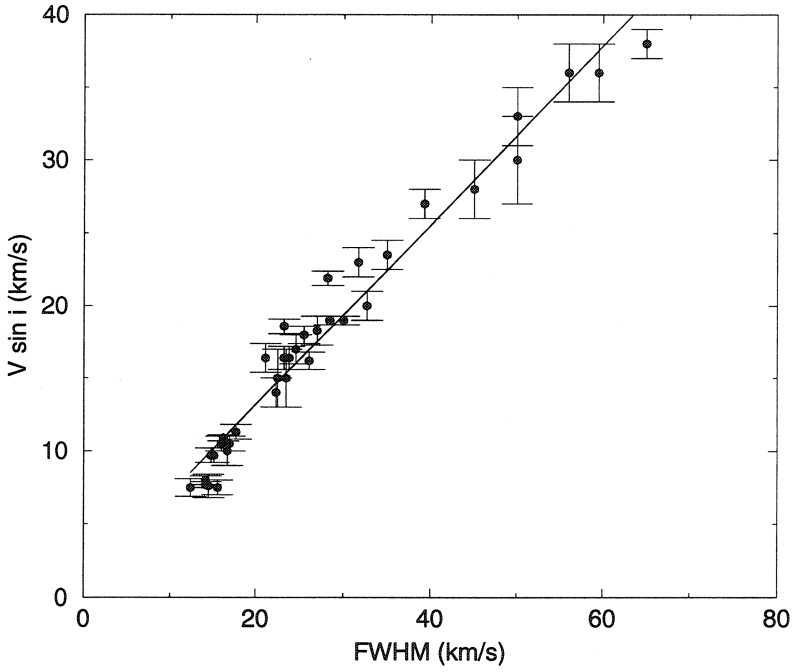

Figure 6.2: Relationship between $v \sin i$ as measured by spectral synthesis comparison and FWHM of Gaussian fits to LSD Stokes I profiles for stars in this survey

6.4 Results

In the survey of 63 Am, HgMn, λ Boo, normal and emission-line stars, during which multiple observations have been made of several stars, we find no significant circular polarization. Thus, we find no evidence that any of the survey stars are magnetic. The criterion for detection of polarization is the statistical test described by Donati et al. (1997) in which reduced χ^2 statistics are computed for the Stokes V profile inside and outside the spectral line. The test quantifies how much the LSD profile deviates from zero in units of the mean error-bar for all the LSD profile resolution elements, both inside and outside the extent of the LSD-extracted spectral line. The statistics are then converted to detection probabilities (Donati 1992) and the probabilities are assessed to determine if significant polarization is detected.

While the detection or non-detection of significant circular polarization does provide an unambiguous diagnosis of a star's magnetic field, we have additionally computed mean longitudinal magnetic fields, B_l, for the stars in our survey in order to make comparisons with previous measurements, and to provide a simple quantitative magnetic field diagnostic which may be analyzed statistically. Longitudinal fields for all observations (except HD 109387, see Sect. 6.4.6) have been calculated from LSD averaged Stokes V and I profiles using Eq. 5.13. Longitudinal fields and associated 1σ uncertainties are given in Table 6.3 for the Am, HgMn, normal and emission-line stars, and in Table 6.4 for stars classified as Ap SrCrEu and Ap Si. In cases where two identical observations were made successively of the same star (indicated by $2\times$ in Column 12 of Table 6.1), the longitudinal field was measured for both observations and then the average calculated and presented in Tables 6.3 and 6.4. The median of the 1σ uncertainties associated with the longitudinal field measurements of all non-magnetic stars is 22 G. We realize that the non-detection of longitudinal fields does not preclude the existence of highly complex fields, or even simple fields observed at unfavorable phases, and thus stress that it is the *detection or non-detection of significant circular polarization in LSD profiles which is the basis for our determination of a star having a magnetic field.*

A secondary result of our survey was the new analysis of the observations of spectroscopic binary (SB) stars, or those binaries whose nature is known due to the periodic Doppler shifts observed in their spectral lines. Spectroscopic binaries may be divided into two groups: those where one sees only the lines of one star (SB1) and

Table 6.3: Summary of derived longitudinal magnetic fields ($\pm 1\sigma$) for the Am, HgMn, normal and emission-line stars.

HD number	$B_z \pm \sigma$ (G)	HD number	$B_z \pm \sigma$ (G)	HD number	$B_z \pm \sigma$ (G)	HD number	$B_z \pm \sigma$ (G)
Am stars				**HgMn stars**			
29173	28 ± 32	109485	-26 ± 31	27295	22 ± 34	106625	-29 ± 46
48915	1 ± 7	110380	21 ± 16	63975	100 ± 110	129174	-12 ± 39
	10 ± 6	110951	-2 ± 14	75333	-120 ± 100		-2 ± 29
60178	24 ± 10		8 ± 16	77350	6 ± 35	143807	31 ± 17
73709	66 ± 39	112412	-1 ± 18		17 ± 36	144206	-24 ± 49
	-58 ± 53	116657	37 ± 67	78316	-37 ± 26	145389	-7 ± 16
78209	3 ± 10	125337	20 ± 23	**Normal stars**			
78362	-5 ± 5	126661	20 ± 23	20902	1 ± 2	110379	20 ± 8
	-3 ± 5		-41 ± 35	24760	130 ± 140		-9 ± 12
89021	66 ± 22	141675	42 ± 26	41753	120 ± 420	114710	5 ± 4
90277	-9 ± 20	141795	-7 ± 15	61421	2 ± 5	118216	39 ± 18
95418	-4 ± 15		-7 ± 15	82328	0 ± 4	123299	-29 ± 30
95608	-3 ± 21		1 ± 12	87737	4 ± 14	124850	3 ± 5
97633	9 ± 12	159560	33 ± 34		6 ± 13	126660	-2 ± 7
108642	-15 ± 17	195479	15 ± 53	95382	-80 ± 43	128167	8 ± 13
	11 ± 18	214994	-32 ± 20	8353	120 ± 120	144284	3 ± 8
108651	-14 ± 56			99028	20 ± 8	147394	33 ± 87
Emission-line stars				104321	-93 ± 53	155763	41 ± 43
103287	-140 ± 120					160762	13 ± 43
108844	66 ± 52						
163472	150 ± 330						

Table 6.4: Longitudinal magnetic field measurements for the stars classified as Ap SrCrEu, Si.

HD number	HJD (2,440,000+)	$B_z \pm \sigma$(G)	Note
		Ap SrCrEu, Si Stars	
60179	11612.445	26 ± 13	Probably not magnetic Ap
74521	11612.414	634 ± 17	
108662	11612.536	-604 ± 23	
108945	11612.571	109 ± 44	
115735	11600.658	10 ± 380	
116656	11587.679	-9 ± 16	Probably not magnetic Ap
120198	11601.673	-209 ± 74	
125248	11599.671	-10 ± 43	
	11612.680	-1496 ± 43	
140160	11606.630	230 ± 120	
148112	11602.688	-81 ± 47	
148330	11599.730	52 ± 37	

those where one may see both stars' lines (SB2). Our high signal-to-noise ratio mean Stokes I profiles for the observed spectroscopic binaries allow for the measurement of component radial velocities, which may be used in orbit and component mass determinations.

6.4.1 Am stars

No significant Zeeman circular polarization (according to the statistical test described by Donati et al. 1997) was detected for any of the 35 observations of all 25 Am stars. Twenty-four observations imply longitudinal fields significant at less than 1σ. For nine observations we infer longitudinal fields significant at greater than 1σ, with one of those between 2σ and 3σ, and another at 3σ. The 3σ detection is not thought to be significant because we observe no coherent signal in the Stokes V profile (see section under HD 89021).

The median of the 1σ longitudinal field standard errors for the Am stars is 18 G. In comparison, typical longitudinal field measurements previously obtained for Am stars (e.g. Borra & Landstreet 1980, Landstreet 1982) were null detections with σ's of 50 to 200 gauss. Our longitudinal field standard errors are all less than 50 G except for observations of the faintest stars ($V_{\rm mag} > 6$) and/or stars with relatively large rotation velocities ($v \sin i > 50$ km s^{-1}).

HD 29173, HD 112412, HD 195479, HD 214994

We detect no circular polarization in the spectral lines of HD 29173, HD 112412, HD 195479 or HD 214994, stars for which magnetic fields have been reported using other methods. In Fig. 6.3 we show LSD Stokes I and V mean signatures for two of these stars. The S/N obtained for HD 112412 (330:1) is slightly lower than the median S/N (370:1) obtained for Am stars in this study, while that obtained for HD 195479 (110:1) is one of the lowest S/N obtained in this study. The Stokes V values inside the line for HD 112412 has a peak-to-peak amplitude of 0.02% while that for HD 195479 has a peak-to-peak amplitude of 0.08%, both of which are smaller than the truly significant profile for HR 1099 which was 0.1% (see Fig. 6.1).

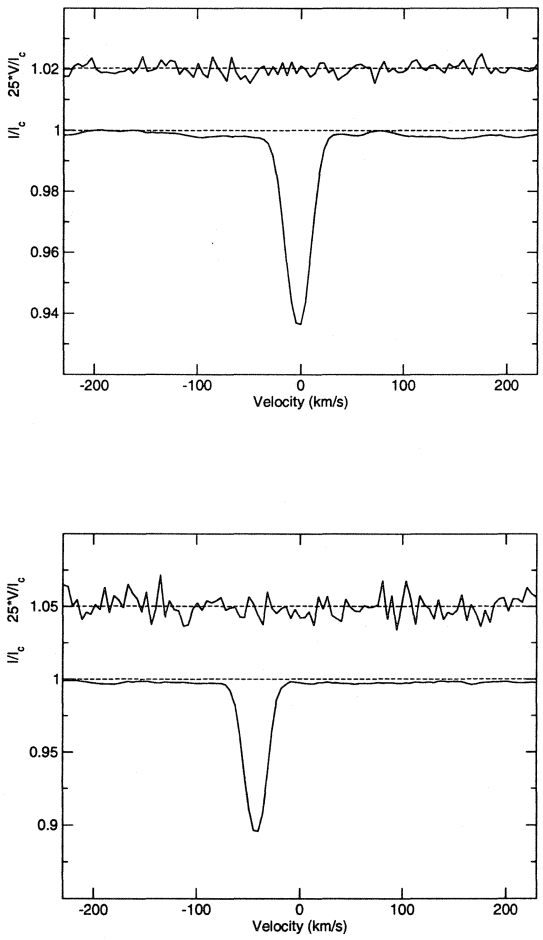

Figure 6.3: LSD mean Stokes I and V profiles of the Am star HD 112412 (top) observed on HJD 2450859.724 and the Am SB1 HD 195479 (bottom) observed on HJD 2450860.738. Note that, for display purposes, the Stokes V profiles have been expanded by a factor of 25 and shifted upward by 1.02 (upper) and 1.05 (lower).

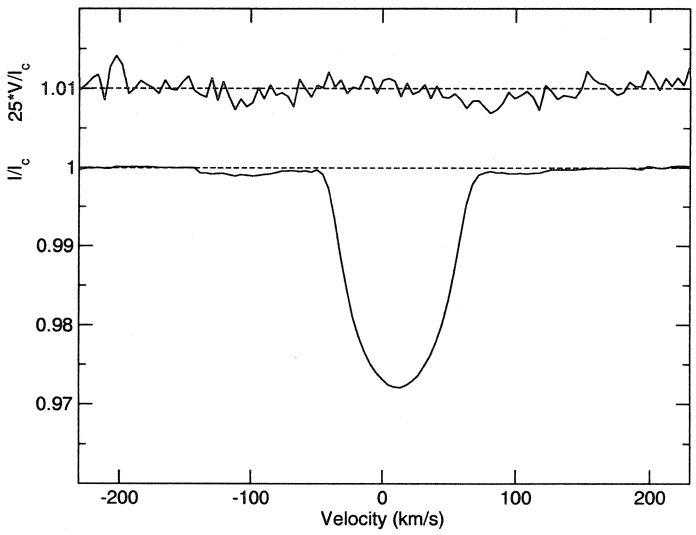

Figure 6.4: LSD mean Stokes I and V profiles of the Am star HD 89021, observed on HJD 2451579.681. Although a longitudinal magnetic field is detected at the 3σ level for this star, no significant polarization is seen in its Stokes V profile. Note that, for display purposes, the Stokes V profile has been expanded by a factor of 25 and shifted upward by 1.01.

HD 48915 (Sirius)

Our observations of Sirius show no evidence for a magnetic field, and our two longitudinal field measurements are non-detections with $\sigma = 6$ and 7 G. It is interesting to note that, while these standard errors are among the smallest we achieve in this study, similar precision has been achieved for Sirius using photoelectric polarimetric analysis of single lines by Borra et al. (1973), which gave null measurements of longitudinal field having σ as low as 9 G. Our observations do not confirm the measurements by Severny (1970) who reported a significant field of 38 G for Sirius.

HD 89021

The measurement of the longitudinal field of HD 89021 is 66 ± 22 G, which would seem to indicate a significant 3σ detection. An examination of its LSD profiles, shown in Fig. 6.4, reveals no coherent signal in Stokes V, and we tentatively conclude that this measurement is spurious. We plan to re-observe this star in future in order to verify this conclusion.

HD 108642

Two observations of HD 108642 (on HJD 2450851.636 and 2451197.710) show the mean line of the secondary in the unpolarized LSD profile. This object is well known as an SB1 and was discovered to be SB2 by Boesgaard (1987). The two observations of this system show a much weaker secondary mean line with approximately the same low rotation velocity (i.e., < 10 km s^{-1}) as the primary (Fig. 6.5). Using the radial velocities of both components from both observations, we determine the systemic velocity (the radial velocity of the binary system) to be $V_0 = -2 \pm 2$ km s^{-1}. Harper's (1929) orbital elements for this system include the systemic velocity $V_0 = +1.78 \pm 0.37$ km s^{-1}, which is consistent with our value. Using our measurements of the radial velocities of each component in each observation, we then compute the mass ratio, $\mathcal{M}_1/\mathcal{M}_2 = v_2/v_1 = 1.9 \pm 0.1$. From the reasonable assumption that the observed effective temperature and surface gravity ($T_{\rm eff} = 8100 \pm 300$ K and $\log g = 4.1 \pm 0.3$; Landstreet 1998) correctly describe the primary, we find the mass of the primary $\mathcal{M}_1 = 1.9 \pm 0.4\ \mathcal{M}_\odot$ from its position on the $\log T_{\rm eff} - \log g$ diagram (using the theoretical evolutionary tracks for solar metallicity calculated by Schaller et al. 1992). This, in combination with the mass ratio, gives the secondary mass $\mathcal{M}_2 = 1.0 \pm 0.2\ \mathcal{M}_\odot$. This simple analysis therefore suggests that the secondary component of HD 108642 is a solar-mass dwarf, and the luminosity ratio, L_1/L_2, of the two components would be about 15. We may further substitute for the masses in the mass function defined as,

$$f(\mathcal{M}) = \frac{P v_1^3}{2\pi G} = \frac{(\mathcal{M}_2 \sin i)^3}{(\mathcal{M}_1 + \mathcal{M}_2)^2} \tag{6.2}$$

which arises from Kepler's third law, where P is the orbital period and i the orbital inclination. Harper (1929) determined the value of $f(\mathcal{M}) = 0.0857$, which, using our values of the stellar masses, would imply that the inclination of the orbital plane is $i \simeq 64°$.

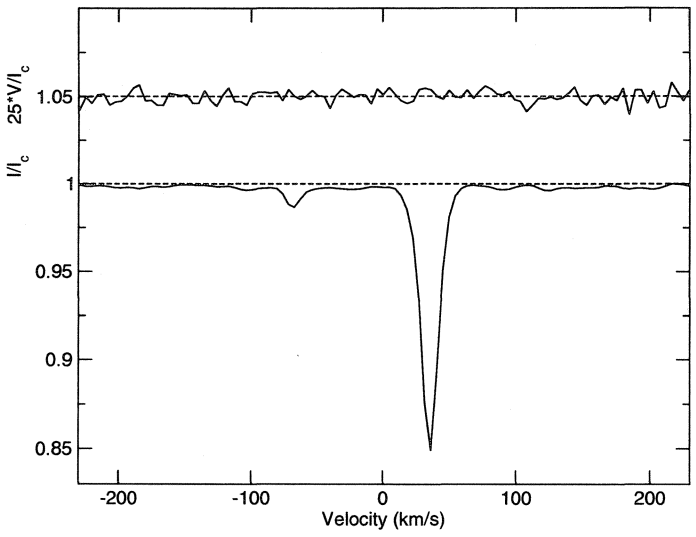

Figure 6.5: LSD mean Stokes I and V profiles of the Am SB2 HD 108642, observed on HJD 2450851.636. The weak mean line of the secondary is clearly visible. Note that, for display purposes, the Stokes V profile has been expanded by a factor of 25 and shifted upward by 1.05.

HD 110951

We have detected the mean lines of both components of the SB2 HD 110951. This system is one in which the lines of the secondary indicate that it is hotter than the primary, implying evolution of the primary off the main sequence (Mitton & Stickland 1979). While detection of the lines of the secondary in this system had been reported previously (Mitton & Stickland 1979), its projected rotation velocity remained highly uncertain. Since this system is thought to contain a pulsating δ Del star (the primary; Mitton & Stickland 1979), it is potentially very interesting for detailed study. From our first observation of HD 110951, shown in Fig. 6.6, we obtain for the secondary $v \sin i = 80 \pm 10$ km s^{-1}(where the error bar takes into account the uncertainty due to blending with the mean line of the primary), consistent neither with the results of Mitton & Stickland (1979) nor those of Kurtz et al. (1976) (who

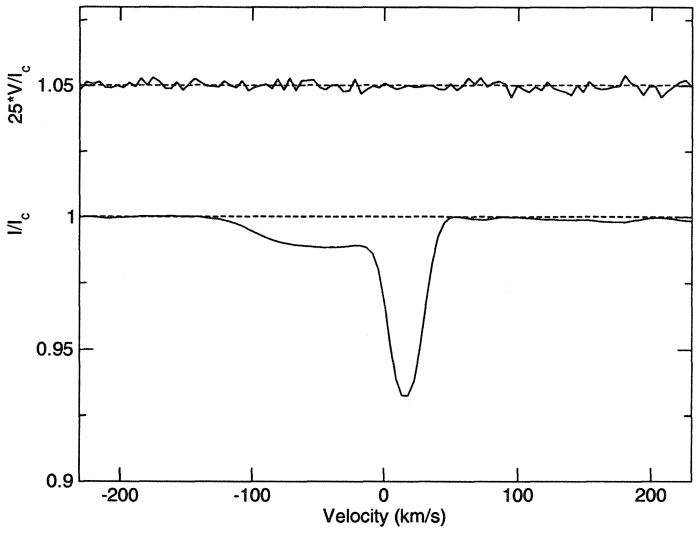

Figure 6.6: LSD mean Stokes I and V profiles of the Am SB2 HD 110951, observed on HJD 2450856.595. Mean lines of both components are visible. Note that, for display purposes, the Stokes V profile has been expanded by a factor of 25 and shifted upward by 1.05.

report $v \sin i = 140$ km s^{-1} and $v \sin i \sim 50$ km s^{-1} respectively). The $v \sin i$ of the sharper-lined component is 19 ± 3 km s^{-1}, which is consistent with that obtained by Kurtz et al. 1976.

HD 125337

We have detected the lines of both components of the SB2 HD 125337 in its LSD line profile which is shown in Fig. 6.7. It is apparent that one star is sharp-lined, and we estimate from the FWHM of its LSD profile that it has $v \sin i < 10$ km s^{-1}, although with some uncertainty due to the difficulty in the fit of a Gaussian to the broader lined component. We did not find it possible to accurately estimate the rotation velocity of the broad-lined component using our simple method, but its LSD profile is consistent with an approximate value of 50 km s^{-1}.

6.4.2 HgMn stars

No significant circular polarization is detected for any of the 12 observations of all 10 HgMn stars. All 12 observations imply longitudinal fields significant at less than 2σ, with nine significant at less than 1σ. The median 1σ longitudinal field standard error for the observations of HgMn stars is 39 G. Typical previous longitudinal field measurements of HgMn stars include those made by Borra & Landstreet (1980) which were non-detections with typical σ's of 180 G.

HD 27295

No significant circular polarization is detected for HD 27295, although Hubrig & Castelli (2001) show evidence of magnetic intensification of Fe II lines for HD 27295, implying a possible magnetic field for this star. Chountonov (2001), used a "back-and-forth" magnetometry method (an efficient CCD spectropolarimetry technique described by Chountonov et al. (2000)) and found its longitudinal field to be $B_z = +30 \pm 20$ G.

HD 78316 (κ Cnc)

No significant circular polarization is detected for HD 78316. Hubrig (1998) observed this star and used a diagnostic method sensitive to the value of $\langle B^2 + B_z^2 \rangle$ (the "quadratic field") and found it to be 2.7 kG, significant at the 6.3 σ level. Hubrig

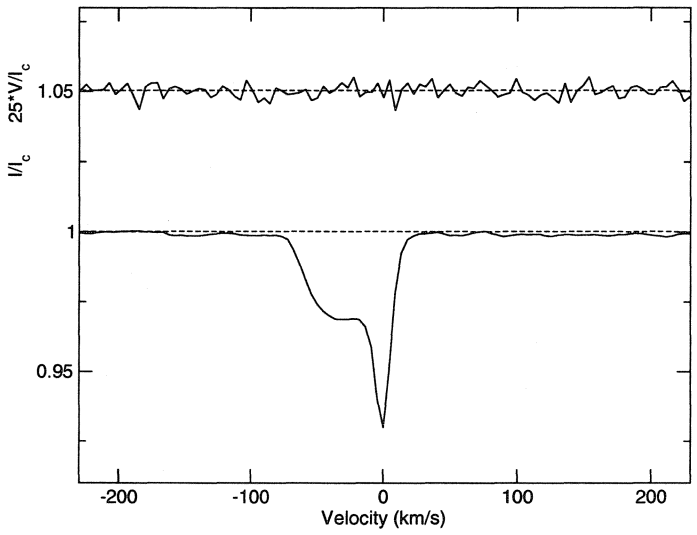

Figure 6.7: LSD mean Stokes I and V profiles of the Am SB2 HD 125337, observed on HJD 2451603.675. The lines of both the sharp-lined component and broad-lined component are visible. Note that, for display purposes, the Stokes V profile has been expanded by a factor of 25 and shifted upward by 1.05.

(1998) also mentioned measurements of the longitudinal field of HD 78316 as being "...of the order of few hundred gauss at levels above 3σ" which would appear in a future, and as yet unpublished, paper. Since the diagnostics used to detect magnetic fields in HgMn stars have been primarily related to Fe II lines, we recomputed the LSD profiles for HD 78316 using only the Fe II lines in its spectrum. As expected, the resultant average profile was noisier (because fewer lines are used in the average, and lines other than Fe II, which may be blended in, are ignored) but still no significant circular polarization was observed. The corresponding longitudinal magnetic field measurement was $B_z(\mathrm{Fe}) = -24 \pm 41$ G, as compared to the measurement made using LSD profiles extracted from all spectral lines, $B_z = -37 \pm 26$ G.

Our longitudinal field measurement is also in contrast to the measurements made by Babcock (1958) and Preston et al. (1969), which seem to show periodic magnetic variability for HD 78316, with longitudinal fields ranging between +250 and −150 G, but with large uncertainties. Our non-detection is supported, however, by a non-detection made by Chountonov (2001) which implied a longitudinal field of $B_z = +50 \pm 30$ G.

6.4.3 λ Boo stars

The two λ Boo stars studied here, HD 110411 (ρ Vir) and HD 125162 (λ Boo) were studied by Bohlender & Landstreet (1990) using a Hβ Zeeman analyzer. Their measurements of the longitudinal fields resulted in non-detections with errors of around 200 G. Our measurements do not provide any detections of magnetic fields, but our errors are much larger ($\sigma = 500$ G for HD 110411 and $\sigma = 900$ G for HD 125162). Stars with the λ Boo chemical peculiarity are a good example of those which are not suitable for analysis with the LSD technique. The low abundance of iron-peak elements (responsible for most of the lines in the visible spectrum of an A-type star), with the resulting low density of rather weak lines, as well as the high projected rotation velocities typical of this class of star, mean that one is averaging fewer, weaker lines and the multiplex advantage of the LSD technique is greatly reduced. It should be noted that many O and early B-type stars may also be poor candidates for analysis with the LSD technique for the same reasons as for the λ Boo stars.

6.4.4 Normal stars

No significant circular polarization is detected for any of the 24 observations of 22 normal (i.e. non-chemically peculiar, non-emission-line) stars. All 24 observations imply longitudinal fields significant at less than 3σ, with 20 significant at less than 2σ, and 17 significant at less than 1σ. The median 1σ longitudinal field standard error for the normal stars is 13 G. Previous longitudinal field measurements by Landstreet (1982) of some normal stars on our list also show no evidence for magnetic fields but have standard errors with a median value of 55 G, and ranging from $\sigma = 7$ G (for HD 61421, Procyon) to $\sigma = 300$ G (for one observation of HD 160762, a B3IV star).

HD 20902 (α Per)

HD 20902 is extremely well suited to the LSD technique, since it is quite bright, has a high line density due to its spectral type (F5Ib) and a moderately low projected rotation velocity of 20 km s^{-1}. We have measured its longitudinal field to be $B_z = 1 \pm 2$ G, finding no significant circular polarization. Borra & Landstreet (1973) did not detect a longitudinal field in this star, with $\sigma = 60$ G.

HD 61421 (Procyon)

We do not detect any significant circular polarization for HD 61421. Our corresponding longitudinal field measurement of 2 ± 5 G has one of the lowest errors in our survey, but it is not a large improvement over other measurements for this well-studied star. Landstreet (1982), using a coudé line profile scanner with polarization module, reported two non-detections with $\sigma = 7$ G. Borra et al. (1984) made a longitudinal field measurement using circular spectropolarimetry of many lines simultaneously, in a technique resembling LSD, and found $B_z = -7.5 \pm 5.9$ G. Bedford et al. (1995), using a magneto-optical-filter spectrometer, made 12 measurements resulting in null detections with $\sigma = 0.7 - 1.8$ G. Plachinda & Tarasova (1999) used a coudé spectropolarimeter along with their "Flip-Flop Zeeman Measurement" technique and measured the longitudinal field of HD 61421 to be $B_z = -1.34 \pm 1.0$ G.

HD 98353

HD 98353 (55 UMa) has been classified as a λ Boo type star (Hauck 1986) but was later determined to be of spectral type A2 Va by Gray & Garrison (1987). It has

also been classified as an A-shell star (Hauck & Jaschek 2000). Horn et al. (1996) suggest that it is the composite nature of the spectrum of this triple system that has led to its being mis-classified, and that HD 98353 is not peculiar in any other way. Therefore, we have treated it as a normal star and do not find any significant circular polarization or evidence for a magnetic field in this star. The error in the longitudinal field measurement for this star, 120 G, is the largest for any A type star we have studied, except for the rapidly rotating emission-line star, HD 103287 and the λ Boo stars. We suspect it is the composite nature of the average line profile for HD 98353 which does not allow us to obtain a more precise result.

HD 110379 (γ Vir A)

Babcock (1958) reported the field for HD 110379 to be $B_z = -390 \pm 50$ G. Boesgaard (1974) also detected a field for this star, varying between ~ -300 G to $\sim +400$ G, but with the variability seemingly unrelated to rotation. One measurement by Landstreet (1982) was a null with $\sigma \approx 50$ G. Our two measurements of the longitudinal field of this star, separated by 13 days, both non-detections with $\sigma \approx 10$ G, do not confirm the existence of a longitudinal field of several hundred gauss.

HD 123999

HD 123999 is a known SB2, and our radial velocity measurements for the primary and secondary, given in Table 6.1, are in agreement with Fig. 3 of Boden et al. (2000).

6.4.5 Ap SrCrEu and Si stars

The 11 stars classified as Ap SrCrEu and Si which were observed as part of the survey include five stars for which no fields have ever previously been detected, as well as six stars which are known to be magnetic. Of the stars previously not known to be magnetic, we have detected circular polarization in two; no significant polarization is detected for three others, with two observations implying longitudinal fields significant at less than 1σ and one at 2σ. The observations of the known magnetic stars show the expected circular polarization and corresponding longitudinal fields, except in the cases of HD 148112 and HD 148330, where we do not conclusively detect a magnetic field in one measurement of each star. The longitudinal fields and associated 1σ uncertainties are listed in Table 6.4.

HD 60179, HD 116656

Although HD 60179 and HD 116656 are classified as having the characteristic chemical peculiarities associated with magnetic fields, we detect no circular polarization in their spectral lines. A comparison of sections of their spectra to other, non-chemically peculiar stars we have observed does not show the marked difference in the strengths of spectral lines of elements which one expects for the Ap SrCrEu type stars. For example, we do not observe markedly strong chromium lines for any either of these stars, and found Cr lines to be of similar strength to the Cr lines of Sirius, While this is not conclusive evidence that these stars are misclassified as magnetic peculiars, it suggests that misclassification is likely, especially since neither of these stars is identified as having variable photometry or line strengths (Catalano & Renson 1984 and supplements).

A measurement of the longitudinal field of HD 116656 on HJD 2451578.717 (our first observation) was not performed because of the blending of the line of the secondary with that of the primary, but no significant circular polarization was detected for that observation.

HD 74521

The longitudinal field of this magnetic Ap star has been measured in the past with σ = 100–300 G (Mathys 1991, Bohlender et al. 1993) and, as mentioned by Mathys (1991), "the variability of (the longitudinal field) in HD 74521 is far from being indisputably established." There is also some uncertainty concerning the period of variation of HD 74521, if any such variation exists. Our single longitudinal field measurement of HD 74521, while very precise, is nearly at the mean of the previous field measurements and does little to confirm any variation.

HD 108662

The longitudinal field of HD 108662 was previously studied by Babcock (1958), Preston et al. (1969) and Rustamov & Khotnyanskii (1980). It shows field variations between approximately +200 to −800 G. Our single longitudinal field measurement, $B_z = -604 \pm 23$ G, is much more precise than any previous, and is in reasonable agreement with the observed field variation of previous measurements, when phased with the ephemeris of Rice & Wehlau (1994). More observations are necessary to

improve the period.

HD 108945

This is the first detection of circular polarization for the A2pSr star HD 108945 previously announced by Shorlin et al. (2001). Its LSD profiles are shown in Fig. 6.8, and clearly show a characteristic Stokes V profile for a magnetic star, which is "definitely detected" as determined by LSD (Donati et al. 1997). The asymmetry of the Stokes I profile is probably due to inhomogeneous chemical distributions on the stellar surface, a common feature of magnetic Ap stars. Although our single longitudinal field measurement, $B_z = 109 \pm 44$ G, is significant at less than 3σ, the detection of significant circular polarization in the Stokes V profile reveals this to be definitely a magnetic Ap star.

HD 115735

HD 115735 has the highest rotation velocity of any of the canonically magnetic Ap stars we observed, and while we do not detect significant circular polarization for it, it does not appear that it is misclassified or non-magnetic. Zverko (1984) shows that it is peculiar in that it has weak helium lines, although silicon does not seem to be of higher than normal abundance. Because of its high rotation velocity, HD 115735 is an example of a star which is not well-suited for our detection method.

HD 120198

The longitudinal field of HD 120198 (84 UMa) has been measured by Borra & Landstreet (1980) and Wade et al. (1998), with typical standard errors of ≈ 150 G for the most recent observations. The variation evident in these measurements has allowed Wade et al. (1998) to determine the magnetic geometry for this star. Our single measurement, $B_z = -209 \pm 74$ G, when phased with the data of Wade et al. (1998) using their ephemeris, is in good agreement with the best-fit sinusoidal curve in their Fig. 1, and shows clearly that the field is variable.

HD 125248

HD 125248 (CS Vir) is an extremely well-studied magnetic Ap star, with many longitudinal field measurements made by authors from Babcock (1958) to Leone & Catan-

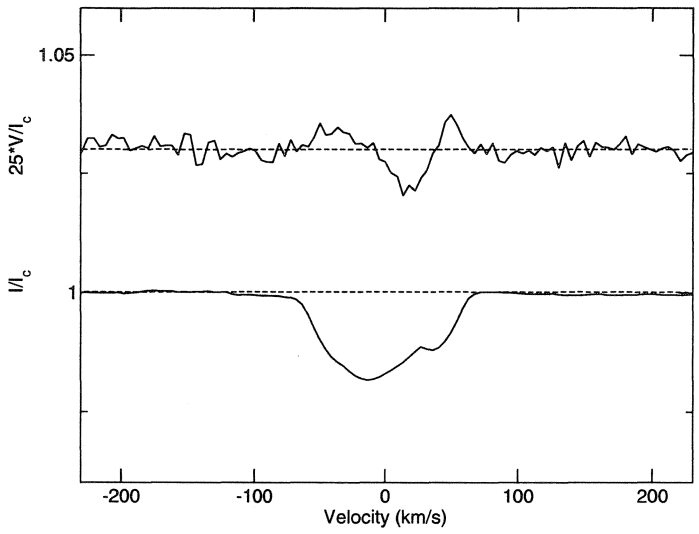

Figure 6.8: LSD mean Stokes I and V profiles of the Ap Sr star HD 108945, observed on HJD 245162.571. A characteristic Stokes V profile for a magnetic Ap star may be seen. A "bump" in the Stokes I profile may also be seen, likely due to chemical abundance inhomogeneity on the stellar surface. Note that, for display purposes, the Stokes V profile has been expanded by a factor of 25 and shifted upward by 1.03.

zaro (2001). Typical standard errors of previous longitudinal field measurements have been hundreds of gauss, while we have made two measurements, both with $\sigma = 43$ G. Our measurements are in nearly perfect agreement with the purely sinusoidal longitudinal field curve seen in Fig. 6 of Mathys & Hubrig (1997), when phased with their ephemeris. Our measurements are not in agreement, however, with the somewhat anharmonic best-fit longitudinal field curve in Fig. 10 of Leone & Catanzaro, when phased with their ephemeris. The curve of Leone & Catanzaro includes longitudinal field measurements made over the past fifty years from all available sources. Our data suggest that the longitudinal field of HD 125248 varies as described by Mathys & Hubrig.

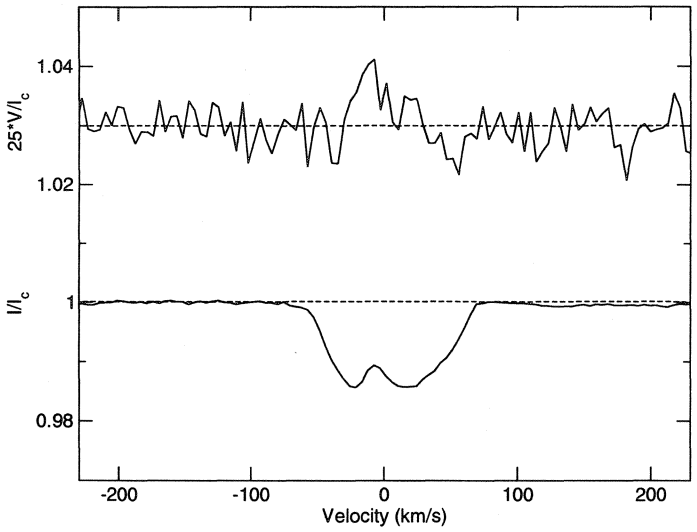

Figure 6.9: LSD mean Stokes I and V profiles of the A0 SrCr star HD 140160, observed on HJD 2451606.630. Significant polarization is seen in the Stokes V profile. Note that, for display purposes, the Stokes V profile has been expanded by a factor of 25 and shifted upward by 1.05.

HD 140160

The longitudinal field of HD 140160 is not well-studied, with eight observations by Landstreet et al. (1975) and a single longitudinal field measurement by Borra & Landstreet (1980), none of which is significant at a 3σ level. Leroy et al. (1993) observed HD 140160 using their broadband linear polarization method and found very low polarization. Our longitudinal field measurement, $B_z = 230 \pm 120$ G is significant at less than the 2σ level, but the large amplitude of the circular polarization in the LSD Stokes V profile seen in Fig. 6.9, which is a "definite detection" according to the statistical test described by Donati et al. (1997), provides the first unambiguous detection of a magnetic field in this star.

HD 148112

HD 148112 (ω Her) was observed by Borra & Landstreet (1980) and found to have a consistently negative longitudinal field, with some apparent variation between -570 G and -15 G, significant at less than 2σ. Hatzes (1991) reported Doppler imaging of this star which shows inhomogeneities in the surface abundance of chromium, as is often seen in magnetic Ap stars. Our single observation does show a negative value of $B_z = -81 \pm 47$ significant at between 1 and 2σ, but we do not conclusively detect a significant circular polarization signature.

HD 148330

HD 148330 was found to be magnetic by Žižňovský & Romanyuk (1990), with a longitudinal field varying between -600 and 200 G. We find no evidence for a magnetic field in our single observation of this star, but this is not inconsistent with the longitudinal field curve shown by Žižňovský & Romanyuk. When phased with their ephemeris, using a period of 4.288404 days, our longitudinal field measurement of $B_z = 52 \pm 37$ G is consistent with their near-zero longitudinal field measurements around phase 0.33. The non-detection of circular polarization in the LSD Stokes V profile is to be expected near polarity reversal for a star with low projected rotation velocity, when observed with only moderate S/N.

Ap Star Summary

Our survey of stars with magnetic Ap peculiarities may be divided into two groups: stars with and without previous field detections. For those with previous detections, we have greatly improved the precision of longitudinal field measurements over those made in other studies. In the cases of HD 120198 and HD 125248, our new measurements may be used to more accurately describe each star's field variation with rotation. For HD 148112 and HD 148330, our non-detections are consistent with either (a) observations at unfortunate phases or (b) very weak fields, of the order of the fields previously observed in the Ap star ϵ UMa ($B_z \leq 100$ G, Wade et al. (2000)).

Of the stars without previous magnetic field detections, we have found two with new and unambiguous circular polarization profiles implying that they are definitely magnetic. Of the other three, two are likely to be mis-classified as having Ap-like peculiarities, and one, HD 115735, is not well-suited to our detection technique.

6.4.6 Emission-line stars

No significant circular polarization is detected in three emission-line stars, and the uncertainties in their inferred longitudinal fields are relatively large, due to high rotation velocities, relative faintness, and in the cases of the hottest examples, the relatively low number of lines in their spectra. Emission spikes in the spectrum of HD 109387 (κ Dra) made it impossible to extract LSD line profiles and thus to measure a longitudinal magnetic field.

6.5 Analysis

It is useful to examine the reasons why there is such wide range in longitudinal field standard errors in this survey, with values varying from 2 G to hundreds of gauss, or even 10^3 G if the λ Boo stars are considered. Examining Eq. 2.7 and Eq. 2.8 and assuming that the stellar magnetic fields are large-scale and produce a net longitudinal field, it may be seen that the longitudinal field scales as

$$B \sim \frac{V}{\mathrm{dI/d}\lambda} \tag{6.3}$$

so that the uncertainty in B scales as

$$\sigma(B) \sim \frac{\sigma(V)}{\mathrm{dI/d}\lambda} \tag{6.4}$$

in a single line. The uncertainty in V scales as the inverse of the signal-to-noise ratio of the data, which we abbreviate as S. The slope of the line profile depends on two parameters: the depth and the width of the line. In almost all of the survey stars, line broadening is dominated by rotation. As $v \sin i$ increases, the line becomes both wider and shallower, which implies that $\mathrm{dI/d}\lambda$ scales with $(v \sin i)^2$. In the case of LSD profiles, the noise in the V profiles is reduced by a factor of $\sqrt{N}$, where N is the total number of lines used to compute the average profile. Thus, the uncertainty in longitudinal field measurements scales approximately as

$$\sigma \sim (v \sin i)^2 \, \mathrm{S}^{-1} \, N^{-1/2}. \tag{6.5}$$

Using this approximation helps to explain why the longitudinal field standard errors are so variable from star to stars. For example, an increase of $v \sin i$ by a factor of 4 and a decrease of number of lines by a factor of 10, as one may reasonably expect

to be the case for a hot star compared to a cool star, would result in a more than hundred-fold increase in standard error in longitudinal field.

Aside from the variation of line depth with $v \sin i$, the *intrinsic* average line depth also affects the uncertainty in longitudinal field. Therefore, the very best candidates for field detection and measurement using this technique are stars with low $v \sin i$ and many intrinsically strong lines. The LSD technique provides less precise results for stars with intrinsically weak lines, high $v \sin i$ and/or few lines. This simple relationship explains the success of the LSD technique in measuring longitudinal fields in slowly rotating F, A and late B stars, especially those with chemical peculiarities that increase both intrinsic line depth as well as the number of lines found in their spectra. It also explains the relative failure of the LSD technique for the λ Boo and early B stars and other relatively fast rotators which have fewer lines in their spectra.

For the stars in which no significant polarization was detected, the measured values of B_z with 1σ error-bars are plotted against stellar effective temperature in Fig. 6.10 in order to illustrate the very low standard errors achieved by using this method to measure fields, as well as the relative levels of success along the mid to upper main sequence. This figure includes only stars with $\sigma < 50$ G, since those stars with larger uncertainties are the ones with high rotation velocities, fewer lines or lowest S/N, and are examples of stars for which our technique is not well-suited.

A histogram of the values of $z = |B_z|/\sigma$ for the same stars, compared to a normal distribution, is shown in Fig. 6.11. It may be seen that in no longitudinal field measurement is the 3σ level exceeded, and that the distribution is somewhat over-concentrated towards zero. A truly normal distribution would exceed the 1σ level in one-third of the measurements. Since the 1σ level is exceeded in only approximately one-quarter of the measurements, this is an indication that perhaps the error-bars computed by LSD are a slight overestimate of the true uncertainty.

The distributions of the values of $|B_z|+1\sigma$ and $|B_z|+3\sigma$ for stars with no significant polarization, with $\sigma < 50$ G, are shown in Fig. 6.12. This distribution allows us to define envelopes of the upper limits on longitudinal field measurements for the stars best-suited to our method. These envelopes should be good indicators of the upper limits on longitudinal fields of the entire population of Am, HgMn and normal F, A and late B type stars. The 1σ envelope in Fig. 6.12 allows us, with 67% confidence, to rule out for this population the existence of any longitudinal field larger than 90 G, and to say that at least half of the population will have longitudinal fields less than

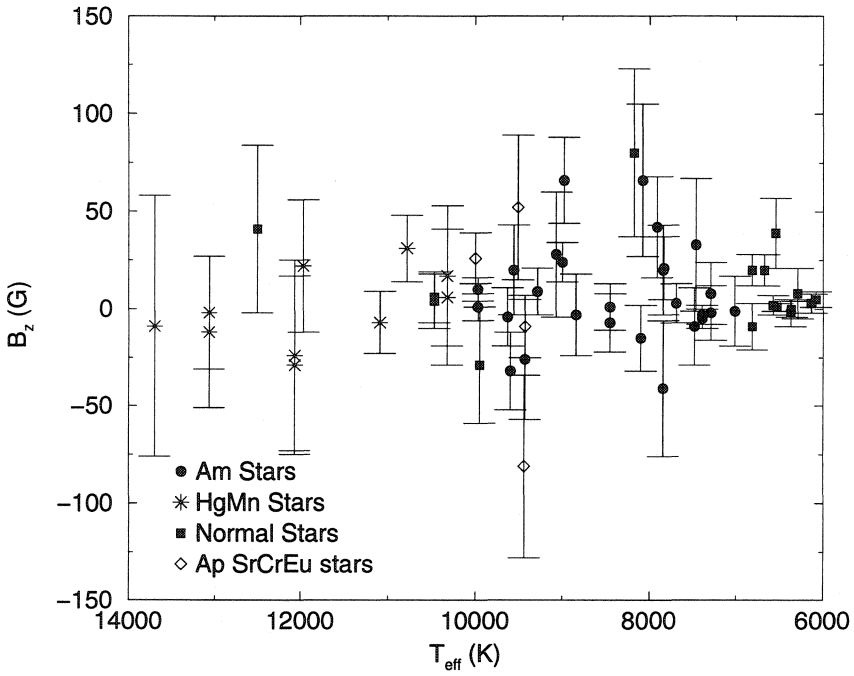

Figure 6.10: B_z measurements of stars for which no significant polarization was detected in the survey. In order to best visualize the most precise measurements, the nine with $\sigma > 50$G have been excluded from the figure. The other 64 are shown. Points corresponding to multiple measures of the same stars, or to stars with identical $T_{\rm eff}$ have been offset on the x-axis. The improvement in standard error with decreasing $T_{\rm eff}$ is apparent.

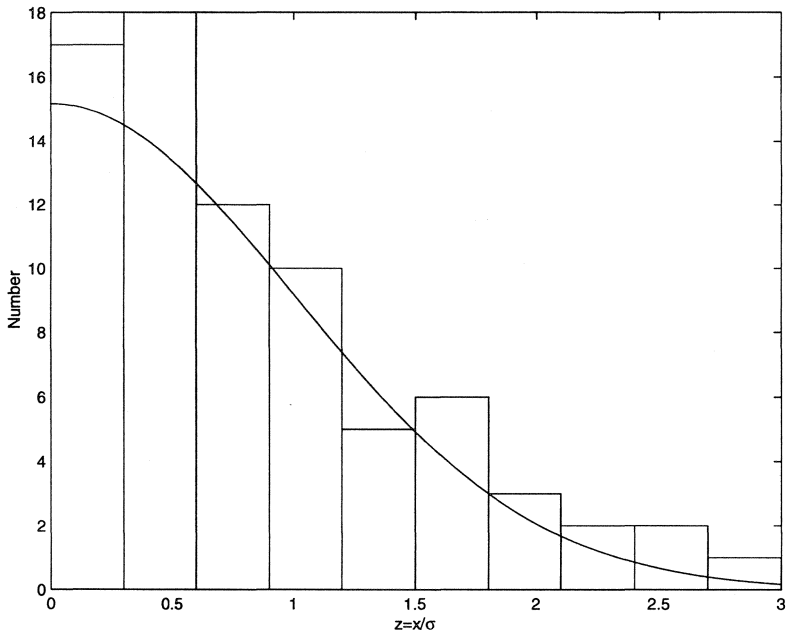

Figure 6.11: Histogram of $z = x/\sigma$, where $x = |B_z|$, compared with a normal distribution.

40 G. The 3σ envelope defines an extreme upper limit on longitudinal fields for this population. Even at the 3σ confidence level (99.7%), at least half the stars have fields less than 70 G. It is instructive to contrast these values with longitudinal fields as large as 5 kG observed in some magnetic Ap SrCrEu stars (Mathys 1991, Hill et al. 1998) and a median of around 300 G (Bohlender & Landstreet 1990).

Assuming that the stellar magnetic fields are *not* large-scale in nature, but are similar to those in cool active stars, the chances of detecting circular polarization signatures in LSD profiles is *increased* for stars with larger $v \sin i$, up to $v \sin i \approx 50$ km s^{-1}. Light originating from regions of opposite magnetic polarity will be increasingly Doppler separated by increased rotation velocity, thus decreasing the amount of cancellation in the overall Stokes V profile, which will make it easier to detect. Since we do not detect polarization signatures in any Am, HgMn, and normal stars, including the fastest rotators, we conclude that they do not have fields similar to those of cool active stars. This conclusion is supported by the lack of secondary indicators of magnetic activity such as flares, spots, etc.

The observations presented in this survey therefore do not support the general

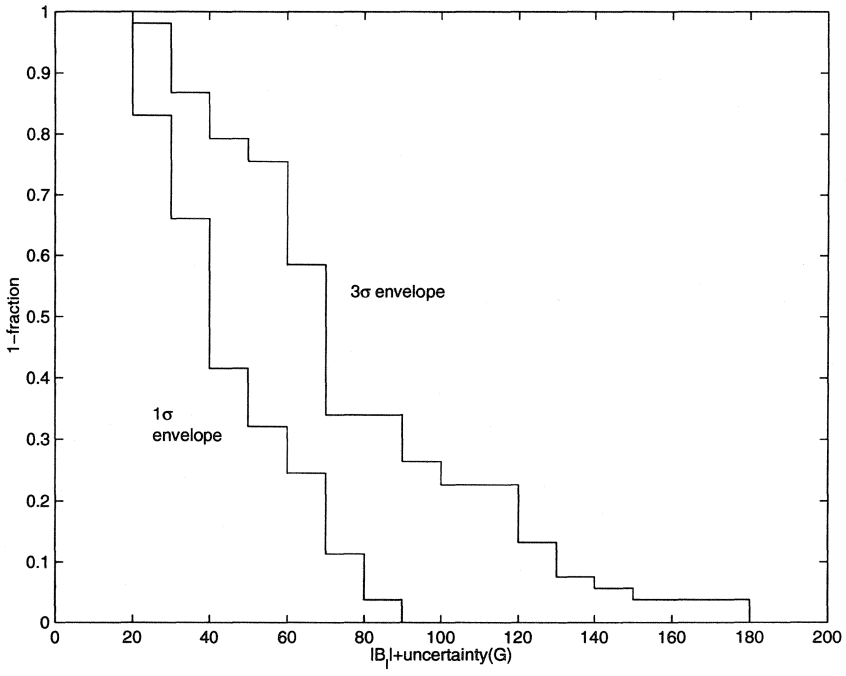

Figure 6.12: Distribution of the absolute value of longitudinal field measurements plus 1σ and 3σ for stars with $\sigma < 50$ G.

existence of strong, complex magnetic fields, with topologies similar to, or simpler than, those observed in active late-type stars, in the photospheres of Am or HgMn stars. Since the existence of *ordered* fields is also ruled out by these and earlier observations (cited in Section 6.1), we conclude that the Am and HgMn stars in general do not display magnetic fields currently detectable by means which investigate circular polarization. Since the detectability of magnetic features of opposite polarity using circular spectropolarimetry depends of the size and separation of such features, as well as the rotation velocity of the star, the limits of field strength and/or complexity one might expect to be able to detect could be estimated, but are left to future work. There have also been suggestions that toroidal fields may exist in these stars and that perhaps such fields would escape detection by circular polarization methods, but we are able to observe circular polarization for general geometries of toroidal fields in a rotating star using the LSD technique, due to the Doppler separation of the components of the Stokes V profile originating from the approaching and receding limbs of the star. In fact, toroidal field topologies in cool, active stars have been detected and even reconstructed previously using the LSD technique (Donati & Collier Cameron 1997).

This result leads us to conclude that either the magnetic fields detected by line profile methods (discussed in Section 6.1) in these objects have topologies still considerably more complex than those found in active late-type stars, or that the reported detections of magnetic fields in these stars are spurious. The first conclusion cannot be excluded, although it would invoke a new kind of astrophysical phenomenon (the existence of strong stellar magnetic fields which are highly complex topologically on a small scale, *and* which cover a large portion of a star's surface). This option should be entertained within the context of our current knowledge of the kinds of magnetic fields which exist in stars: weak fields which are mildly topologically complex (in Sun-like stars and active late-type stars), and strong fields which are topologically simple (in the magnetic A and B type stars). The second conclusion is in principle also quite reasonable, since the reported field detections discussed in Section 6.1 are based upon measurements of the very subtle differential broadening of single pairs of spectral lines in the presence of a magnetic field, measurements susceptible to systematic errors, especially due to uncertainties in atomic physics and line blending.

References

Abt, H. A., & Morrell, N. I. 1995, ApJS, 99, 135

Adelman, S. J. 1996, MNRAS, 280, 130

Adelman, S. J., Gulliver, A. F., Kochukov, O. P., & Ryabchikova, T. A. 2002, ApJ, 575, 449

Babcock, H. W. 1958, ApJS, 3, 141

Babcock, H. W. 1967, in The Magnetic and Related Stars, ed. R. C. Cameron, (Mono Book Corporation, Baltimore)

Bedford, D. K., Chaplin, W. J., Davies, A. R., et al. A&A 1995 293, 377

Bikmaev, I. F., Musaev, F. A., Galazutdinov, G., Savanov, I. S., & Savel'eva, Yu. Yu. 1998, Astronomy Reports, 75, N1

Boden, A. F., Creech-Eakman, M. J., & Queloz, D. 2000, ApJ, 536, 880

Boesgaard, A. M. 1974, ApJ, 188, 568

Boesgaard, A. M. 1987, ApJ, 321, 967

Bohlender, D. A., & Landstreet, J. D. 1990, MNRAS, 247, 606

Bohlender, D. A., Landstreet, J. D., & Thompson, I. B. 1993, A&A, 269, 355

Borra, E. F., Edwards, G., & Mayor, M. 1984, ApJ, 284, 211

Borra, E. F., & Landstreet, J. D. 1973, ApJ, 185, 139L

Borra, E. F., & Landstreet, J. D. 1980, ApJS, 42, 421

Borra, E. F., Landstreet, J. D., & Vaughan, A. H. 1973, ApJ, 185, 145L

Borra, E. F., Landstreet, J. D., & Thompson, I. B. 1983, ApJS, 53, 151

Castelli, F. 1991, A&A, 251, 106

Catalano, F. A., & Renson, P. 1984, A&AS, 55, 371

Chountonov, G., Murzin, V. A., Ivashchenko, N. G., & Afanasieva, I. V., 2000, in *Magnetic Fields of Chemically Peculiar and Related Stars*, eds. Yu.V. Glagolevskij & I.I. Romanyuk, 249

Chountonov, G. 2001, in ASP Conf. Ser. 248, *Magnetic Fields Across the H-R Diagram*, eds. G. Mathys, S. Solanki, & D. Wickramasinghe, 385

Conti, P. S. 1969, ApJ, 156, 661

Donati, J.-F. 1999, MNRAS, 302, 457

Donati, J.-F., Semel, M., & Rees, D. E. 1992, A&A, 265, 669

Donati, J.-F., & Collier Cameron, A. 1997, MNRAS, 291, 1

Donati, J.-F., Semel, M., Carter, B. D., Rees, D. E., & Collier Cameron, A. 1997, MNRAS, 291, 658

Gray, R. O., & Garrison, R. F. 1987 ApJS, 65, 581

Harper, W. E. 1929, Pub. DAO, 3, 315

Hatzes, A. P. 1991, MNRAS, 253, 89

Hauck, B. 1986, A&A, 154, 349

Hauck, B., & Jaschek, C. 2000, A&A, 354, 157

Hauck, B., & Mermilliod, M. 1998, A&AS, 129, 431

Hill, G. M., Bohlender, D. A., Landstreet, J. D., et al. 1998, MNRAS, 297, 236

Horn, J., Kubát, J., Harmanec, P., Koubsky, P., Hadrava, P., Simon, V., Stefl, S. & Skoda, P. 1996, A&A, 309, 521

Hubrig, S. 1998, Contributions of the Astronomical Observatory Skalnaté Pleso, 27, 296

Hubrig, S., & Castelli, F. 2001, A&A, 375, 963

Kurtz, D. W., Breger, M., Evans, S. W., & Sandmann, W. H. 1976, ApJ, 207, 181

Landstreet, J. D. 1982, ApJ, 258, 639

Landstreet, J. D. 1988, ApJ, 326, 967

Landstreet, J. D. 1998, A&A, 338, 1041

Landstreet, J. D., Borra, E. F., Angel, J. R. P., & Illing, R. M. E. 1975, ApJ, 201, 624

Landstreet, J. D., Barker, P. K., Bohlender, D. A., & Jewison, M. S. 1989, ApJ, 344, 876

Lanz, T., & Mathys, G. 1993, A&A, 280, 486

Leone, F., & Catanzaro, G. 2001, A&A, 365, 118

Leroy, J. L., Landolfi, M., & Landi Degl'Innocenti, E. 1993, A&A, 270, 335

Mathys, G. 1988, in Elemental Abundance Analyses, (Inst. Astr. Univ. Lausanne, Chavennes-des-Bois), 82

Mathys, G. 1991, A&AS, 89, 121

Mathys, G., & Hubrig, S. 1995, A&A, 293, 810

Mathys, G., & Hubrig, S. 1997 A&AS, 124, 475

Mathys, G., & Lanz, T. 1990, A&A, 230, L21

Mitton, J., & Stickland, D. J. 1979, MNRAS, 186, 189

Moon, T. T., & Dworetsky, M. M. 1985, MNRAS, 217, 305

Plachinda, S. I., & Tarasova, T. N. 1999, ApJ, 514, 402

Preston, G. W. 1974, ARAA, 12, 257

Preston, G. W., Stepien, K., & Wolff, S. C. 1969, ApJ, 156, 653

Rao, S. S., Abhyankar, K. D., & Nagar, P. 1990, ApJ, 365, 336

Rustamov, Yu. S., & Khotnyanskii, A. N. 1980, SvAL, 6, 202

Schaller, G., Schaerer, D., Meynet, G., & Maeder, A. 1992, A&AS, 96, 269

Severny, A. 1970, ApJ, 159, 73L

Shorlin, S. L. S., Landstreet, J. D., Sigut, T. A. A, et al. 2001, in ASP Conf. Ser. 248, Magnetic Fields Across the H-R Diagram, ed. G. Mathys, S. Solanki, & D. Wickramasinghe, 423

Smith, M. G. 1974, ApJ, 189, 101

Uesugi, A., & Fukuda, I. 1985, *Revised Catalogue of Stellar Rotational Velocities*, Department of Astronomy, Kyito Univ., Japan

Wade, G. A., Donati, J.-F., Landstreet, J. D., & Shorlin, S. L. S. 2000, MNRAS, 313, 851

Wade, G. A., Hill, G. M., Adelman, S. J, Manset, N., & Bastien, P. 1998, A&A, 335, 973

Žižňovský, J. & Romanyuk, I. I. 1990, BAICz, 41, 118

Zverko, J. 1984, BAICz, 35, 294

Chapter 7
Investigations into LSD mean polarization profiles

7.1 Introduction

7.1.1 Motivation

The two recent advances in the field of observational stellar spectropolarimetry, namely the use of the MuSiCoS spectropolarimeter and the development of the LSD averaging technique, have led to a number of important results. MuSiCoS spectropolarimetric data include the first linearly polarized stellar spectra (Stokes Q and U) ever obtained, as well as spectra in Stokes I and V. Individual line profiles in all four Stokes parameters, from MuSiCoS observations, have been used to obtain the first detailed model of the magnetic field structure of an Ap star (Kochukhov et al. 2004). LSD averaged profiles of MuSiCoS Stokes V spectra have made possible the measurement of longitudinal fields in magnetic Ap stars with greatly improved precision. The new data are consistent with, and a major improvement over, previous measurements (Wade et al. 2000b). Average LSD Stokes V profiles have made possible precise and convincing arguments against the existence of fields in a number of contested stars (Chadid et al. 2004, Wade et al. 2002, this thesis Chapter 6). Finally, non-zero LSD average Stokes Q and U profiles have been detected in MuSiCoS spectra, with an important increase in S/N over the signal in individual profiles (Wade et al. 2000a). For most of the stars observed by Wade at al (2000a), Stokes Q and U signatures are *only* observed in the LSD mean profiles, not for any individual line. Furthermore, these mean profiles are the first linear polarization line profile data available for these stars. Accurate and representative linear polarization data in line profiles provide essential input for realistic stellar magnetic field modelling because of the strong constraint

such data furnish on the transverse components of stellar fields.

One unresolved issue is whether or not the LSD profiles are useful for modelling magnetic fields, and this has not been rigorously tested. In order for LSD profiles to be considered as reasonable descriptors of how a star's magnetic field affects its spectral lines, then they must be related to the profiles in individual lines. While it may be *theoretically* possible to model a star's field by synthesizing a large portion of stellar spectrum (e.g., 2000 Å in the case of MuSiCoS) in four Stokes parameters, calculating synthetic LSD mean profiles from the synthetic spectra and comparing the synthetic LSD profiles to the observed LSD profiles, the iterative nature of the modelling procedure requires many synthesis steps. This procedure would be impractical in terms of computation time, given the large number of lines and width of spectrum required to be synthesized in each iteration as the parameters describing the star's magnetic field are varied in order to find a model which fits the data.

If, however, the LSD mean profiles can be treated as being the profiles for a single line of known characteristics, then an iterative modelling procedure becomes computationally reasonable. The question posed here is whether it is possible to ensure that this is actually the case. A first step is to ensure that all the lines that are included in the LSD averaging have the "same" shape in their Stokes profiles (i.e., all Stokes V the same shape, all Stokes Q the same shape, etc.). If this is the case, the LSD mean profiles will have the largest possible signal to noise ratio (no disparately shaped profiles will be included in the average), and the treatment of the LSD mean profiles as those of a single line may be valid, since the mean profile and single line profiles are similar in shape. In order to ensure that the multiplex gain advantage of using the LSD technique is maximized, one requires a large number of lines to be included. Thus, the best case for modelling LSD data is for observations in which most, if not all, spectral lines have the same shapes in their individual Stokes profiles.

The second step is to ensure that the way in which the average is taken, i.e., the weight given to any one profile in the average, reflects the true contribution of each profile to the overall average. We emphasize here that each profile in a given set of polarized stellar spectra of course has an amplitude and that an averaging procedure must weight each one according to its amplitude. But in real observations, the amplitudes are often unmeasurable, especially in linear polarization, which is the reason why the LSD technique is needed. Therefore the averaging must be done using weights based upon parameters for each line that influence the polarization profile

amplitudes. The LSD theory, discussed in Section 5.1.2, uses the approximation that each polarization profile is a scaled version of the mean profile, where the scaling factor is the weighting, $w = g\lambda d$ for Stokes V profiles and $w = g^2\lambda^2 d$ for Stokes Q and U profiles. Here g is the mean Landé factor (also written as $\bar{g}$), λ the wavelength and d the depth of each line. These scaling factors are derived assuming a weak field, a weak line and no rotational broadening. These approximations are not perfectly valid for stars with strong magnetic fields, and usually do not accurately describe the cases in which LSD is to be used.

We know that individual polarization profiles, for any given star, may differ in shape and amplitude depending on a line's depth, wavelength, magnetic sensitivity and Zeeman splitting. The star's magnetic field strength and rotation velocity will also influence the shape and size of any individual profiles. We also know that the assumption of individual polarization profiles being similar enough to average using a simple scaling relationship is an approximation. The goal of the study that follows is to determine if, and for what ranges of stellar and line parameters, the scaling approximations are reasonably correct. In what cases do most lines appear similar enough to average, and what scaling factors are valid to be used in the averaging? And can we determine the equivalent atomic parameters of the LSD line profiles needed for modelling? Please note that the effects of varying λ has not been examined in these exploratory tests. Future tests should address this, but since λ varies by less than 30% over a MuSiCoS spectrum while d can have any between 0 and 1, and B can vary by orders of magnitude in observationally interesting parameter space, the effect of scaling with wavelength is secondary.

7.1.2 An overview

The study of the LSD technique and its approximations began with some preliminary synthetic polarized line profiles that showed that the Stokes V signature of different lines appeared similar, while those in Stokes Q and U did not. This has led to the question: In the parameter space relevant to stars and their spectral lines (B, $v \sin i$, d, g), is there some "region" in which a large number of Stokes Q and U profiles are "similar enough" to compute LSD mean profiles from which can be deduced the Stokes profiles of a single line? And, in this region of parameter space, what is the amplitude weighting of each profile used in the average, as deduced from line parameters.?

The study has been accomplished by the synthesis of unpolarized and polarized spectra at a variety of field strengths and rotation velocities, in order to identify if and in what cases individual profiles do appear qualitatively similar. In those regimes of adequate similarity, new synthetic profiles were generated in order to test the effects of the line parameters on the shapes and amplitudes of the profiles. The scaling relationships from the LSD theory have been tested, and the range of parameter space over which they, or other new relationships, are appropriate has been determined.

While LSD mean profiles, in both circular and linear polarization, have been calculated and interpreted for a wide variety of stellar observations, (e.g. Magnetic Ap stars, Wade et al. 2000a, 2000b; Be stars, Neiner et al. 2003; Cool active stars, Petit et al. 2004), this study is the first test of the applicability of LSD averaging, and of its scaling relationships for amplitude weighting. While results using circularly polarized LSD profiles have been consistent, both internally and with other studies, the linearly polarized LSD profiles have only broad-band linear polarization studies to be compared with. Thus, the sort of rigorous testing presented here is a nearly unique way to test the LSD averaging technique as applied to mean Stokes Q and U profiles. This study is intended to be somewhat exploratory in nature, given the wide range of parameter space which may be considered for realistic stars and spectral lines.

7.2 Synthesizing polarization profiles

7.2.1 The code

The generation of synthetic spectra to be used in the testing process is done using the code ZEEMAN, described by Landstreet (1988) and Landstreet et al. (1989). ZEEMAN is a standard line profile synthesis code that calculates polarized and unpolarized line profiles for a model with a given magnetic field, abundance distribution, and model atmosphere, in a user-specified spectral window. It does so by dividing the visible disk into a number of representative points where it calculates local (in the star's frame) intensity and polarization profiles for spectral lines in the chosen window, based upon the local field, local abundance and the transfer of polarized light outward through the atmosphere. The local profiles are then summed over the stellar disk, each appropriately Doppler shifted according to the rotation velocity and

convolved with an instrumental profile to produce the final profiles. Line profile synthesis of ZEEMAN has been tested by Landstreet and collaborators, as well as in the literature in comparison to other codes that generate spectra for magnetic stars (Wade et al. 2001), all with satisfactory results.

7.2.2 The lines

In order to investigate the validity of using the polarization profiles of many different spectral lines to compute average Stokes profiles, as is done by LSD, a series of real spectral lines (i.e. lines with real atomic parameters) were synthesized in unpolarized and polarized light. Lines were chosen from a VALD line list (Kupka et al. 1999, Ryabchikova et al. 1998) as generated for the Ap9000 LSD line mask (see Section 5.2.1 for details). From that list, 27 strong lines of Fe and Cr were chosen for synthesis, because a primary goal is to evaluate the use of LSD in studying Ap stars, which often have spectra rich in lines of these two elements. The chosen lines are listed in Table 7.1. For convenience in calculation, the wavelengths were shifted so that they could all be synthesized in a reasonably small window of spectrum, and the values of wavelength at which each line was synthesized is in column 3 of the table. These wavelengths will be used to identify each line in plots later in this chapter. As may be seen, the chosen lines cover a wide range in values of average Landé factor, $\bar{g}$, as well as combinations of g and J in the levels, which affect the Zeeman splitting.

7.2.3 Stellar parameters

Spectra in all four Stokes parameters were calculated for a model star with $T_{\rm eff}$ = 9000 K and $\log g = 4.0$. It is not expected that the results will strongly depend on the values of $T_{\rm eff}$ and $\log g$. Thus, all calculations were carried out for a single stellar model. For this first exploratory study, a very simple field structure was adopted. The rotation axis was chosen to have inclination $i = 90°$ (i.e., in the plane of the sky). A dipolar magnetic field was chosen with obliquity angle $\beta = 90°$, so that the positive magnetic pole points exactly at the observer at the phase defined as 0.00. Three rotational phases were considered: 0.00, 0.15 and 0.25 of a rotation cycle, measured from the phase at which the dipole axis is parallel to the line of sight. In order to investigate the effects of both rotation and magnetic field strength on profiles, spectra were calculated for a grid of parameters with $B_{\rm polar} = B = 500, 1000, 2000, 4000$ &

Species	True $\lambda(\AA)$	Test $\lambda(\AA)$	$\log(gf)$	J_1	J_2	g_1	g_2	$\bar{g}$
Fe II	4508.2880	6108.0	-2.250	1.5	0.5	0.400	-0.020	0.500
Fe II	4515.3390	6111.0	-2.450	2.5	2.5	1.020	1.070	1.040
Fe II	4520.2240	6114.0	-2.600	4.5	3.5	1.310	1.290	1.340
Fe II	4522.6340	6117.0	-2.030	2.5	1.5	1.020	1.150	0.920
Fe II	4534.1680	6120.0	-3.330	1.5	2.5	0.400	1.070	1.570
Fe II	4541.5240	6123.0	-2.790	1.5	1.5	0.400	1.150	0.770
Fe II	4549.4740	6126.0	-2.020	3.5	2.5	1.210	1.350	1.030
Cr II	4554.9880	6129.0	-1.282	3.5	3.5	1.240	1.430	1.330
Fe II	4555.8930	6132.0	-2.160	3.5	3.5	1.210	1.290	1.250
Cr II	4558.6500	6135.0	-0.449	4.5	3.5	1.330	1.430	1.160
Cr II	4565.7400	6138.0	-1.820	2.5	1.5	0.920	1.180	0.720
Fe II	4576.3400	6141.0	-2.920	2.5	2.5	1.020	1.350	1.180
Fe II	4582.8350	6144.0	-3.090	2.5	3.5	1.020	1.290	1.630
Fe II	4583.8370	6147.0	-1.860	4.5	3.5	1.310	1.400	1.140
Cr II	4588.1990	6150.0	-0.627	3.5	2.5	1.240	1.380	1.060
Cr II	4592.0490	6153.0	-1.221	2.5	2.5	1.030	1.380	1.200
Cr II	4616.6290	6156.0	-1.361	1.5	1.5	0.410	1.180	0.790
Cr II	4618.8030	6159.0	-0.840	2.5	1.5	1.030	1.180	0.910
Fe II	4629.3390	6162.0	-2.330	4.5	4.5	1.310	1.320	1.310
Cr II	4634.0700	6165.0	-0.990	1.5	0.5	0.410	0.010	0.510
Fe II	4731.4530	6168.0	-3.000	2.5	3.5	2.000	1.400	0.650
Cr II	4824.1270	6171.0	-0.970	4.5	4.5	1.340	1.340	1.340
Cr II	4876.3990	6174.0	-1.460	1.5	1.5	0.420	0.410	0.410
Cr II	4876.4730	6177.0	-1.940	3.5	2.5	1.250	1.020	1.520
Fe II	4923.9270	6183.0	-1.320	2.5	1.5	2.000	2.400	1.690
Fe II	5018.4400	6189.0	-1.220	2.5	2.5	2.000	1.870	1.930
Fe II	5169.0330	6194.0	-1.303	2.5	3.5	2.000	1.700	1.330

Table 7.1: Lines synthesized to study Stokes profiles

6000 G and $v \sin i = 5, 10, 15, 20$ & 25 km s^{-1} as well as 30 km s^{-1} for the two strongest field values. These are typical values characteristic of most of the magnetic Ap stars for which MuSiCoS data are available.

The values of the abundance of Fe and Cr were initially chosen to resemble those found in magnetic Ap stars, but all test lines were found to be very strong in this case. The abundance values were reduced to a level where some of the lines being synthesized were still very strong, but others were considerably weaker, allowing us to study the effects of line depth on the profiles. The final abundance values $\log(N(\mathrm{Fe})/N(\mathrm{H})) = -5.3$ and $\log(N(\mathrm{Cr})/N(\mathrm{H})) = -5.0$ were used in the synthesis. The abundance of each element was taken to be constant over the surface of the star.

All spectra were synthesized as if convolved with an instrumental profile (such as introduced in actual observations with a spectrographic instrument) resulting in a resolving power of $\lambda/\Delta\lambda = 42000$, which is slightly better than is the case for MuSiCoS data.

7.2.4 Coherence regimes

Stokes V and Q profiles were examined for the grid of test spectra calculated over the range of B and $v \sin i$ defined above. Stokes U spectra were also calculated in the synthesis procedure, but the symmetry due to the choice of rotation and magnetic axes causes the Stokes U profiles to be nearly zero. This is an expected result, and one that causes the simplification of the data being analyzed. Since Stokes Q and U are interchangeable, if the geometry of the star is simply rotated by 45° in the plane of the sky, the results for Stokes Q profiles are applicable to both sets of linear polarization spectra.

Stokes V

Stokes V profiles were examined visually at all three phases in the full set of test computations to discover for what ranges of $B_{\mathrm{polar}} =$ "B" and $v \sin i$ the Stokes V profiles of most individual lines are closely similar in shape (apart from any scalable variations in amplitude). Ranges of B and $v \sin i$ for which profiles are similar in shape will be called "coherence regimes".

The striking result is that in *all* test spectra, the Stokes V profiles are very similar in shape to one another. A subset of the lines for two of the test cases are shown in

Figs. 7.1 and 7.2, but the robustness in the shapes of V profiles is found in every spectrum synthesized. Clearly, the use of LSD to compute average Stokes V profiles is quite promising given that, at least qualitatively, the fundamental LSD approximation of similarity in form is clearly valid.

Stokes Q

Stokes Q profiles were examined visually at all three phases in the full set of computations to identify B vs. $v \sin i$ coherence regimes. The complete set of Stokes Q test cases are shown in Figs. 7.3 to 7.7 for a subset of the lines.

The range of values of B and $v \sin i$ in which similar Stokes Q profiles are found (coherence regimes) may be seen by examining the figures in detail. It may be seen that test spectra at low $v \sin i$ values and low field strengths do not have coherently shaped profiles at all phases. As field strength increases, so must the rotation velocity in order for the profiles to be similar in shape. For the spectra for the highest field strengths, coherently shaped profiles (to some degree) may be seen at both high and low rotation velocities. One obvious disparity is in the profiles of the lines placed at 6141 Å and 6144 Å compared to the others, especially at high field strengths. These two lines are the weakest lines in the section of test spectrum shown, and their profiles, compared to the profiles of stronger lines, are an indication that line depth is a variable whose effect must be carefully studied.

From examination of such figures, we have identified regions in the B-$v \sin i$ diagram where the Stokes Q profiles are reasonably similar (if only for the strongest lines at large values of B). These coherence regimes are identified in Fig. 7.8. In order to further examine the behaviour of Stokes Q profiles with stellar and line parameters, we have concentrated our tests to the following pairs of (B, $v \sin i$): (500 G, 20 $\mathrm{km\,s^{-1}}$), (1000 G, 20 $\mathrm{km\,s^{-1}}$), (2000 G, 20 $\mathrm{km\,s^{-1}}$), (4000 G, 5 $\mathrm{km\,s^{-1}}$), (4000 G, 25 $\mathrm{km\,s^{-1}}$), (6000 G, 5 $\mathrm{km\,s^{-1}}$) and (6000 G, 30 $\mathrm{km\,s^{-1}}$).

7.3 Tests

In the coherence regimes, further testing was necessary to quantify the similarity between polarization profiles, and to examine the effects of the variables which are discussed in the LSD theory (see Section 5.1.2) as being important to the scaling of

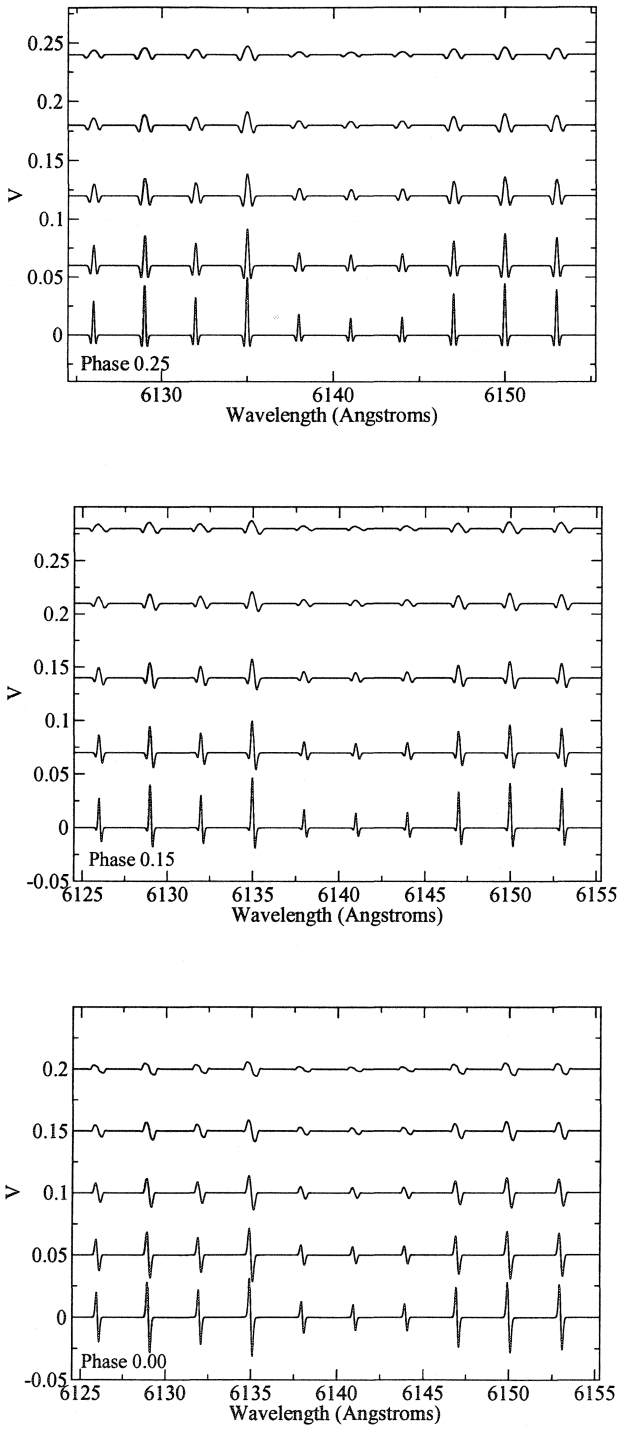

Figure 7.1: Stokes V test profiles at $B = 1000$ G. $v \sin i$ values are 5, 10, 15, 20 & 25 $\mathrm{km\,s^{-1}}$ from bottom to top in each plot. The rotational phase of each is shown.

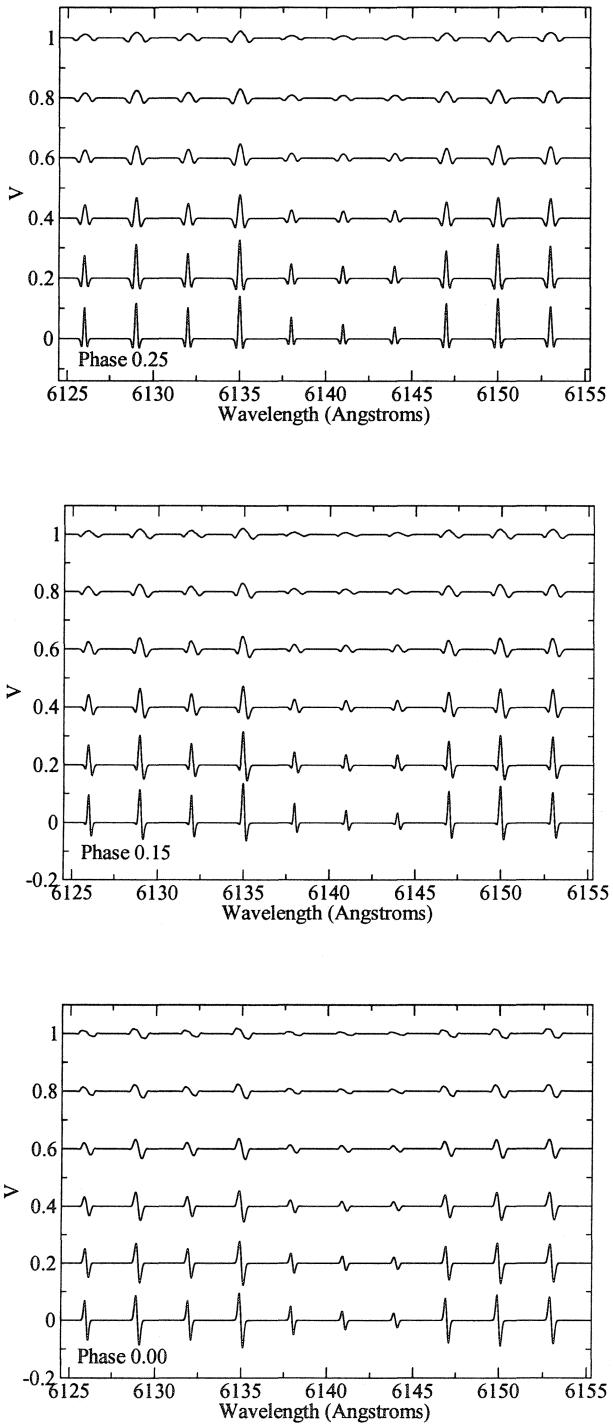

Figure 7.2: Stokes V test profiles at $B = 4000$ G. $v \sin i$ values are 5, 10, 15, 20, 25 & 30 $\mathrm{km\,s^{-1}}$ from bottom to top in each plot. The rotational phase of each is shown.

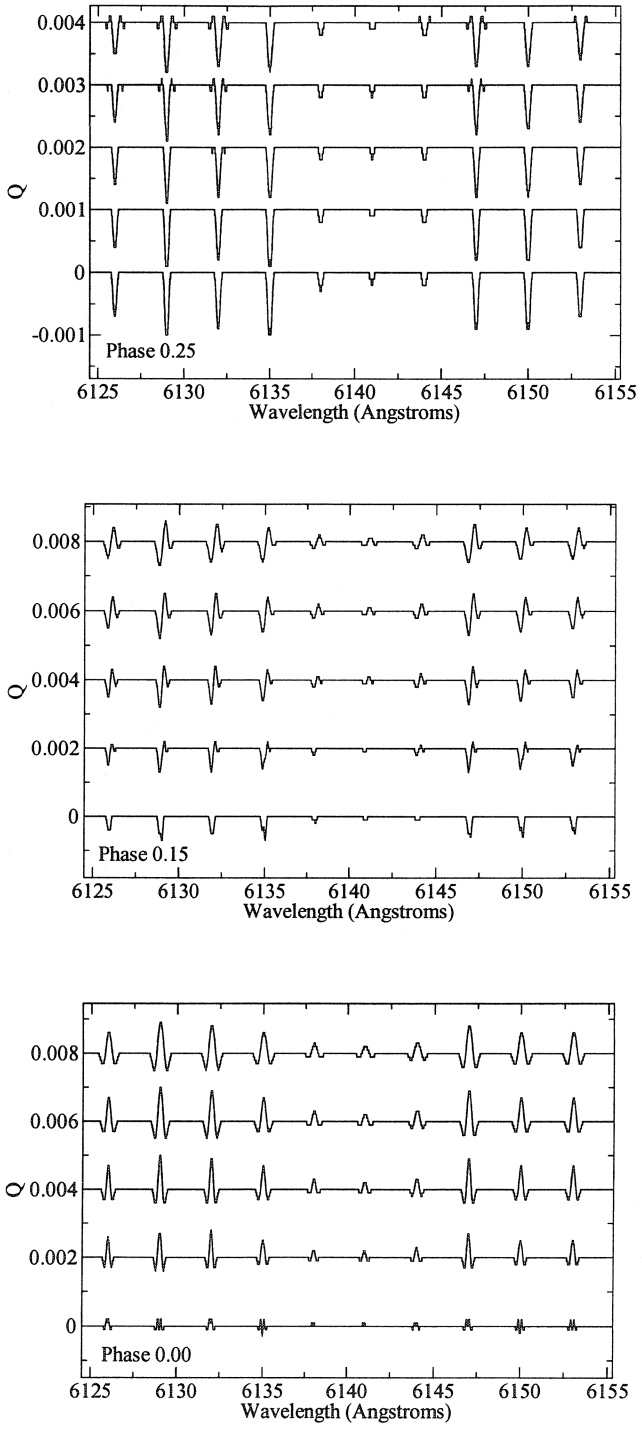

Figure 7.3: Stokes Q test profiles at $B = 500$ G. $v \sin i$ values are 5, 10, 15, 20 & 25 $\mathrm{km\,s^{-1}}$ from bottom to top in each plot. The rotational phase of each is shown.

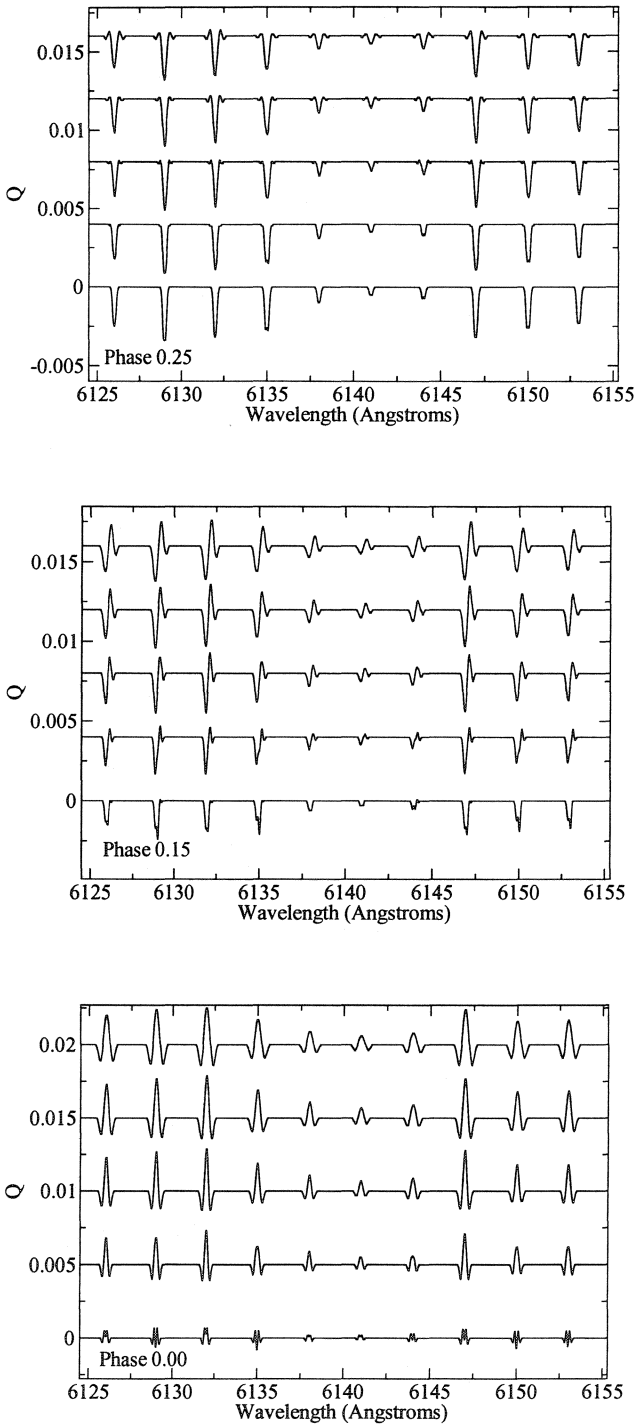

Figure 7.4: Stokes Q test profiles at $B = 1000$ G. $v \sin i$ values are 5, 10, 15, 20 & 25 $\mathrm{km\,s^{-1}}$ from bottom to top in each plot. The rotational phase of each is shown.

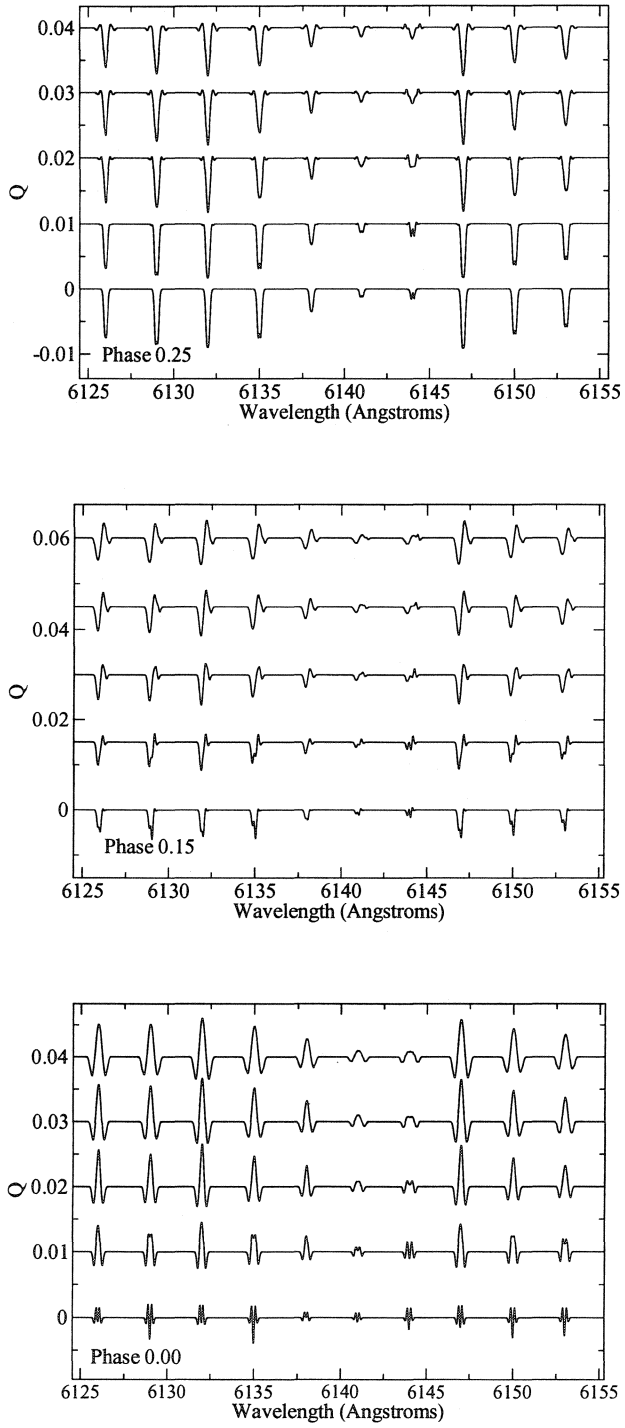

Figure 7.5: Stokes Q test profiles at $B = 2000$ G. $v \sin i$ values are 5, 10, 15, 20 & 25 $\mathrm{km\,s^{-1}}$ from bottom to top in each plot. The rotational phase of each is shown.

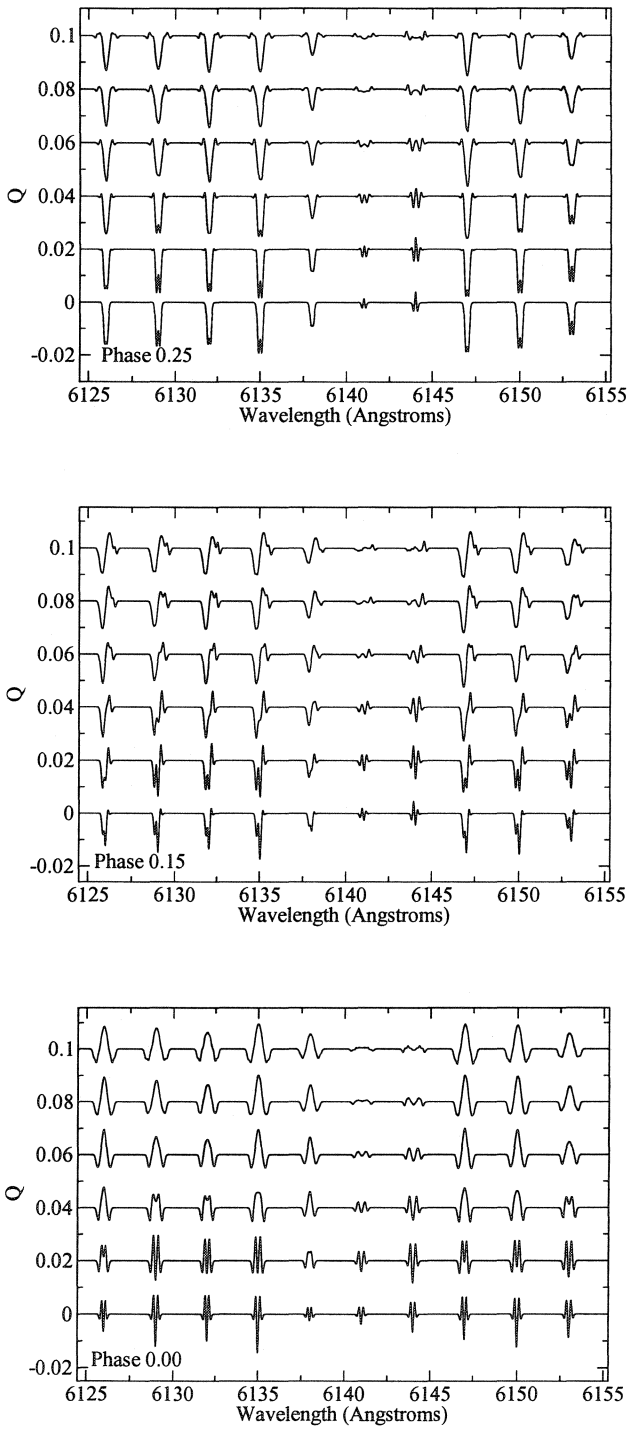

Figure 7.6: Stokes Q test profiles at $B = 4000$ G. $v \sin i$ values are 5, 10, 15, 20, 25 & 30 $\mathrm{km\,s^{-1}}$ from bottom to top in each plot. The rotational phase of each is shown.

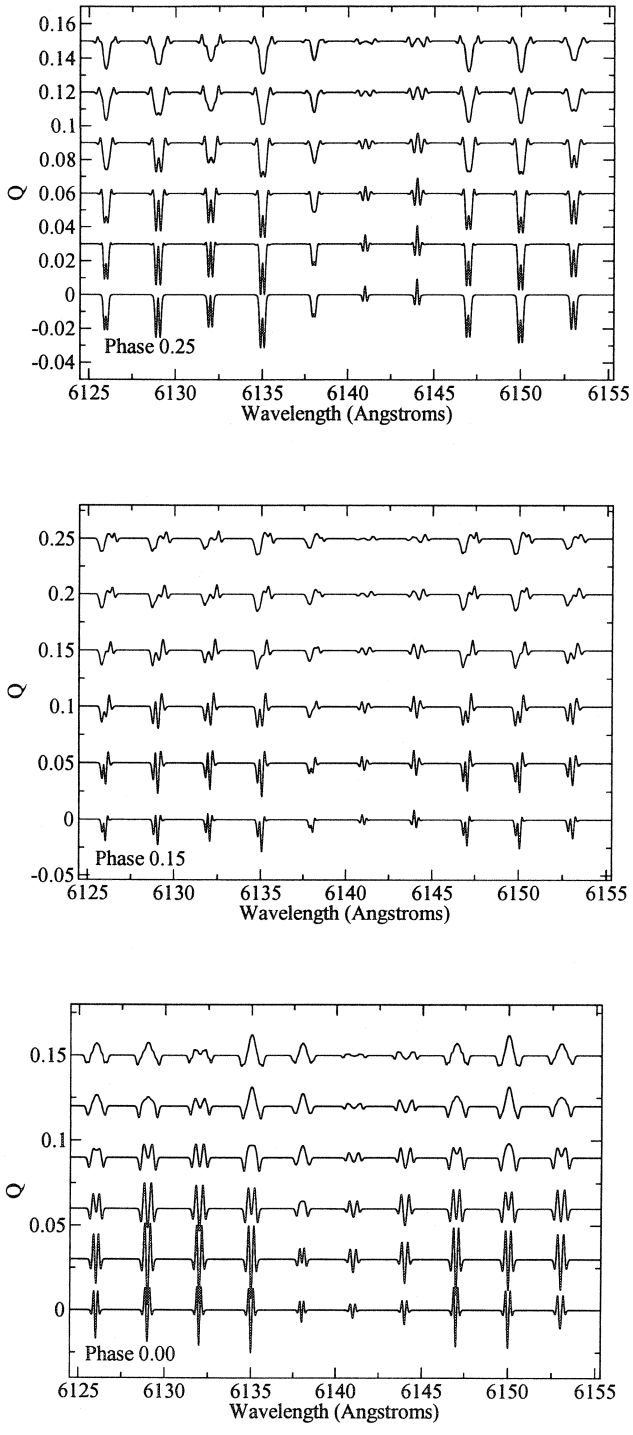

Figure 7.7: Stokes Q test profiles at $B = 6000$ G. $v \sin i$ values are 5, 10, 15, 20, 25 & 30 $\mathrm{km\,s^{-1}}$ from bottom to top in each plot. The rotational phase of each is shown.

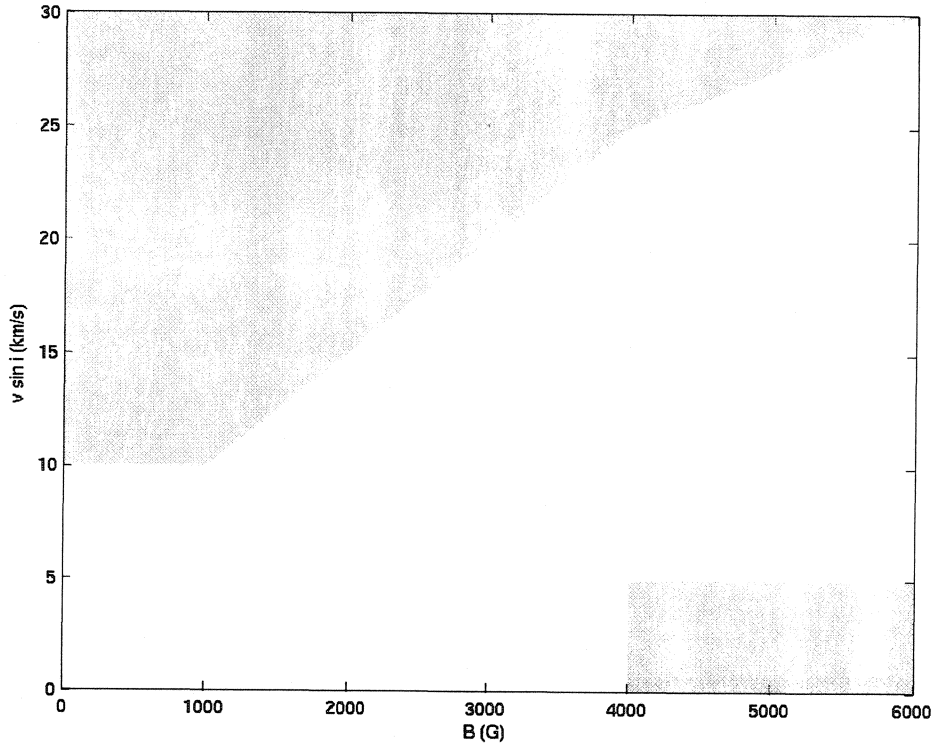

Figure 7.8: Shaded regions are the approximate regimes of $v \sin i$ vs. B in which most Stokes Q polarization profiles have similar shapes. The B ordinate may be considered to be approximately equal to $\bar{g}B$, since most lines have mean Landé factors near 1

the profiles. The effects of varying line depth, Landé factor, magnetic field strength and also rotation velocity were examined.

7.3.1 Line depth

New test spectra were synthesized at the chosen values of B and $v \sin i$ in the previously identified coherence regimes. Stellar and magnetic field parameters were kept the same as previous tests. The new spectra were made up of test lines, identical is all aspects other than their value of $\log(gf)$. Lines were synthesized with values in the range of $-0.4 > \log(gf) > -3.2$, resulting in a range of central line depths, d, (as measured at high resolution and $v \sin i = 0$ km s^{-1}) of $0.73 > d > 0.14$ of the continuum. This definition of d is the same as in the scaling weights, w, used by LSD theory, with larger values of d corresponding to stronger lines.

Stokes V

Examination of the Stokes V profiles shows a monotonic increase of their amplitudes corresponding to increasing line depth. Two examples of the tests of the effect of line depth, for the (1000 G, 20 km s^{-1}) and (4000 G, 25 km s^{-1}) cases, are shown in Figs. 7.9 and 7.10 as plots of V vs. $\log(gf)$. The amplitudes of the Stokes V profiles for both examples were measured at phase 0.00 and plotted with respect to central line depth for the profiles synthesized over the larger range of $\log(gf)$ as discussed above. These relationships are shown in Figs. 7.11 and 7.12.

The relationship seen in Figs. 7.11 and 7.12 is a linear dependence on d for a weak subset of lines ($d \leq 0.5$) and a non-linear dependence for the strongest lines ($d > 0.5$). This is contrary to the linear d dependence in the scaling weights for Stokes V profile in the LSD theory. The likely cause is that as the lines become deeper, they begin to saturate and the line depth grows more slowly with increasing line absorption (whether resulting from increased abundance or, in this test case, increased values of $\log(gf)$). Therefore d does not grow as quickly as V amplitude, and a non-linear relationship between the two arises.

An interesting question is whether or not this non-linearity is important. Adopting a single linear scaling with d certainly is a good description for the weaker set of lines. It also holds approximately true up to $d < 0.6$. Lines stronger than this depth deviate from a linear scaling relationship with d. It appears that one could treat the situation

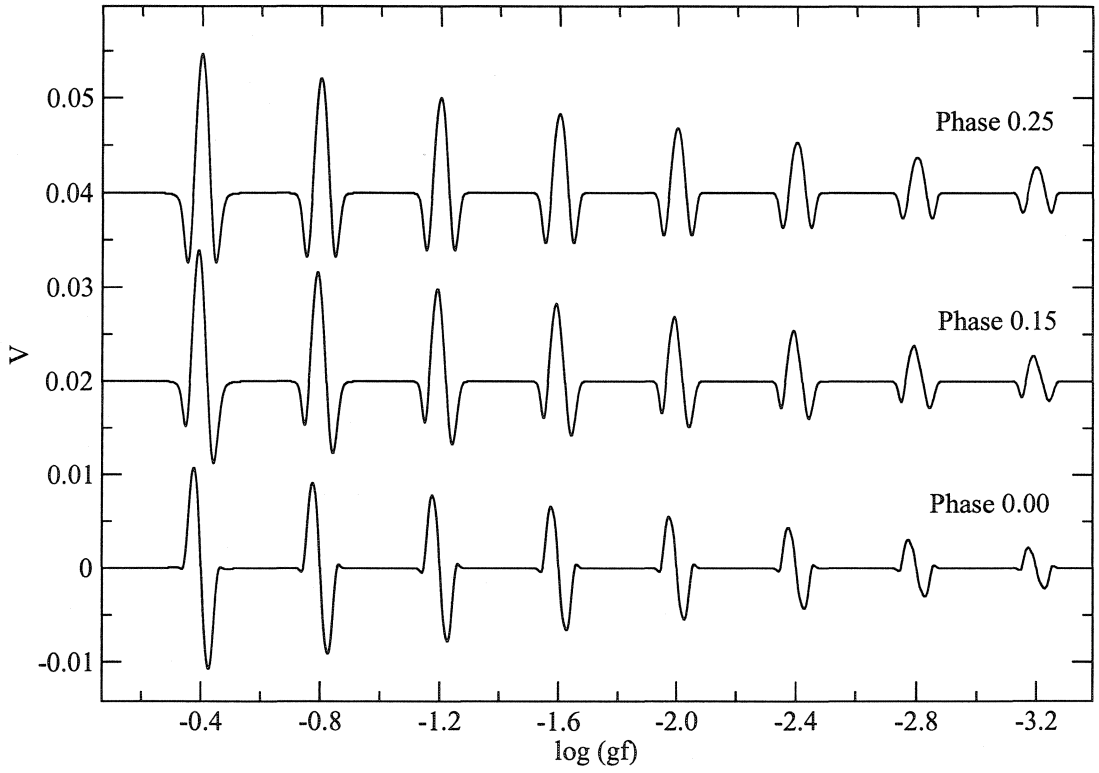

Figure 7.9: $B = 1000$ G,$v \sin i = 20$ km s^{-1}. Stokes V profiles at all phases with $\log(gf)$

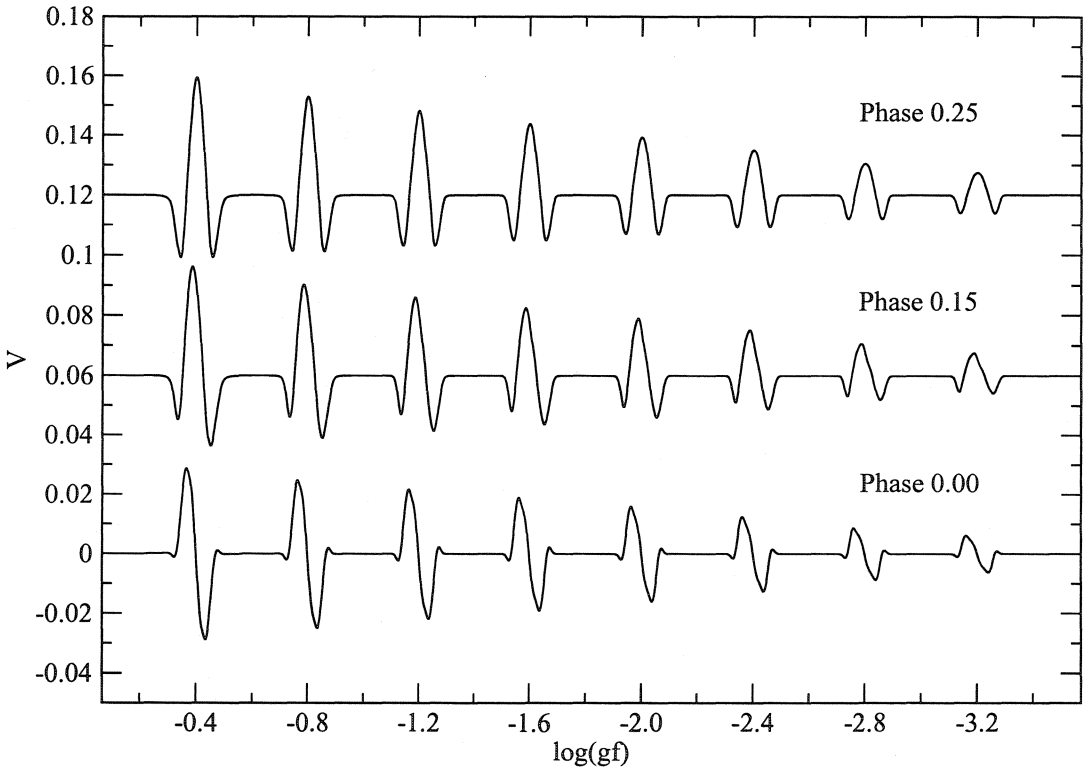

Figure 7.10: $B = 4000$ G,$v \sin i = 25$ km s^{-1}. Stokes V profiles at all phases with $log(gf)$

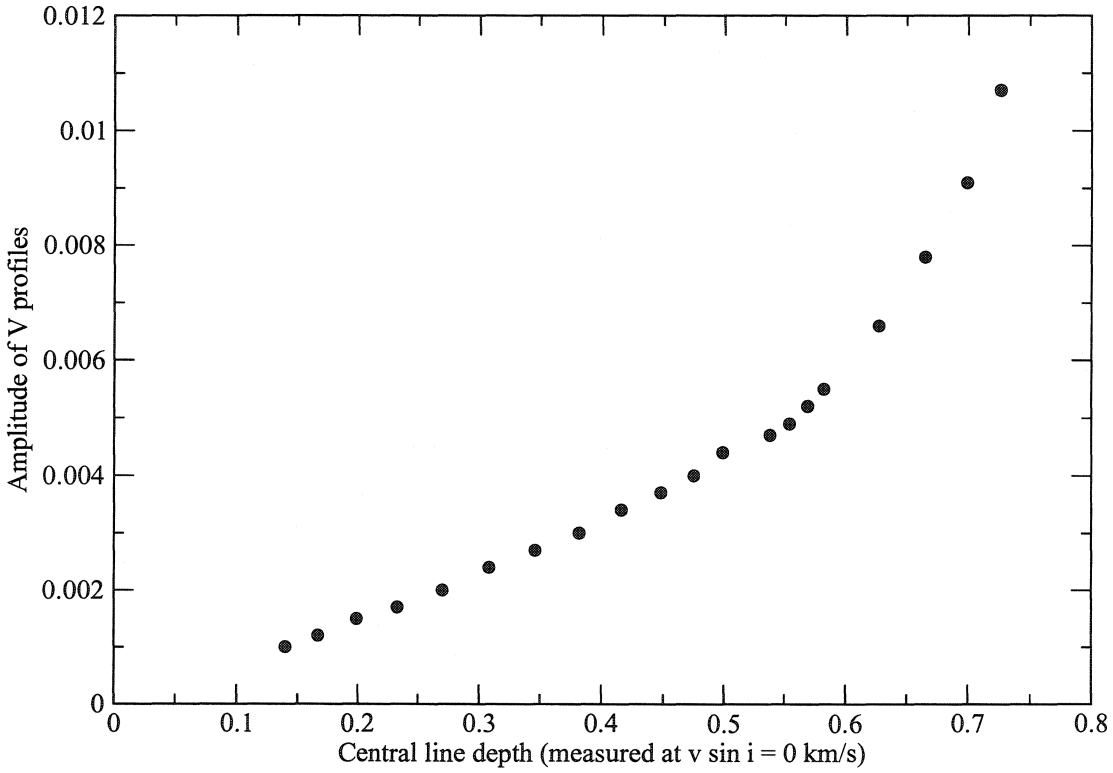

Figure 7.11: $B = 1000$ G,$v \sin i = 20$ km s^{-1}. Amplitude of the Stokes V profiles at phase 0.00 with d

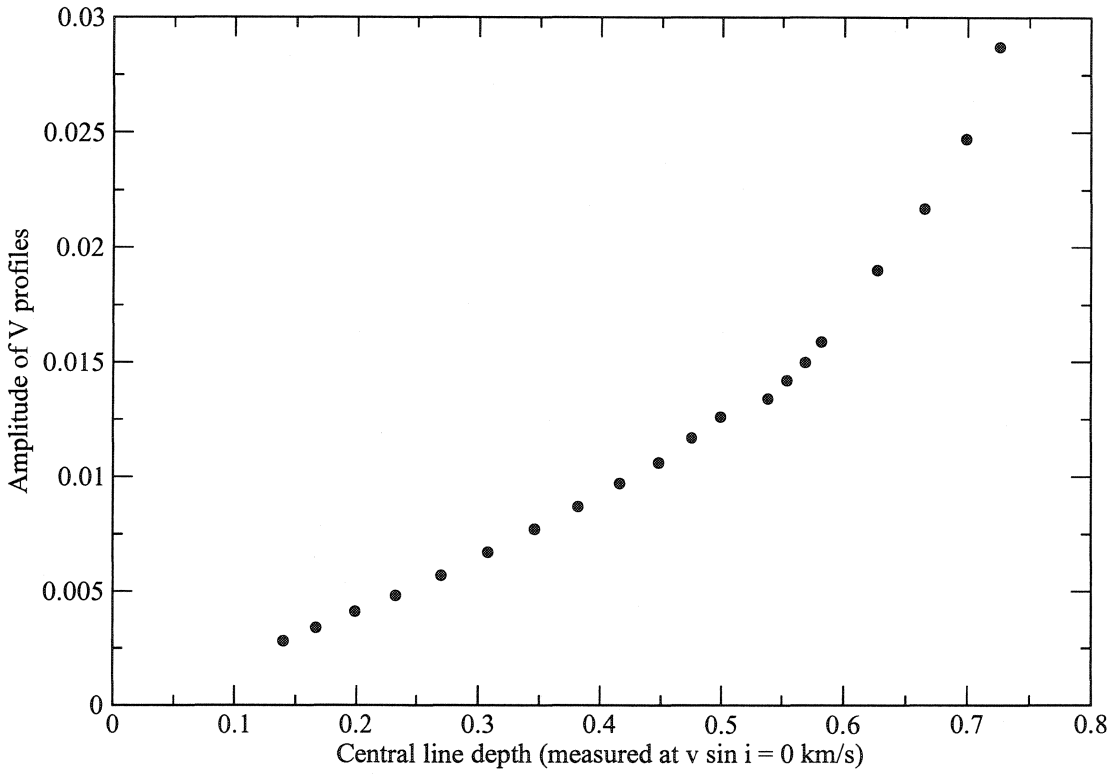

Figure 7.12: $B = 4000$ G,$v \sin i = 25$ km s^{-1}. Amplitude of the Stokes V profiles at phase 0.00 with d

in one of three possible ways: Use only lines weaker than some depth, say $d < 0.6$, and a linear scaling, use all lines with two different scaling relationships based upon a depth criterion, or use a common scaling for all lines.

The first option is potentially reasonable since there are many lines in a real spectrum to choose from, and there will be more weak lines than strong ones. Circular polarization signals are relatively strong in any individual line in the magnetic stars likely to be modelled, and one probably does not need to include the very strongest ones to obtain an LSD mean signature with good S/N. One potential concern is that if one neglects to include the strongest lines in the LSD line mask (thereby removing them from the averaging process), then they will be unaccounted for in the deconvolution procedure. The final LSD mean Stokes V signature from a given spectrum will potentially be contaminated by the unaccounted for strong signatures from blended and neighbouring strong lines. The revision of the LSD line masks to include only weaker lines would certainly have to be tested on real spectra, to see how it would affect the LSD mean V profiles, and deduced field strengths, B_z.

If one decides to retain the strong lines in the averaging, then the decision must be made whether to leave the scaling linear over the whole range of d (as is the current LSD procedure) or to alter it to some power-law for some range in d, as indicated by the above analysis. Our recommendation is to retain the linear scaling, but to note that this will introduce some systematic error in the LSD mean V profiles, as well as in any deduced quantity such as longitudinal field obtained from such profiles. The error will be introduced as a result of the strongest lines including some extra polarization amplitude in their profiles that will be unaccounted for by a linear scaling. The resulting LSD mean profiles will then be slightly more difficult to interpret than if the averaging had been done in a more precise way. Also, measures of longitudinal field from LSD Stokes V profiles will be slightly different than field measurements made using other techniques. The agreement that previous LSD longitudinal field measurements have shown with other types of longitudinal field measurements, even though linear scaling was assumed (see Fig. 1.3, Wade et al. 2000b), reassure us that this approximate scaling appears in almost all cases to be adequate, if not perfect.

Stokes Q

The tests of the depth dependence of Stokes Q profiles revealed that the profiles do *not* exhibit a monotonic dependence on line depth, and that the nature of the

dependence is based on whether the lines are weak or strong. As line depth initially increases, the amplitudes of their corresponding Q profiles increase monotonically to a maximum near $d \sim 0.6$. For depths greater than this value, they *decrease* with increasing d.

In the cases of tests with stronger fields (4000 and 6000 G), only the the Stokes Q profiles corresponding to d greater than some value (near, but not necessarily equal to, the value of d above which the amplitudes decrease) have similar shapes. An example of this may be seen in Fig. 7.13. In this example, the Q profiles corresponding to $\log(gf) \geq -2.0$ ($d \geq 0.6$ in these tests) have the same shape. In the 6000 G cases, only profiles with $\log(gf) \geq -1.6$ ($d \geq 0.65$) are similar in shape. In these strong fields cases, the Q profiles for the coherently shaped strong lines differ in amplitude by only 10% at 4000 G and 6% at 6000 G.

For weaker fields (500 and 1000 G), the Stokes Q profiles retain their shape over the entire range of d as tested (see 7.14), and their amplitudes have been measured as a function of depth. The relationship between the amplitude of the Stokes Q profile at phase 0.00 and line depth in the (1000 G, 20 $\mathrm{km\,s^{-1}}$) case is shown in Fig. 7.15. The relationship has two regions where a linear description of Q amplitude with d is valid. There is a range of approximate linearity between $0.55 > d > 0.25$, which does not appear to extend to the weakest lines. Lines stronger than that range exhibit the strong line behaviour, while weaker lines have amplitudes that are approaching the numeric limit of the computations. In the stronger line region, $d > 0.6$, there is a linear relationship but in the opposite sense. Here, Q profiles decrease in amplitude as lines become stronger.

The question is how to include this depth dependence into the LSD averaging procedure. While one might be tempted to only include lines with depths in the the linear, intermediate range which is obvious in Fig. 7.15, one would be neglecting the possibly very important contribution of strong Q profiles from the strongest lines, as well as allowing for contamination from blended and neighbouring lines, which would be unaccounted for in the average. Since Stokes Q profiles are so weak, the multiplex gain of LSD must be maximized by including as many strong Q profiles in the average as possible. The inclusion of weak lines in the average would be inadvisable for stars with strong fields, given that their shapes are not similar to one another over a wide range in d.

Constraining the LSD line mask to include only strong lines, on the other hand, is

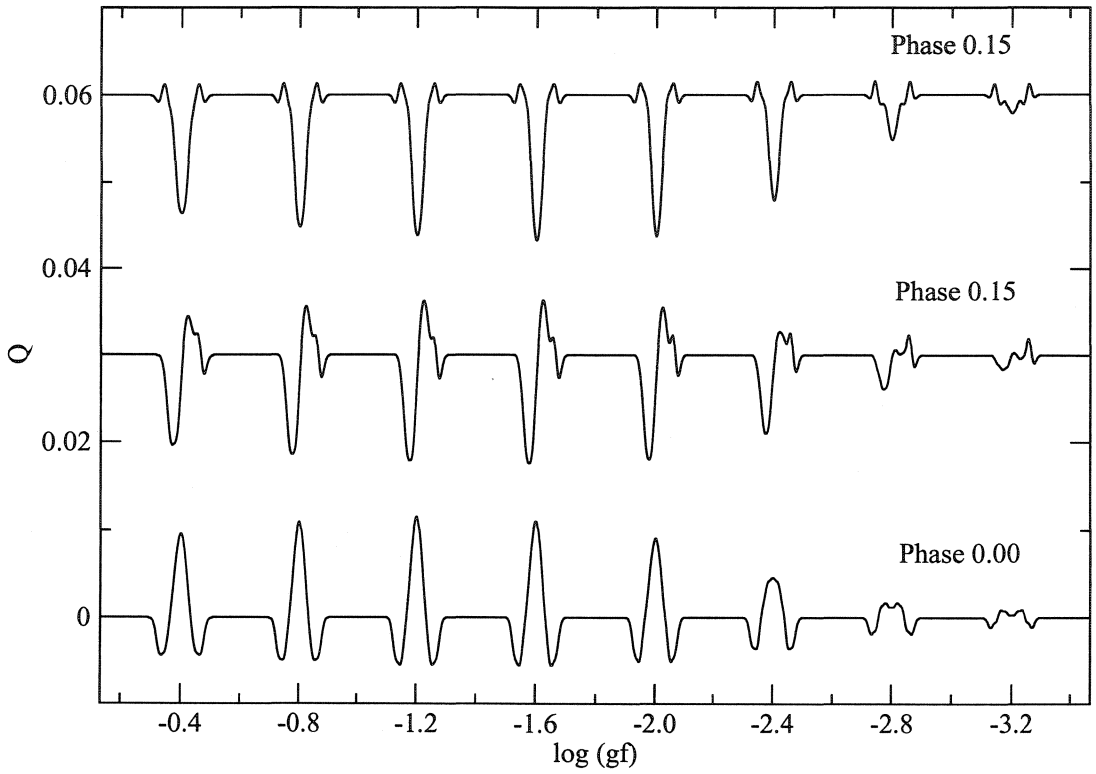

Figure 7.13: $B = 4000$ G, $v \sin i = 25$ km s^{-1}. Stokes Q profiles at three phases with $log(gf)$

quite promising, especially for the regime of strong fields. In this regime, the shapes and amplitudes of Stokes Q profile for the strongest lines change very little with line depth. The treatment of the Q profiles of all strong lines as independent of d for strong field stars (for moderate values of $\bar{g}$) would seem to be a good approximation. In the weaker field cases, it it also possible to approximate the behaviour of strong lines as being independent of d, although doing so introduces more uncertainty than in the strong field case. For example, in the tests at 1000 G, Q amplitudes vary by nearly 30% for lines with depths in the range $d > 0.5$. This level of variation may be too large.

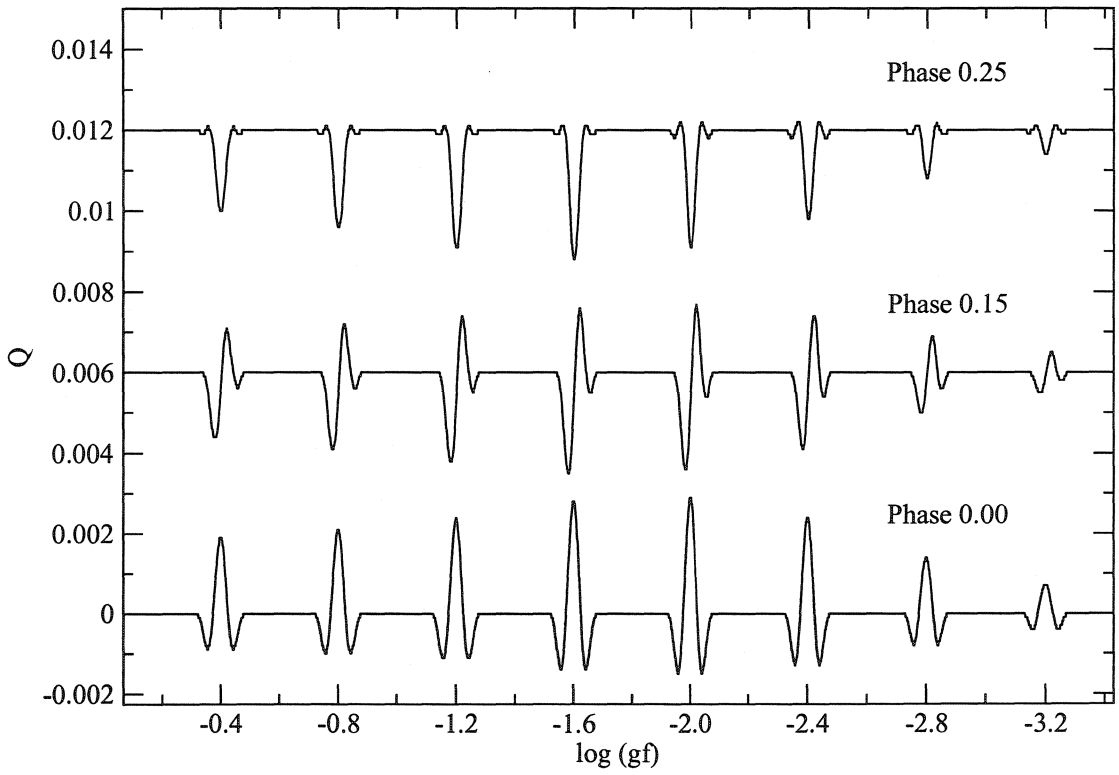

Figure 7.14: $B = 1000$ G,$v \sin i = 20$ km s^{-1}. Stokes Q profiles at all phases with $log(gf)$

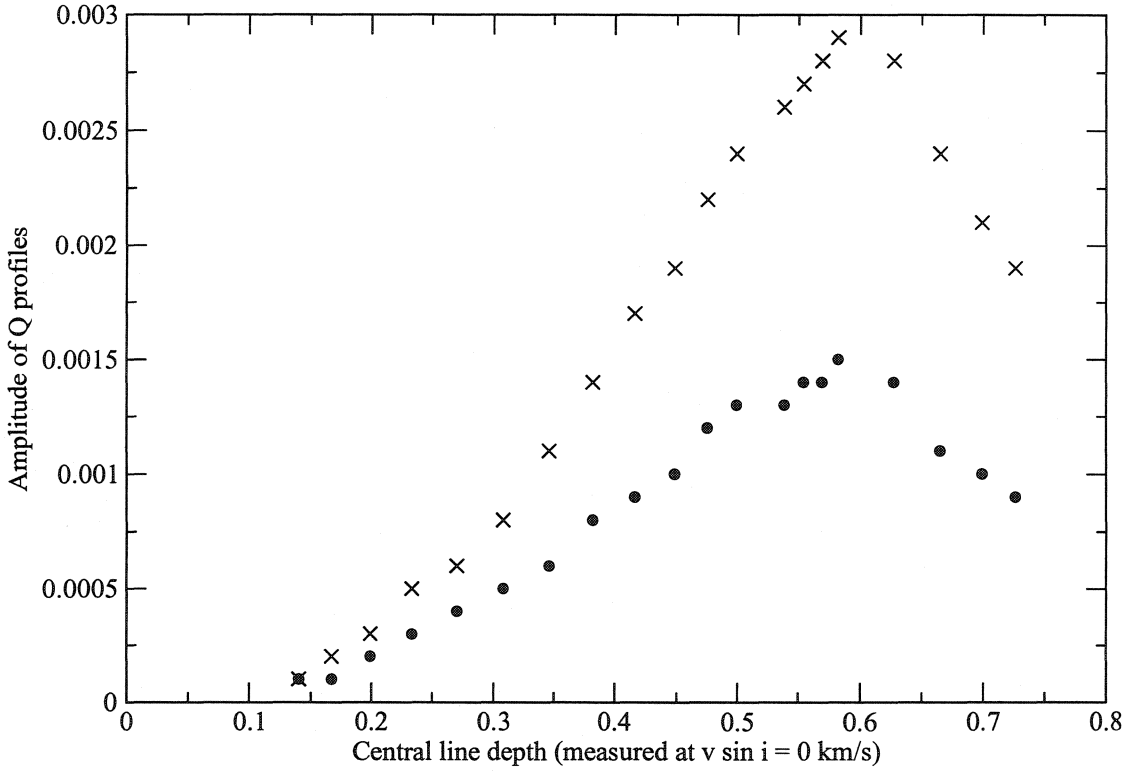

Figure 7.15: $B = 1000$ G,$v \sin i = 20$ km s^{-1}. Amplitude of the Stokes Q profiles at phase 0.00 with d. Circles are the amplitudes of the negative peaks of the profiles, 'X's are the amplitudes of the positive peaks.

7.3.2 Landé factor and magnetic field

The determination of the scaling of the Stokes polarization profiles with mean Landé factor ($\bar{g}$) is inherently tied to the values of stellar magnetic field used in each test, since it is the product $\bar{g}B$ that determines the Landé pattern width that magnetic field produces in any given line. Although the previous coherence regimes were determined at a variety of values of B and for a range of $\bar{g}$ (see Table 7.1), no extreme values of $\bar{g}$ were used, i.e. $\bar{g}$ was always less than 2, which is correct for all but a small number of real spectral lines.

To test the effect of magnetic field, which is manifested in the product $\bar{g}B$, new test spectra were calculated at single values of B (chosen in the coherence regimes) while varying $\bar{g}$ and then at a single value of $\bar{g}$ while varying B. In each single line, any dependence on one of the two variables must be ascribed to their product, whether it is in the scaling of polarization profile amplitudes, or the determination of magnetic regimes where the assumption of coherent profile shapes breaks down. In a given star, $\bar{g}$ will vary from line to line while B will not. Hence, it is useful to examine the Landé factor dependence.

In the new test spectra, stellar and magnetic field parameters were those from Section 7.2.3. The spectra generated to test the effect of varying Landé factor were comprised of test lines similar to the one originally computed at 6132 Å, which is a simple triplet ($g_1 = g_2 = \bar{g}$), in order to simplify its Zeeman splitting. This line was replicated throughout a wavelength window, where each new line was varied in its value of Landé factor in the range of $0.4 < \bar{g} < 2.6$, in increments of 0.2.

The effect of magnetic field strength on the polarization profiles were investigated independently by computing additional test spectra using the set of 27 strong lines from the coherence regime tests, for a range of field strengths from 500 G $< B <$ 6000 G, in 500 G increments. Since the coherence regime tests showed that all field strengths resulted in good coherence in Q profiles at higher rotation velocities, the test spectra were calculated at $v \sin i = 25$ km s^{-1}. Stellar parameters remained unchanged.

Since only the strongest lines show coherence in Q at all field strengths, even at high rotation velocity, the effect of magnetic fields on the polarization profiles was measured in the two strongest lines: the Cr II lines initially synthesized at 6135 Å and 6150 Å, which have respectively $\bar{g} = 1.16$ and 1.06. The amplitudes of both lines' polarization profiles were measured for each spectrum at phase 0.00.

Stokes V

Examining the effects of Landé factor on the Stokes V profiles of the test lines revealed that in all cases of field strength and rotation velocity, the V profiles retain their shape. An example is seen in Fig. 7.16 for the case of (1000 G, 20 $\mathrm{km\,s^{-1}}$), but the behaviour of a monotonic increase in V amplitude with $\bar{g}$ is replicated in all test spectra. Examples of the dependence of the amplitude of Stokes V profiles on Landé factor are shown in Figs. 7.17, 7.18 and 7.19 for tests at (1000 G, 20 $\mathrm{km\,s^{-1}}$), (4000 G, 25 $\mathrm{km\,s^{-1}}$) and (6000 G, 30 $\mathrm{km\,s^{-1}}$). In the case of the smallest field values (500, 1000 & 2000 G), an example of which is shown in Fig. 7.17, the dependence of Stokes V amplitude on $\bar{g}$ is very well described as a linear relationship over the entire range of $\bar{g}$. This corresponds to a linear dependence at least in the range $200 < \bar{g}B =< 5200$ G.

For the case of a stronger field (4000 G), a single linear relationship does a *reasonable* job in describing the relationship between Stokes V amplitude and $\bar{g}$ over the range of Landé factor, but most especially for lower values of $\bar{g}$. There is some indication of a slight deviation from linearity which occurs near $\bar{g} > 1.6$, or $\bar{g}B = 6400$ G. This is further confirmed by examining the relationship between Stokes V amplitude and Landé factor for the (6000 G, 30 $\mathrm{km\,s^{-1}}$) case, as shown in Fig. 7.19. In this case, the deviation from linearity occurs at $\bar{g} = 1.2$, corresponding to $\bar{g}B = 7200$ G. The linear relationship, $V \propto \bar{g}$, is thus found to be a valid approximation in the range $\bar{g}B < 7000$.

The relationship between the amplitudes of the Stokes V profiles and the stellar magnetic field, held at constant values of $\bar{g}$, is shown in Fig. 7.20. This relationship is monotonic such that V amplitudes consistently grow with increasing B. The relationship is approximately linear over the range of magnetic field, which is predicted by the LSD theory from Section 5.1.2. A log-log analysis over the entire range of magnetic field results in a slight non-linearity as $V \sim B^{1.07-1.08}$. If one only takes the data for $B \leq 5000$ G, at which point the line appears visually to begin to curve, then the power-law relationship is as $B^{1.04}$. In either case, a simple linear relationship, $V \propto B$, is an accurate approximation for these data, at least in the range $\bar{g}B \leq 6000$ G.

The question is now how to include lines of varying Landé factor, at a given stellar magnetic strength, in the LSD averaging process. For stars of weak magnetic field, say $B \leq 2000$ G, one may reasonably expect a linear scaling relation to be valid for use in averaging lines of any value of $\bar{g}$ found in a stellar spectrum. For stars with stronger fields, only those lines which satisfy the $\bar{g}B \leq 7000$ G will linearly scale in

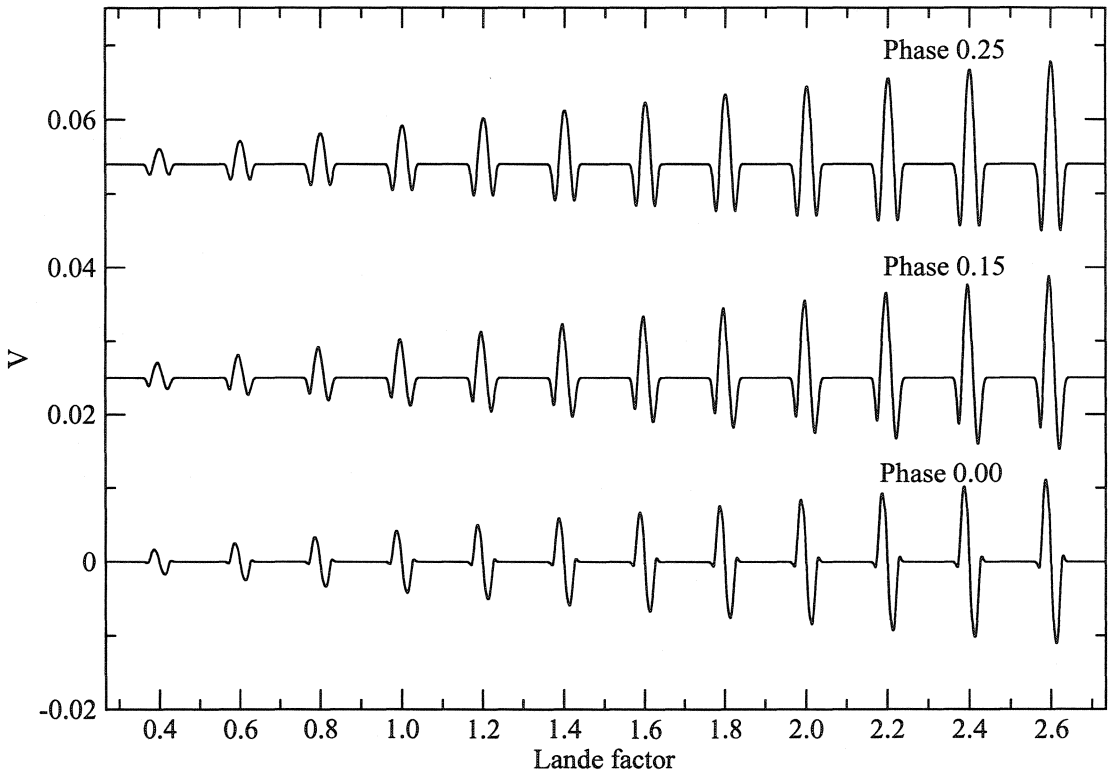

Figure 7.16: $B = 1000$ G, $v \sin i = 20$ km s^{-1}. Stokes V profiles for all three phases as a function of Landé factor.

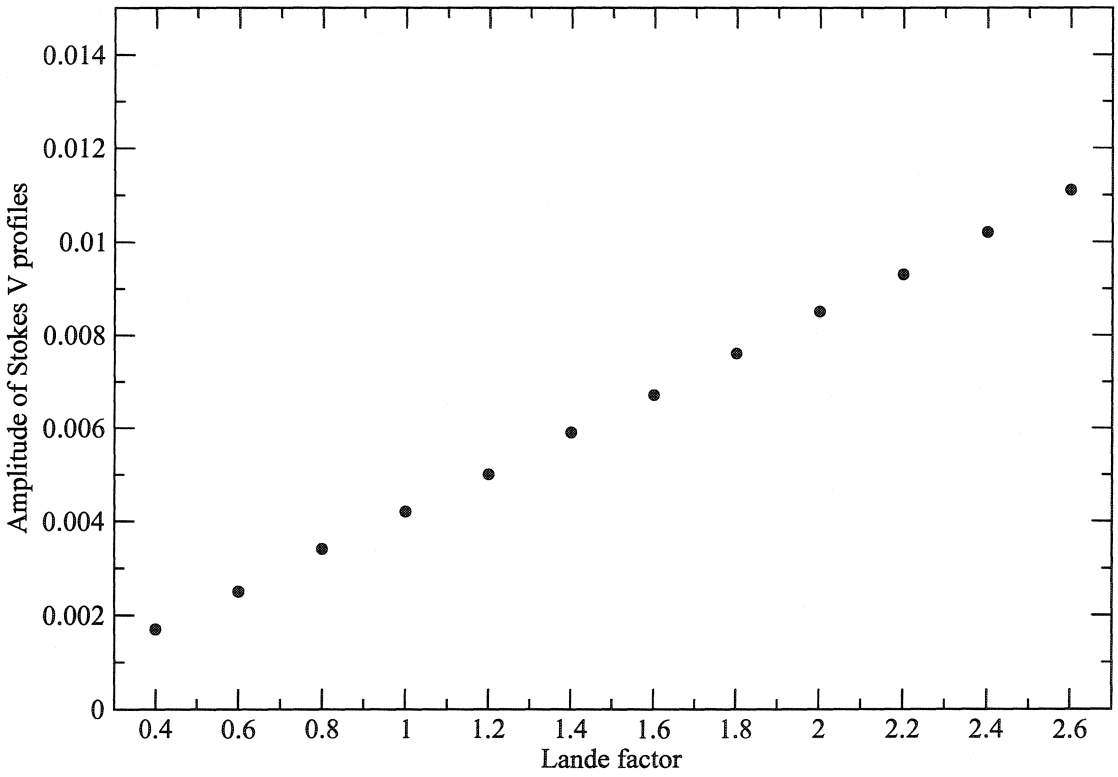

Figure 7.17: $B = 1000$ G, $v \sin i = 20$ km s^{-1}. Amplitude of Stokes V profiles at phase 0.00 as a function of Landé factor

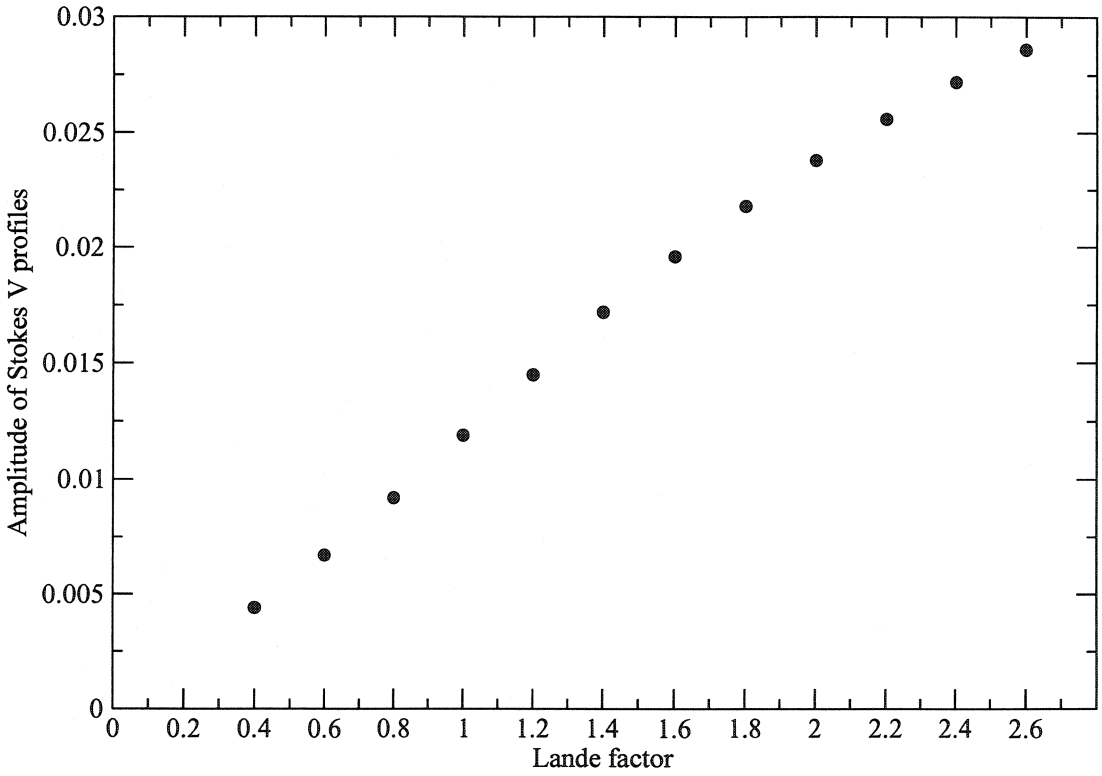

Figure 7.18: $B = 4000$ G, $v \sin i = 25$ km s^{-1}. Amplitude of Stokes V profiles at phase 0.00 as a function of Landé factor

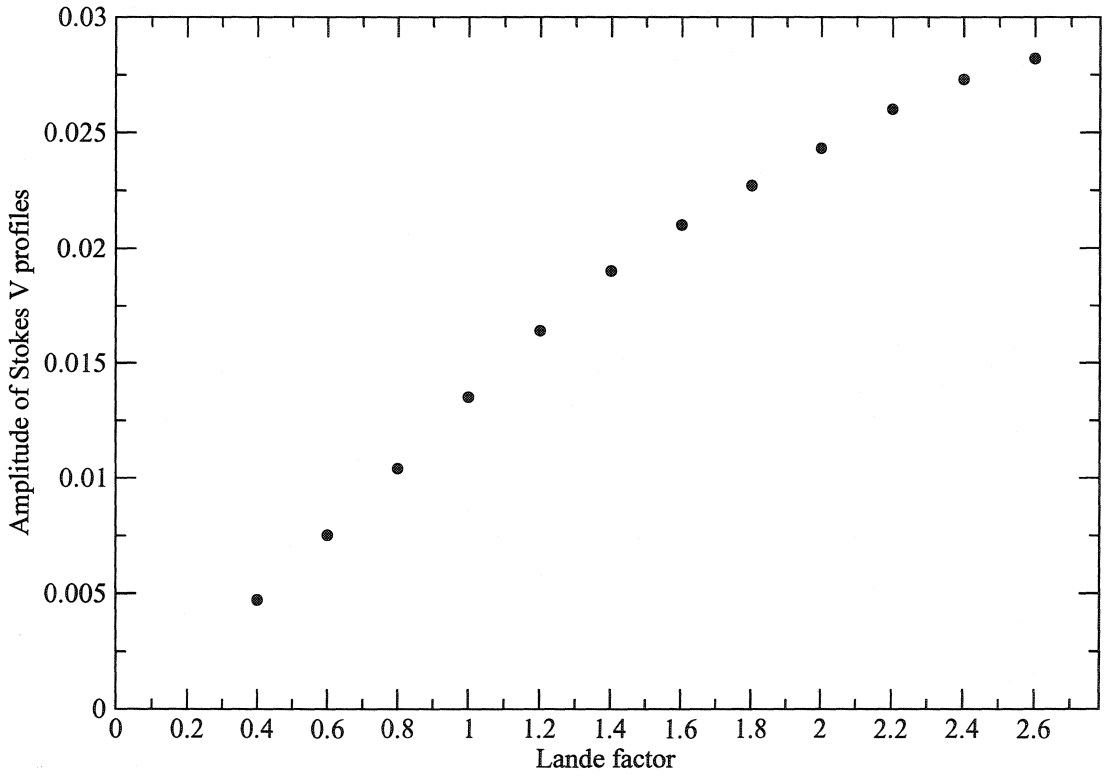

Figure 7.19: $B = 6000$ G, $v \sin i = 30$ km s^{-1}. Amplitude of Stokes V profiles at phase 0.00 as a function of Landé factor

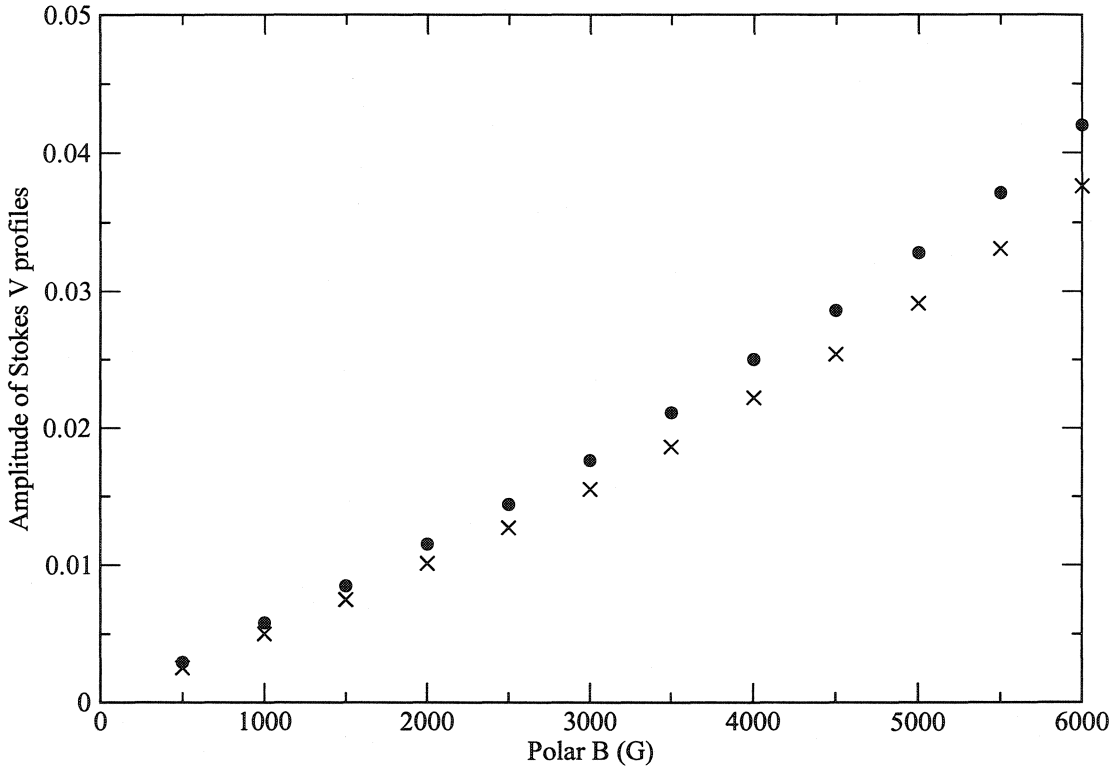

Figure 7.20: Amplitudes of Stokes V profiles, measured at phase 0.00 and $v \sin i = 25$ km s^{-1}, as a function of polar magnetic field. Filled circles are the amplitude of the 6135 Å test line ($\bar{g} = 1.16$), 'X's are of the 6150 Å test line ($\bar{g} = 1.06$)

amplitude with Landé factor. In other words, if a star with a strong field is observed, then using a linear scaling with $\bar{g}$ for Stokes V profiles from lines with even moderate Landé factors will introduce a systematic error in the LSD mean V profiles. The error will be the result of the lines with large values of $\bar{g}$ contributing less polarization signal to the average than is expected from their Landé factors. The stronger the field, the greater this error will be.

The importance of this error, however, is reduced when one considers the nature of the lines that make up a typical stellar spectrum. More than 95% of the spectral lines in a typical Ap spectrum have $\bar{g} < 2$, thus helping to validate the linear scaling for all lines at moderately high values of B, since nearly all the lines will be scaled correctly. At extreme values of B, however, the linear scaling becomes less valid even at moderate $\bar{g}$ values, and the results from using LSD with its current linear scaling weights must be considered in this light. One may be tempted to neglect lines whose values of $\bar{g}$ (for the star's magnetic field strength) correspond to deviations from the linear relationship. This may be a valid treatment, although strong Stokes V signatures for some of the lines with large $\bar{g}$ values may contaminate the averaging process, if left unaccounted for.

Stokes Q

The tests of the mean Landé factor ($\bar{g}$) dependence of the Stokes Q profiles showed that for weak fields (500 and 1000 G), the shapes of the profiles remained similar and the amplitudes increased with increasing $\bar{g}$ (see 7.21). The relationship between the amplitude of the Stokes Q profiles and $\bar{g}$ for the tests at (500 G, 20 $\mathrm{km\,s^{-1}}$) and (1000 G, 20 $\mathrm{km\,s^{-1}}$), measured at phase 0.00, may be seen in Figs. 7.22 and 7.23. Each plot shows the monotonic increase in the size of the profiles with Landé factor. The relationship for the 500 G case is approximately linear for $\bar{g} > 1.2$, while in the 1000 G case, it is linear for $\bar{g} > 0.6$, both corresponding to $\bar{g}B > 600$ G. It must be noted that the linear dependence used in LSD scaling is of the form $Q = A\bar{g}$ (A some proportionality constant), and not $A\bar{g} + C$ (C some intercept).

Examining the plot for the 500 G case, and concentrating on the points for values of $\bar{g} < 1.2$, a quadratic relationship, $Q \propto \bar{g}^2$, describes the data very well. Caution must be stressed not to over-interpret this result since the amplitudes at the lowest field strengths and Landé factors are near the numeric limit of the calculations.

For strong fields at high rotation velocity, the Q profiles initially grow with in-

creasing $\bar{g}$. Then the profiles begin to change shape and Q profiles generally become smaller in peak-to-peak amplitude, but increasingly complex. As $\bar{g}$ increases further, the profiles continue to change shape and begin to increase in amplitude once again. The may be seen in the example of Fig. 7.25. For this example, the Stokes Q profiles maintain their similar shape only at $\bar{g} \leq 1.2$, corresponding to $\bar{g}B < 4800$ G. For the 6000 G test at $v \sin i = 30$ km s^{-1}, the Stokes Q profiles retained their coherence for $\bar{g} \leq 0.8$, again corresponding to $\bar{g}B < 4800$ G. in each case, the amplitudes of the Stokes Q profiles change very little as Landé factor is varied, while they remain coherent in shape.

For the strong field cases at low rotation velocity, Stokes Q profiles do grow initially with Landé factor, but their shapes change as $\bar{g}$ varies from the 0.4 to some intermediate value. An example is shown in Fig. 7.24 for the (4000 G, 5 km s^{-1}) case. Here, coherent profiles exist in all three phases only at $\bar{g} \geq 2.2$, or $\bar{g}B \geq 8800$ G. The test profiles for the (6000 G, 5 km s^{-1}) case exhibit the same behaviour with Landé factor, becoming coherent in shape for $\bar{g} \geq 1.6$, or $\bar{g}B \geq 9600$ G. After becoming coherently shaped in each case, the amplitudes of the Stokes Q profiles change very little in amplitude with increasing $\bar{g}$.

The relationship between the amplitudes of the Stokes Q profiles and the stellar magnetic field, holding $\bar{g}$ constant, is shown in Fig. 7.26. The increase of Q amplitudes with B is approximately linear over the range 1500 G $< B <$3500 G. As the field increases past about 4000 G, the Q amplitudes increase more slowly until they level off at 5500 G, and then decrease. The B^2 dependence of the Q profiles as given in the LSD theory from Section 5.1.2, is not an accurate description of these data, although there may be a region of $Q \propto B^2$ dependence which exists for $B(= \bar{g}B) < 1000$ G.

In order to account for the dependence on Landé factor in Stokes Q profiles to be used in the LSD averaging, one must treat three cases separately: weak fields, strong fields with low rotation velocity and strong fields with high rotation velocity. In the case of weakest fields, for $\bar{g}B < 1000$ G, our data are not inconsistent with a quadratic scaling of $V \propto (\bar{g}B)^2$, which is what is used as the scaling weights from the LSD theory. As $\bar{g}B$ increases, this quadratic relationship begins to be a poorer representation of the data, and is differs from the observed relationship between Q and B (or $(\bar{g})$ by more than 50% by the time $\bar{g}B$ reaches 2500 G. But for weak-field stars, say of $B < 1000$ G, the inclusion of lines in the averaging over the entire range of possible Landé factors, and using a quadratic scaling is a valid way to perform

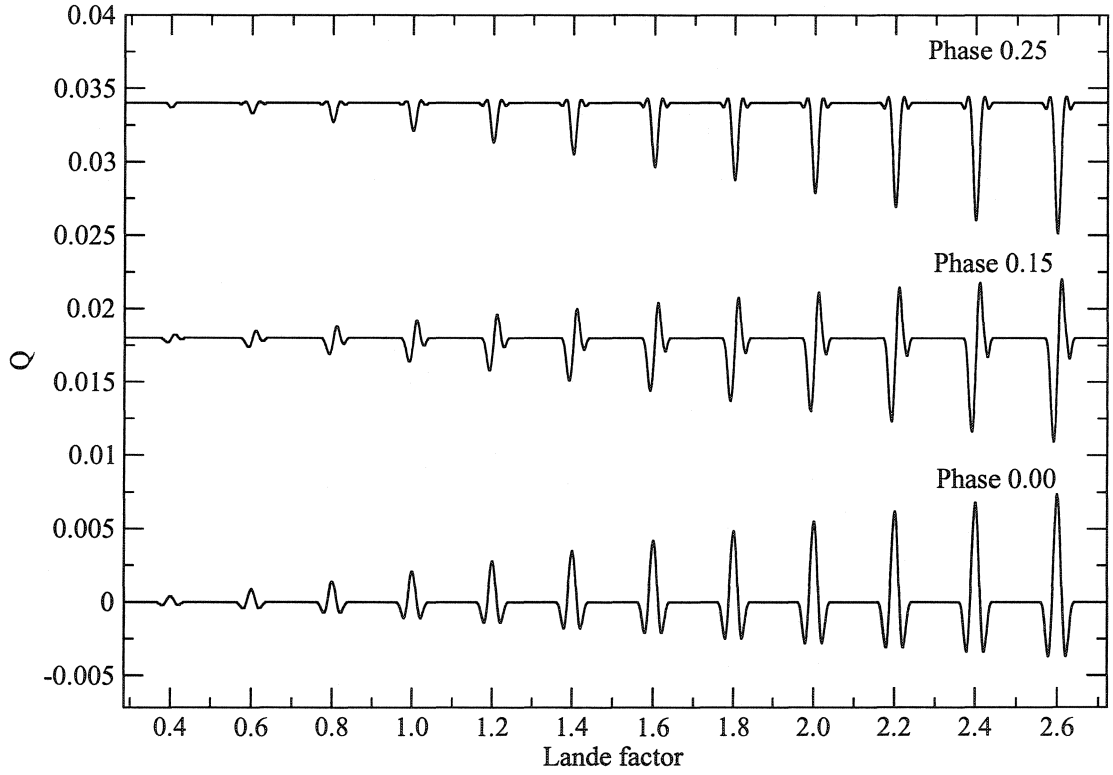

Figure 7.21: $B = 1000$ G, $v \sin i = 20$ km s^{-1}. Stokes Q profiles at all phases as a function of Landé factor.

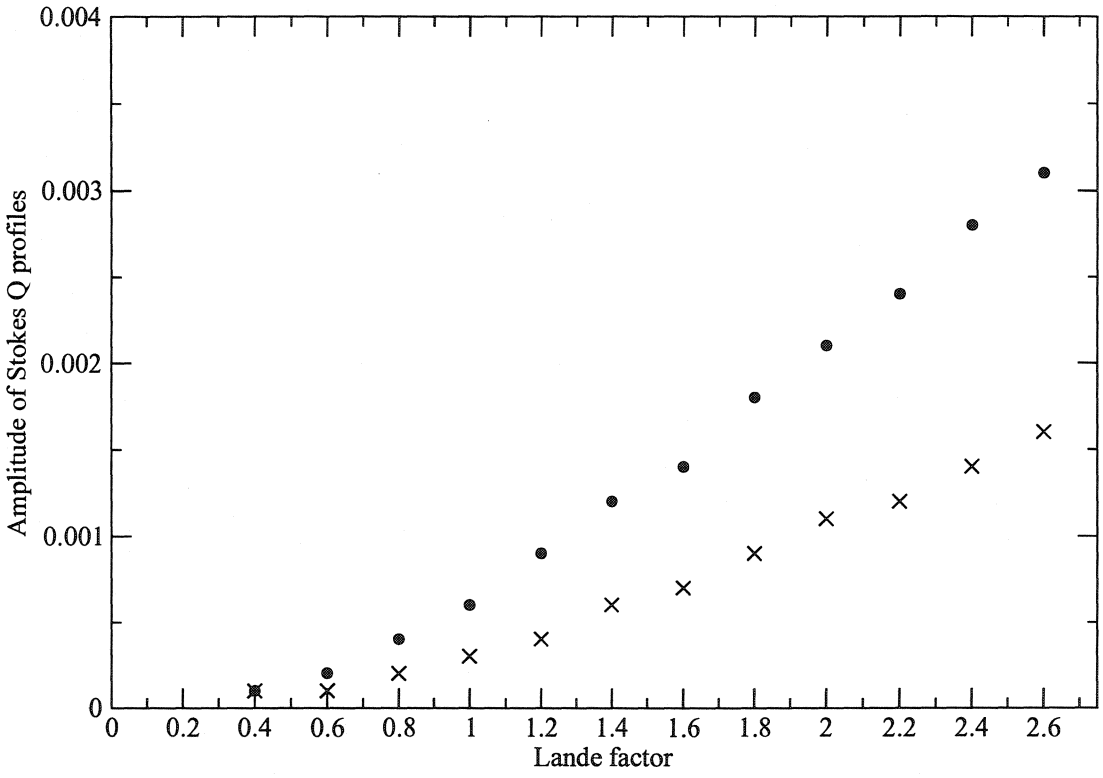

Figure 7.22: $B = 500$ G, $v \sin i = 20$ km s^{-1}. Amplitude of Stokes Q profiles at phase 0.00 as a function of Landé factor. Circles are the amplitudes of the positive peak of each profile, 'X's are those of the negative peak.

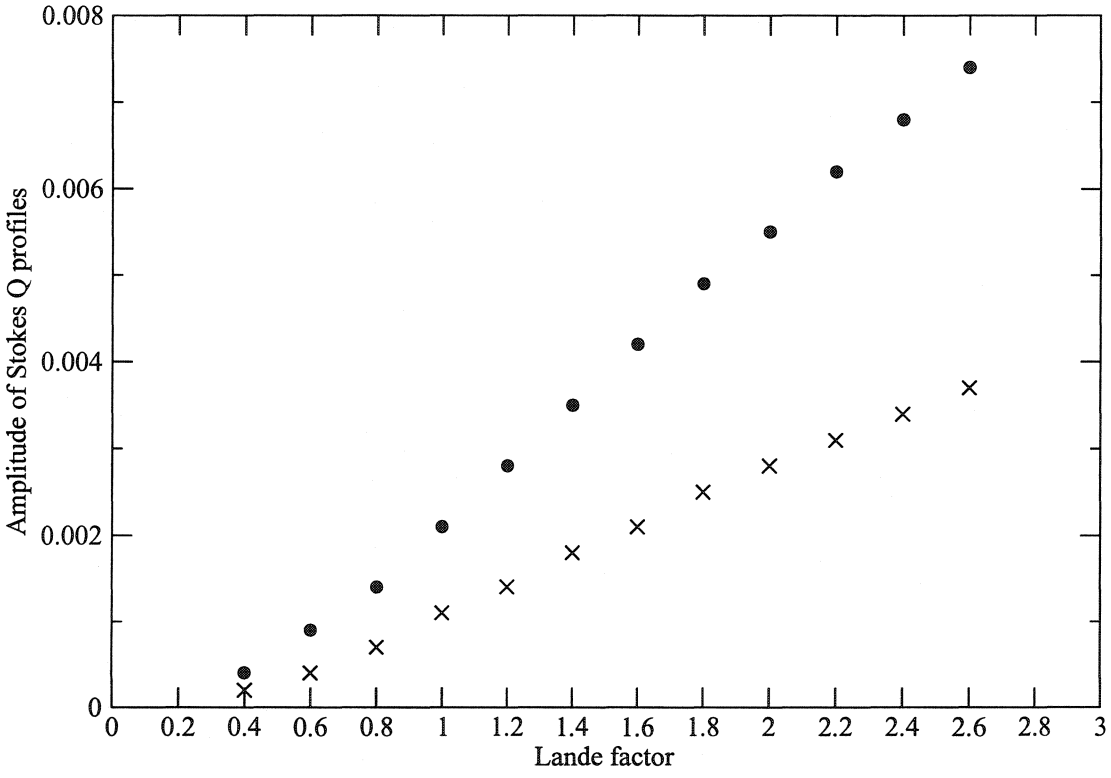

Figure 7.23: $B = 1000$ G, $v \sin i = 20$ km s^{-1}. Amplitude of Stokes Q profiles at phase 0.00 as a function of Landé factor. Circles are the amplitudes of the positive peak of each profile, 'X's are those of the negative peak.

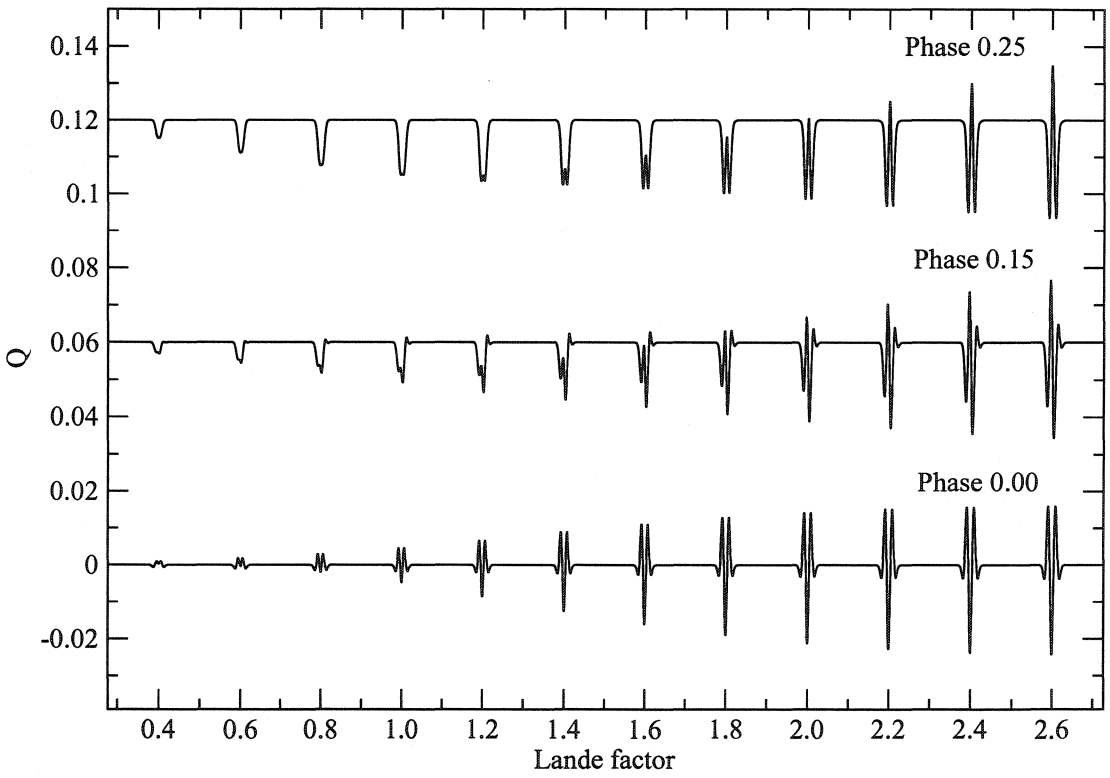

Figure 7.24: $B = 4000$ G, $v \sin i = 5$ km s^{-1}. Stokes Q profiles at all phases as a function of Landé factor

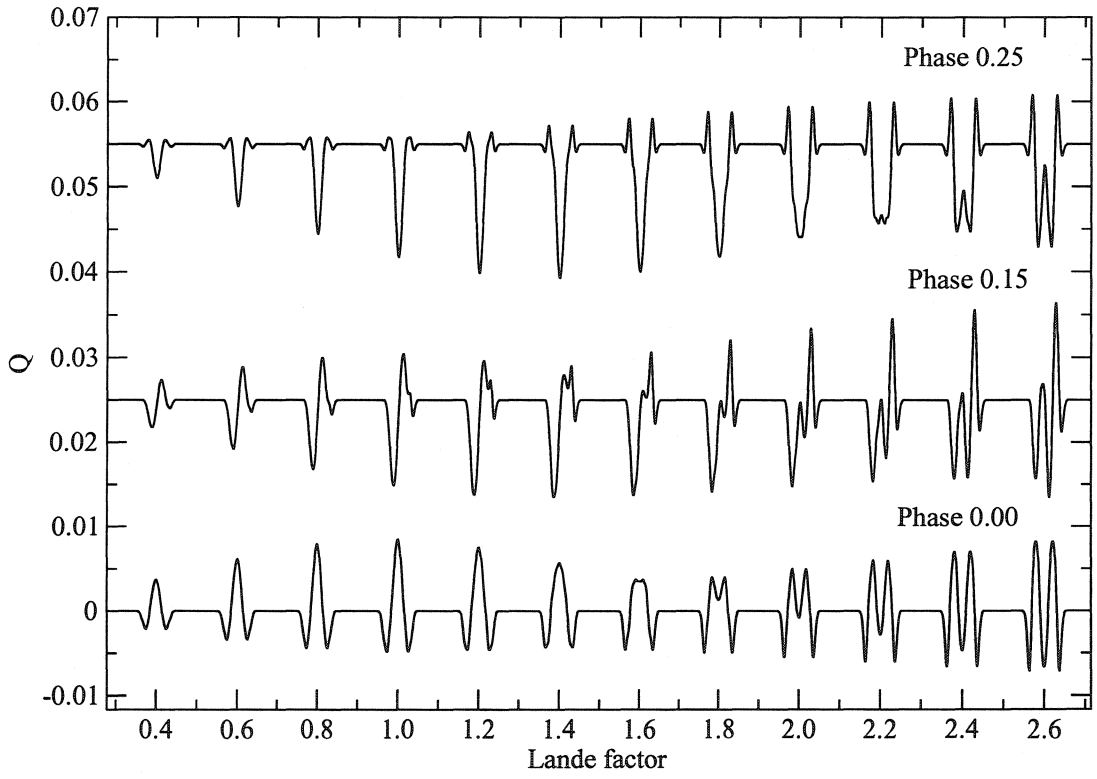

Figure 7.25: $B = 4000$ G, $v \sin i = 25$ km s^{-1}. Stokes Q profiles at all phases as a function of Landé factor

LSD.

For strong field stars at high rotation velocity, one is strongly restricted in which line profiles may be included in the LSD averaging. Only lines for which $\bar{g}B$ is less than about 5000 G are found to be coherent in shape, across a range of $\bar{g}$ values, in the above tests. Therefore, only those lines that satisfy that criterion, for the star's magnetic field strength value, should be used in the average. As B increases, profiles from lines with an increasingly smaller range of $\bar{g}$ values may be added coherently. At some extreme field strengths, it may only be possible to find coherence in profiles from lines with a very small range in Landé factor, say some $\bar{g} \pm 0.1$. One advantage in this regime of strong fields and high rotation velocity is that if an adequate number of lines can be found for which the $\bar{g}B < 5000$ G criterion is satisfied, then the amplitudes of the profiles are relatively independent of $\bar{g}$.

For the case of strong fields and low rotation velocity, coherently shaped profiles are found only at the *highest* values of Landé factor. Again, one is restricted to only including coherently shaped Stokes Q profiles in the LSD averaging, which is satisfied only for values of $\bar{g}B$ greater than about 9000 G. At field strengths of 4000 G, a stellar spectrum will likely have few or no lines which fit this criterion. But this criterion of coherent shape will be easier to meet for stars with even stronger magnetic fields (and low $v \sin i$), and not harder as it is for the strong field, high rotation velocity case. Performing LSD on the Stokes Q spectra of stars in the strong field and low rotation velocity regime will be somewhat simplified in that, once the criterion for $\bar{g}B > 9000$ G is met, the amplitudes of the profiles are relatively independent of Landé factor.

7.3.3 Rotation velocity

According to theory, the local polarized line profiles, as originating from local regions of the stellar disk, are approximately dependent on the shape of the local unpolarized line profile in the following way. Stokes V profiles scale as the first derivative of the line profile with wavelength, $\mathrm{d}I/\mathrm{d}\lambda$, while linear polarization profile depend on the second derivative of the line profile, $\mathrm{d}^2I/\mathrm{d}\lambda^2$. Assuming (although with no strong theoretical justification) that this behaviour extends to the case $v \sin i \neq 0$ leads to the conclusion that the amplitude of the Stokes V profiles should be reduced with increasing $v \sin i$. Linear polarization profiles may or may not be affected in the

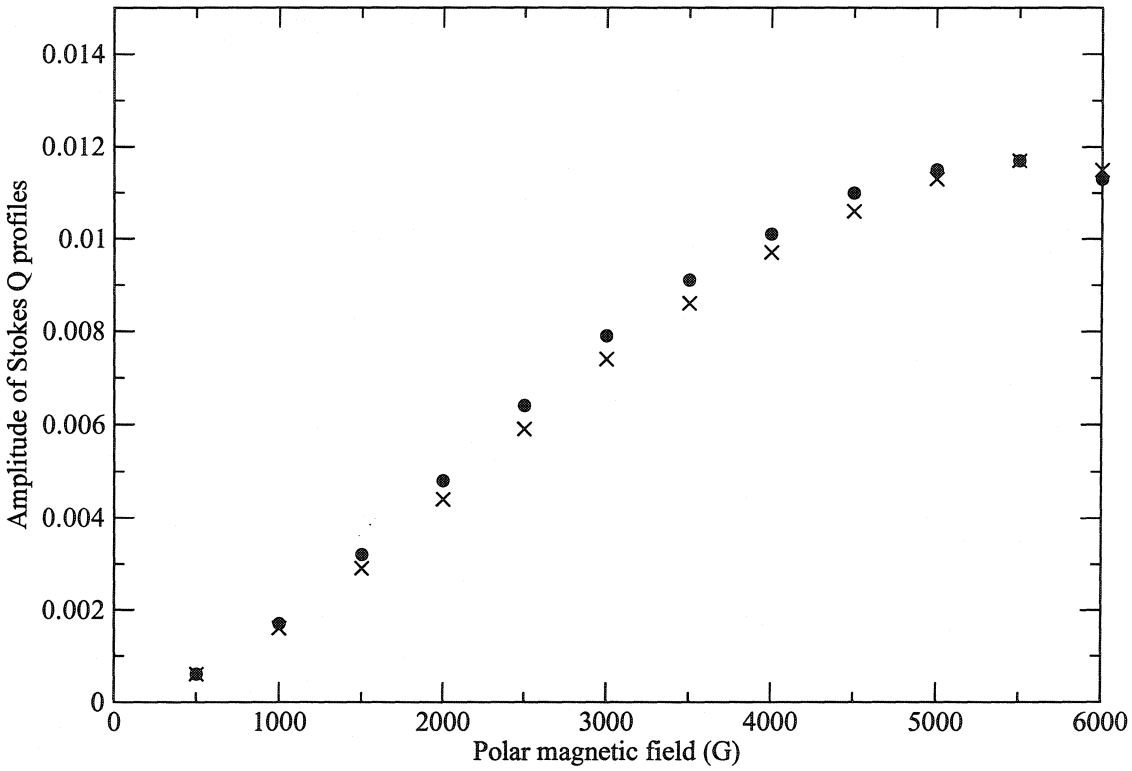

Figure 7.26: Amplitudes of Stokes Q profiles, measured at phase 0.00 and $v \sin i = 25$ km s^{-1}, as a function of polar magnetic field. Filled circles are the amplitude of the 6135 Å test lines ($\bar{g} = 1.16$), 'X's are of the 6150 Å test lines ($\bar{g} = 1.06$)

same way. Since rotation velocity does not enter the model that predicts the simple dependence of the polarization profiles on $\bar{g}$, B, λ and d, we must explore its actual effects numerically.

Stokes V

Analysis of the dependence of Stokes V profiles on rotation velocity was performed by measuring the amplitudes of Stokes V profiles for a given test line at constant magnetic field over the range of $v \sin i$. The test spectra used to determine the coherence regimes (see Figs. 7.1 and 7.2) were used in this analysis. The relationship between Stokes V profile amplitudes and rotation velocity is shown in Fig. 7.27 for the test lines at 6135 Å and 6150 Å, for the test cases with $B = 500$ and 1000 G.

The result is a monotonic decrease in Stokes V amplitude with increasing $v \sin i$. In the cases of $B = 500$ and 1000 G, if one neglects the points for $v \sin i = 5$ km s^{-1}, then the relationship is well described by a power law where $V \sim (v \sin i)^{-1.5}$. This dependence is interesting when compared to Eq. (6.5), the approximate scaling that relates the uncertainty in longitudinal field measurements from LSD mean Stokes V profiles to, among other parameters, $v \sin i$. In that approximation, $\sigma(B_z) \sim (v \sin i)^2$, since the V profile amplitudes scale with the slope of the unpolarized (I) line profiles, which scales approximately as $(v \sin i)^{-2}$. The observed power law is fairly close to the predicted relationship, although not exactly the same, and the fact that rotation velocity influences the Stokes V amplitudes in the same sense as predicted is some justification for the explanation of how errors in longitudinal field uncertainty scale with $v \sin i$. The same power law relationship. $\sim (v \sin i)^{-1.5}$ is also seen for tests with stronger magnetic fields, but only if the two lowest values of rotation velocity are neglected, i.e., only in the range $v \sin i = 15 - 30$ km s^{-1}.

Stokes Q

The dependence of Stokes Q profiles on rotation velocity is difficult to quantify generally because the coherence regimes in most cases exist for limited ranges of $v \sin i$. Coherently shaped Q profiles are available over a range in $v \sin i$ only for the tests at 500 and 1000 G. At those values of magnetic field, the amplitudes of the Stokes Q profiles were measured for the strong test lines at 6135 Å and 6150 Å for spectra synthesized over the range $10 \leq v \sin i$ (km s^{-1}) ≤ 25. The relationship is shown in

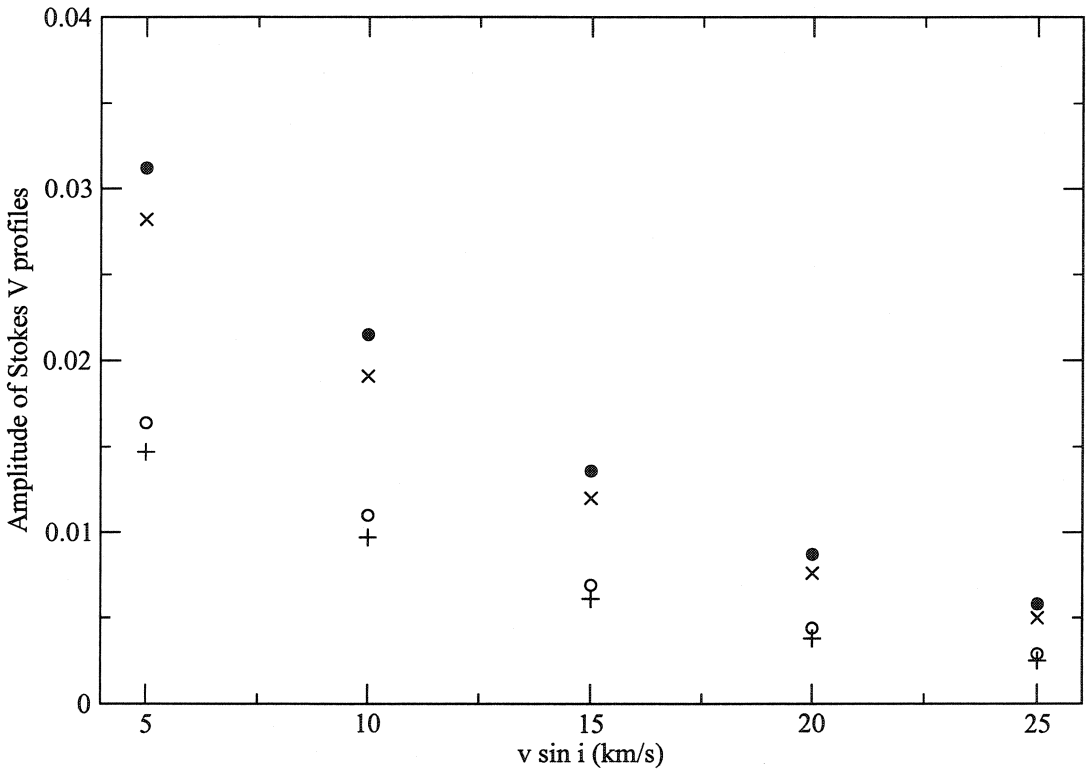

Figure 7.27: Amplitudes of Stokes V profiles, measured at phase 0.00 and $B = 500$ and 1000 G, as a function of rotation velocity. Filled Filled circles are the amplitude of the 6135 Å test line at $B = 1000$ G, 'X's are of the 6150 Å test line at $B = 1000$ G. Empty circles are of the 6135 Å test line at $B = 500$ G and '+'s are of the 6150 Å test line at 500 G.

Fig. 7.28. It is apparent that, while the change in slope of the unpolarized (I) line profile, brought on by rotation velocity, is most important for the Stokes V profiles, the same is not true for the Stokes Q profiles. In the regime of coherently shaped Q profiles, for which the relationship in Fig. 7.28 holds, the Q amplitudes are approximately independent of $v \sin i$, although this may be be true at even larger values of $v \sin i$.

The main influence of rotation velocity on Stokes Q amplitudes in the "competition" between the spreading of the polarization signal over a broader spectral window due to increased $v \sin i$ (thus diluting the Q amplitude) and the moving of regions of cancelling linear polarization to different parts of the line (thus potentially increasing Q amplitude).

7.4 Conclusions

7.4.1 Circular polarization profiles

In this first exploratory study of the relationship of individual line profiles to LSD mean profiles, it has been found that the Stokes V profiles are extremely robust in shape over the entire range of line parameters, field strengths and rotation velocities examined in this study. The applicability of the LSD technique to provide an average circular polarization profile derived from many lines in a stellar spectrum is well validated by these experiments. The scaling of Stokes V profiles is also well described by the weights in the LSD theory; the profile amplitudes scale linearly with Landé factor and field strength in the sense $V \propto \bar{g}B$, up to polar field values of several kilogauss. For larger values of $\bar{g}B$, however, the linear relationship breaks down somewhat, although it is never a very poor description in our tests even up to $\bar{g}B =$ 7000 G. Therefore, we conclude that the current weights in the LSD theory, which scale linearly with $\bar{g}$, are appropriate for the calculation of mean Stokes V profiles. Only in the strongest field cases must some caution be taken to either exclude lines with very high values of $\bar{g}$, or to acknowledge that any LSD mean V profiles which are calculated using the linear scaling are systematically in some degree of error, due to the few lines which have high values of Landé factor contributing less polarization signal to the average than is predicted from their value of $\bar{g}$.

The amplitudes of the Stokes V profiles also scale linearly with line depth, d, as

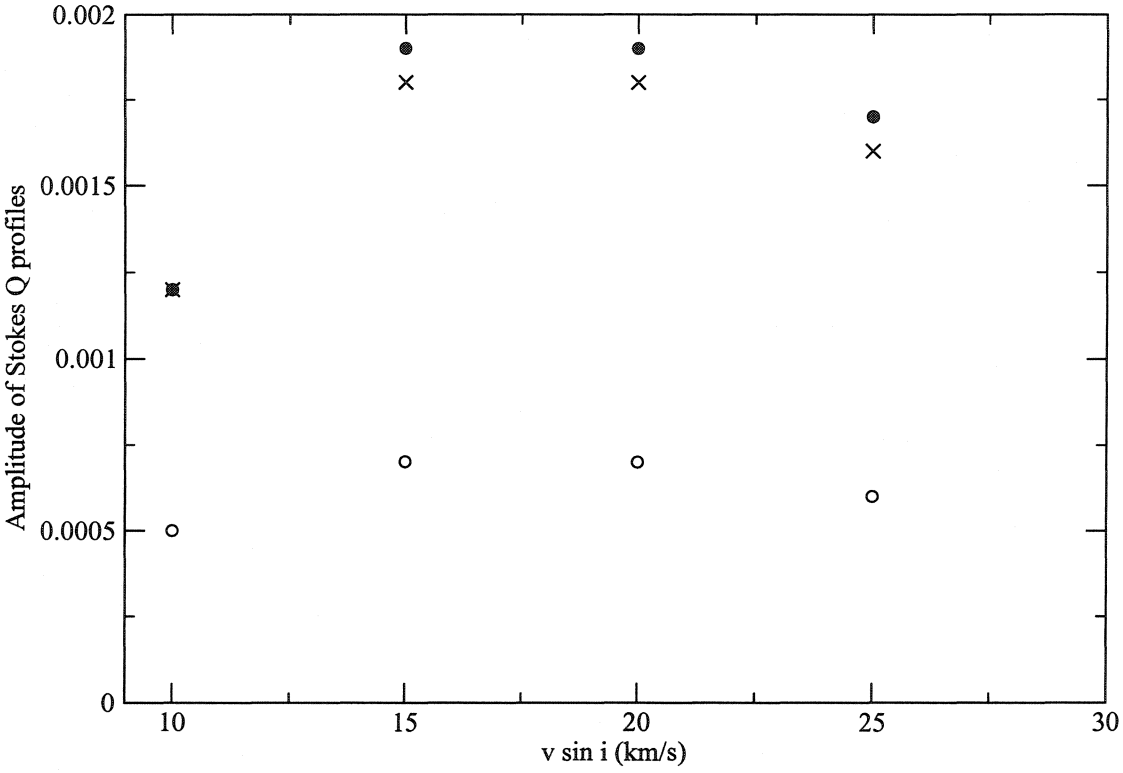

Figure 7.28: Amplitudes of Stokes Q profiles, measured at phase 0.00 and $B = 500$ and 1000 G, as a function of rotation velocity. Filled circles are the amplitude of the 6135 Å test line at $B = 1000$ G, 'X's are of the 6150 Å test line at $B = 1000$ G and empty circles are of both the 6135 Å and 6150 Å test lines at $B = 500$ G

is predicted by LSD theory, but only up to a value of $d \sim 0.5$ or 0.6. This critical line depth is due to line saturation effects, and for lines stronger than the critical d, there is a marked deviation from a linear relationship. Still, for most of the lines in a stellar spectrum, V amplitudes do scale linearly with d and we therefore conclude that the current LSD weights, which scale linearly with line depth, are reasonably appropriate to be used in computing mean V profiles. A systematic error will be introduced in using this simple scaling, due to individual V profiles contributing more polarization signal to the average than predicted by their line depth, and this must be acknowledged when presenting and interpreting LSD average Stokes V data.

Finally, the amplitudes of the Stokes V profiles decrease proportionally with $(v \sin i)^{-1.5}$, which is not too different from approximate relationship predicted by the decrease in the slope of unpolarized line profiles with $v \sin i$ ($Q \propto (v \sin i)^{-2}$). The marked reduction in V amplitude does indicate that the effect of rotation velocity on V profiles is the result of the change in the unpolarized line profile's shape.

7.4.2 Linear Polarization profiles

In this first exploratory study, the main conclusion is that for spectral lines between levels having a broad range of Landé factors and quantum numbers, J, which thus have a variety of magnetic sensitivities and Zeeman splitting patterns, there are cases in which their linear polarization profiles have coherent shapes. Since regimes of coherence are found, there are cases of magnetic field strength and rotation velocity which are qualitatively simple to describe. Weaker field stars have coherently shaped profiles at all but the lowest rotation velocities. Stronger field stars show coherence in strong lines at higher rotation velocities and, for the strongest field cases, also at low rotation velocities.

In the weaker field regimes of coherence, Stokes Q amplitudes scale with Landé factor and with field strength. For the lowest values of the product of Landé factor and field strength, the scaling of Q amplitudes is approximately quadratic with $\bar{g}B$. However, a linear scaling is a reasonable, if somewhat rough, approximation from the lowest values of $\bar{g}B$ up to several kilogauss. At larger field strengths, the Q amplitudes in coherently shaped lines are found to be relatively independent of $\bar{g}B$. The important issue, however, becomes one of coherence. The coherence regimes were previously examined in terms of field strength and rotation velocity. We conclude from

this study that the actual parameter space in which coherence regimes are defined is $\bar{g}B$ vs. $v \sin i$. Since the coherence regimes illustrated in Fig. 7.8 were determined for average lines having $\bar{g} \sim 1$, the magnetic field strength ordinate is approximately interchangeable with $\bar{g}B$. But the inclusion of Landé factor in the $\bar{g}B$ product allows for some flexibility in defining coherence regimes as they apply to individual lines.

For example, a star with a strong field and a *low* rotation velocity will have coherently shaped Stokes Q profiles over a wide range in $\bar{g}$ for the lines, since the criterion for coherence in this case is $\bar{g}B$ being greater than some critical value. Thus, the inclusion of many lines in the LSD average, in this case, is valid. But a star with the same strong field and *moderate* rotation velocity may have coherently shaped profiles for only the few lines with low mean Landé factors, since the criterion for coherence in this case is $\bar{g}B$ being less than some critical value. And there will be some stars whose field strengths and rotation velocities do not produce coherently shaped profiles for lines with any realistic values of mean Landé factor.

We conclude, therefore that one is restricted to the regimes of coherence when using LSD averaged Stokes Q profiles for modelling, and that such regimes are in the most clearly seen parameter space of $\bar{g}B$ and $v \sin i$. For weak fields in those regimes, a linear scaling with $\bar{g}B$ is a reasonable approximation. For strong fields, Q amplitudes may be treated as independent of $\bar{g}B$. For intermediate cases, use of either linear scaling with or independence from $\bar{g}B$ will be a source of error.

Investigating the effect of line depth shows that Stokes Q profiles do not exhibit a monotonic behaviour with increasing d. Stokes Q profile amplitudes initially increase with increasing d, then some value is reached after which they actually decrease in amplitude. This behaviour makes it difficult to include lines in the LSD averaging with depths over a large range. We conclude that the best treatment of the effect of line depth in LSD averaging is to include only lines with depth greater than some cut-off value near which the change in behaviour occurs, and to treat their Stokes Q profiles as having amplitudes independent of d. This treatment will certainly be a source of systematic error, the introduction of which may be necessary in order to include the important contributions of such strong profiles to the average. Any error will be reduced for stars with increasing magnetic field strength, whose Q profile amplitudes become increasingly independent of d, and whose Q profile shapes are coherent only at large values of d. Finally, this treatment is a great improvement over the current LSD weights which include a linear scaling with d. In the current

implementation, the profiles from strong lines are contributing much less polarization signal to any average LSD profile than is predicted by a linear scaling with depth, and this source of error will be reduced by treating them as independent of d.

Finally, the amplitudes of Stokes Q profiles are relatively independent of rotation velocity, at least in the range of $v \sin i$ examined here. The influence which rotation velocity has on Q profiles is in the regimes at which either magnetic splitting or rotation dominates the profile shapes, thus defining the regimes of coherence.

7.5 Future work

This study, while exploratory, has been able to provide the first constraint on the regimes of coherence of the shapes of polarization profiles, as well as some investigation of the behaviour of polarization profile amplitudes with the relevant stellar and line parameters in cases in those regimes. Future study is necessary to determine if those regimes extend to higher and lower values of $\bar{g}B$ and $v \sin i$, while remaining in the observation ally relevant portion of parameter space. Also to be determined is whether the relationships between polarization profile amplitudes and line depth, rotation velocity, Landé factor and magnetic field found here may be used in other regions of parameter space.

New series of test spectra should also be generated for more magnetic field geometries, varying i and β, as well as increasing the complexity of the test cases by including higher order multipolar fields and inhomogeneous surface chemical distributions. Such tests would be used to determined whether the coherence regime and scaling relation conclusions obtained for a simple model in this study may be applied in general to stellar observations. On the observational side, LSD mean signatures should be recomputed for spectra such as those used in the Wade et al. (2000a) study, but using the new scaling weight relations determined here, in order to study the effect these new weights may have.

References

Chadid, M., Wade, G. A., Shorlin, S. L. S., & Landstreet, J. D. 2004, A&A, 413, 1087

Kochukhov, O., Bagnulo, S., Wade, G. A., Sangalli, L., Piskunov, N., Landstreet, J. D., Petit, P., & Sigut, T. A. A. 2004, A&A, 414, 613

Kupka, F., Piskunov, N. E., Ryabchikova, T. A., Stempels, H. C., & Weiss, W. W. 1999, A&AS, 138, 119

Landstreet, J.D. 1988, ApJ, 326, 967

Landstreet, J. D., Barker, P. K., Bohlender, D. A., & Jewison, M. S. 1989, ApJ, 344, 876

Neiner, C., Hubert, A.-M., Frémat, Y., Floquet, M., Jankov, S.;,Preuss, O., Henrichs, H. F. & Zorec, J. 2003, A&A, 409, 275

Ryabchikova, T. A., Piskunov, N. E., Stempels, H.,C., Kupka, F., & Weiss, W. W. 1998, Proc. of the 6th International Colloquium on Atomic Spectra and Oscillator Strengths, Victoria BC, Canada , Physica Scripta, T83, 162

Wade, G. A., Donati, J.-F., Landstreet, J. D., & Shorlin, S. L. S. 2000a, MNRAS, 313, 823

Wade, G. A., Donati, J.-F., Landstreet, J. D., & Shorlin, S. L. S. 2000b, MNRAS, 313, 851

Wade, G. A., Bagnulo, S., Kochukhov, O., Landstreet, J. D., Piskunov, N. & Stift, M. J. 2001, A&A, 374, 265

Wade, G. A., Chadid, M., Shorlin, S. L. S., Bagnulo, S., & Weiss, W. W. 2002, A&A, 392, L17

Chapter 8

Summary

8.1 New spectropolarimetric data and analysis techniques

The field of stellar spectropolarimetry, used in the study of stellar magnetic fields, has been greatly enhanced with two recent developments. The use of the MuSiCoS spectropolarimeter to obtain spectra in all four Stokes parameters over a wide spectral window has provided circular polarization data in spectral lines for a wide variety of stars, including normal stars across the mid to upper main sequence, magnetic Ap stars, other chemically peculiar stars, as well as cool active stars. The first linear polarization data in stellar spectral lines have also been provided by the use of MuSiCoS, in observations of magnetic Ap stars. These new and informative observations have been made by a collaboration, including the authour, who designed the observational programme and performed the observations on-site at Pic-du-Midi observatory. The data from this instrument have been found to be particularly challenging to reduce to a usable format, and the data reduction package ESpRIT was developed to perform this task. The installation and use of this package was performed by the authour.

MuSiCoS spectra, which cover a broad range in wavelength, include very many spectral lines. The Least-Squares Deconvolution (LSD) analysis technique was designed to compute average line profiles in all Stokes parameters from all the lines in an entire spectrum. This has led to very high S/N average profiles in circularly polarized light for a variety of stars, as well as in linearly polarized light for magnetic Ap stars. The use of LSD was customized by the authour to ensure that the characteristics of a stellar spectrum, which are used by LSD in the averaging, are a

reasonable description of each actual spectrum as analyzed. LSD profile averaging was also performed by the authour for a survey group of stars, as well as a number of others.

8.2 Magnetic field survey

In a survey designed to attempt the detection of magnetism across the mid to upper Herzsprung-Russell diagram, we have searched for magnetic fields in the photospheres of 22 normal B, A and F stars, four emission-line B and A stars, 25 Am stars, 10 HgMn stars, two λ Boo stars and 11 magnetic Ap stars using circular spectropolarimetry and LSD. In none of the Am or HgMn stars is Zeeman circular polarization detected, from which we conclude that any magnetic fields which generally exist in the photospheres of Am and HgMn stars must be considerably weaker, considerably more complex or of a different structure than those found in active late-type stars. Measurements of the longitudinal magnetic field from each of our polarization spectra also result in no significant detection for any of the stars in our sample, with a median 1σ uncertainty of ± 18 G for Am stars and ± 39 G for HgMn stars. In particular, we detect no fields in the Am stars HD 29173, HD 112412, HD 195479A or HD 214994 or the HgMn star HD 27295, for which non-zero field measurements have been reported.

We also detect no significant circular polarization for any normal star, ranging in spectral type from B0.5 to F9, including dwarfs, subdwarfs, giants and supergiants. The longitudinal field measurements resulted in no significant detections with a median 1σ uncertainty of ± 13 G. No significant circular polarization was detected for any of the emission-line stars, although the uncertainty for these objects is higher. The LSD method was unsuited for the investigation of the two λ Boo stars, as well as the B6IIIpe star, κ Dra.

For the 12 stars classified as magnetic Ap stars, we provide the first detection of a field for HD 108945, as well as a convincing detection for HD 140160. We do not conclusively detect any field in HD 148112 (ω Her) or HD 148330, stars previously shown to be magnetic, although our non-detections are consistent with previous studies. All other stars previously shown to be magnetic are reconfirmed here, and precise longitudinal field measurements have been made. Other stars classified as Ap SrCrEu, but for which no fields have been previously detected, were observed, but we find no evidence for their having fields. We suggest a reinvestigation of their spectral

classifications.

We have furthermore remeasured the lines of the secondary in the spectrum of HD 108642. From our two measurements of the radial velocity separation of the components, we derive approximate values of the primary and secondary mass ($\mathcal{M}_1 = 1.9 \pm 0.4\ \mathcal{M}_\odot$ and $\mathcal{M}_2 = 1.0 \pm 0.2\ \mathcal{M}_\odot$, respectively), the luminosity ratio ($L_1/L_2 \simeq 15$), and the inclination of the orbital plane ($i \simeq 64°$). As well, we obtain a value of the projected rotation velocity of the rapidly rotating secondary component of the SB2 HD 110951, $v \sin i = 80 \pm 10$ km s^{-1}. This value is inconsistent with previously published determinations.

8.3 Investigations of the use of LSD profiles

An exploratory investigation has been made into the applicability and the implementation of the LSD averaging technique for both circular and linear polarization profiles. Test spectra were generated for a model star having a simple magnetic field geometry over a range in both rotation velocity and magnetic field strength. These were examined to determine regimes of (B, $v \sin i$) in which most lines have coherent shapes; a necessary condition if LSD averaged profiles from a stellar spectrum are to be interpretable as representing actual spectral lines. Regimes of coherence were found, and new tests were performed in those regimes to examine the effects of varying line depth, Landé factor, magnetic field strength and rotation velocity.

Such tests reveal that Stokes V profiles are remarkably robust in maintaining their general shape over a wide range of stellar and line parameters, and the LSD averaging technique is validated for use in circularly polarized spectra. The scaling of V profile amplitudes with magnetic field in LSD, $V \propto \bar{g}B$, is a good approximation over the range in Landé factor and magnetic field strength examined here. The scaling of V amplitudes with central line depth in LSD, $V \propto d$, is a good approximation for weak lines, but becomes increasingly inaccurate as lines begin to saturate. Stokes V amplitudes have also been found to scale with rotation velocity as $V \propto (v \sin i)^{1.5}$ in this limited range of $v \sin i$.

Tests reveal that linear polarization profiles are *not* robust in maintaining their general shape over the entire range of stellar and line parameters explored here. Only in a limited region of the parameter space of $v \sin i$ and $\bar{g}B$ are linear polarization profiles coherently shaped. Additionally, only the strongest lines are coherently shaped

in test spectra for strong field cases.

The scaling of linear polarization profile amplitudes with magnetic field strength in LSD, e.g. $Q \propto (\bar{g}B)^2$, is only a good approximation for the very weakest values of $\bar{g}B$, and is a very poor approximation at even moderate values. A linear scaling with $\bar{g}B$ is more appropriate, although as $\bar{g}B$ increases, profile amplitudes become increasingly independent of magnetic field strength and Landé factor.

The scaling of linear polarization profile amplitudes with central line depth in LSD, e.g. $Q \propto d$, is only a good approximation for lines weaker than some depth, say $d = 0.5$ to 0.6. Lines deeper than this cut-off value have profiles which decrease in amplitude as d increases. A treatment of all profiles from lines with d greater than some depth criterion could be treated as having amplitudes independent of d, although this will introduce some error. Linear polarization profiles have also been found to be relatively independent of rotation velocity in the limited range explored here.

8.4 Future study

New possibilities in the field of studying stellar magnetic fields using spectropolarimetry have been opened up by the use of MuSiCoS and LSD. Continued surveys of stars which are presumed or predicted to be magnetic, but for which fields have never been detected, are an excellent use of Stokes V data from MuSiCoS, as extracted by LSD. Increased precision in longitudinal field measurements for more magnetic Ap stars will improve magnetic field variation curves, thus improving constraints on the possible models of magnetic field strengths and geometries. Such improvement for a large number of stars will allow for better statistical analysis of such issues as e.g. the angles between stellar rotation and magnetic axes, which lead to constraints on field evolution models.

The use of LSD averaged polarization profiles in all four Stokes parameters, with their high signal-to-noise ratios, which may be truly treated as the profiles of single, interpretable spectral lines that can then be modelled, will provide an extremely important contribution to the field of magnetic field modelling. Such profiles, especially in linear polarization will strongly constrain how a star's field may be described over its surface. In order to provide that constraint, however, the applicability of LSD, especially in linear polarization, must be confirmed for a wider range of parameter

space. The implementation of the current, or any new, scaling weight relationships in LSD must also be confirmed to be reasonable approximations, and the degree of error introduced by such approximations should be quantified by further testing.

Appendix A
Guide to installing and operating ESpRIT

A.1 Unpacking the tarfile

Create a directory in which the tarfile, `esprit.tar`, may be unpacked. It should be four directories down from / , (i.e. `/home/user/lsddir/lsd/` is a good directory, whereas `/home/user/lsd/` is not). The `esprit.tar` file includes the ESpRIT source code and the library files. The library directory `lib/` gets untarred two directories up from the sorce code directory, i.e. it is tarred as

```
./geometry.c
./geometry
etc.
../../lib/libfile.a
../../lib/libplot.a
etc.
```

In addition you will need to create the directories for images and the reduced data. Your file structure should be something like:

`/home/user/lsddir/lsd/`	Source code , scripts and executable. Ensure pwd has 4 fields.
`/home/user/lsddir/esprit/BRUT/`	Directory for raw images.
`/home/user/lsddir/esprit/raw/`	Directory for renamed symbolic links to raw data.
`/home/user/lsddir/esprit/spec/`	Directory for reduced data.
`/home/user/lib/`	Library directory.

The above are referred to as "`lsd/`" "`BRUT/`" "`raw/`" "`spec/`" and "`lib/`" in the following discussion.

You also need to include the `lsd/` directory in your path.

A.2 PGPLOT

You need to have PGPLOT installed. PGPLOT is available (as of April 2003) at `http://www.astro.caltech.edu/~tjp/pgplot/` and is from CalTech in any case. You will need to include the following drivers from the list of drivers when PGPLOT is made.

```
/xdisp
/ps
/cps
/vps
/vcps
/xserve
/null
```

`/xdisp` is the most important for ESpRIT, and is not normally included if you follow the instructions in the PGPLOT installation instructions. Therefore it is advised to reinstall PGPLOT locally even if it is already installed on a system. Check the manual (install-unix.txt) which comes in the PGPLOT tarfile. You will also need to make the c-binding for PGPLOT (CPLGPLOT) as outlined in the PGPLOT installation instructions. The resulting files

```
cpgplot.h
libcpgplot.a
libpgplot.a
```

have to be copied to the same `lib/` directory as the other `lib*.a` files. It is convenient to create an alias for the "`pgdisp`" command in the `pgplot/` directory since it will have to be invoked to open up a display window during ESpRIT sessions.

A.3 Libraries

You need to `make` the `lib*.a` files on your machine. Go to `lib/file/`, `lib/mem/`, `lib/nr0/`, `lib/plot/` and "`make lib`" in each directory and then move the resulting `libfile.a`, `libmem.a`, etc. up to the `lib/` directory.

A.4 Executables

The ESpRIT makefile is currently set for Solaris 2. You should see how to comment/uncomment the pertinent lines for your own system. Ensure that the correct directories are indicated to link in the necessary libraries on your system.

You will have to recompile all the `*.o` files (`cc -c geometry.c`, etc.)in the source directory and then `make` the pertinent executables (`make geometry, make wcal`, etc.) See notes on byte-swapping below before makeing `hpf`.

A.5 Byte-Swapping

ESpRIT executables are defaulted to run in byte-swapping mode. To suppress this, they must be run with a "`-s`" flag (e.g. `geometry -s`). There is at least one script (`reduce_pol`) which invokes an executable, in this case "`polar`" in two places, which needs to be edited to "`polar -s`" if you wish to suppress byte-swapping. I'm not sure if there are other scripts which need this attention.

NOTE: Check in the source "`hpf.c`" to see if `hpf` is currently set to do byte-swapping or not. Byte-swapping is hardcoded in and `hpf` does not currently take a command-line flag to change this. The line "`bswap = 0`" (byte-swapping disabled) or "`bswap = 1`" (byte-swapping enabled) may be edited to change `hpf` to what you wish, and then it will need to be recompiled.

A.6 Scripts

The scripts `addff`, `cfits` and `setup_mus` need to be edited to correspond to your own file structure. In `addff` and `cfits`, the values of "`dir1`" and "`dir2`" need to be set to your `raw/` and `spec/` directories, respectively. In `setup_mus`, "`homedir`" is the `lsd/` directory while "`dir`" is the `esprit/` directory (`/home/user/lsddir/esprit`) The value for "`ref`" indicates the run reference number from Pic-du-Midi. It should be edited to correspond to your own, as the file names from the Pic include that number.

I think that's everything outside of what is on the MuSiCoS homepage

Appendix B

Observation log

B.1 A log of observations made by the author

In the completion of this thesis, the author personally made the following observations at the Pic-du-Midi Observatory n one or more Stokes parameters as shown, either alone or with a second observer, as listed in Table B.1. Comments in Table B.1 refer to the type of star being observed: Hot, Solar-type, HgMn, Am, normal and (magnetic) Ap. The details of the observation procedures and the facilties are found in Chapter 4.

Object	Q	U	V	$t_{exp}(s)$	Comments
			14/01/1999		
HD 199178			•	600	Solar-type
o Peg			•	360	Am
II Peg			•	600	Solar-type
UX Ari			•	360	Solar-type
HR 1099			•	360	Solar-type
HD 24712	•	•	•	600/600/360	Ap
HD 71866	•	•	•	600/600/360	Ap
σ Gem			•	360	Solar-type
HD 81009	•	•	•	600/600/360	Ap
HD 129174			•	360	HgMn
Arcturus	•	•	•	30	Normal
			15/01/1999		
β Cep			•	300	Hot
γ Cas			•	360	Hot
ϵ Per			•	400	Hot
γ Cas			•	600	Hot
σ Gem			•	360	Solar-type
49 Cam	•	•	•	600/600/360	Ap
HD 71866	•	•	•	600/600/360	Ap
α^2 CVn	•	•		300/360	Ap
Closed early because of weather					
			16/01/1999		
Closed because of weather, personnel problems					
			17/01/1999		
Closed because of weather					

Object	Q	U	V	$t_{exp}(s)$	Comments
			18/01/1999		
HD 199178			•	600	Solar-type
II Peg			•	600	Solar-type
γ Cas			•	360	Hot
HD 24712	•	•	•	600/600/360	Ap
θ1 Ori C			•	600	Hot
σ Gem			•	360	Solar-type
49 Cam	•	•	•	600/600/360	Ap
HD 98088	•	•	•	600/600/360	Ap
HD 108642			•	600	Am
Arcturus	•	•	•	30	Normal
			19/01/1999		
HD 199178			•	600	Solar-type
γ Cas			•	400	Hot
HR 1099			•	360	Solar-type
HD 29173			•	360	Am
HD 32633	•	•	•	600/600/360	Ap
σ Gem			•	360	Solar-type
49 Cam	•	•	•	600/600/360	Ap
α^2 CVn	•	•	•	360/360/300	Ap
β CrB	•	•	•	300	Ap
HD 129174			•	360	HgMn
			20/01/1999		
Closed because of weather, computer problems					
			21/01/1999		
Closed because of weather					

Object	Q	U	V	$t_{exp}(s)$	Comments
				22/01/1999	
II Peg			•	600	Solar-type, misaligned
UX Ari			•	360	Solar-type
HR 1099			•	360	Solar-type
HD 32633	•	•	•	600/600/360	Ap
σ Gem			•	360	Solar-type
HD 71866	•	•	•	600/600/360	Ap
HD 77350			•	500	HgMn
HD 110951			•	400	Am
Closed early because of telescope problems					
				23/01/1999	
II Peg			•	600	Solar-type
UX Ari			•	360	Solar-type
HR 1099			•	360	Solar-type
HD 27295			•	360	HgMn
HD 32633	•	•	•	600/600/360	Ap
θ Aur			•	300	Ap
σ Gem			•	360	Solar-type
HD 75333			•	600	HgMn
HD 78362			•	360	Am
HD 98088	•		•	600/600/360	Ap
78 Vir	•	•	•	600/600/360	Ap
ϵ UMa			•	300	Ap

Object	Q	U	V	$t_{exp}(s)$	Comments
			24/01/1999		
β Cep			•	300	Hot
II Peg			•	600	Solar-type
UX Ari			•	360	Solar-type
HR 1099			•	360	Solar-type
HD 32633	•	•	•	600/600/360	Ap
θ Aur			•	300	Ap
HD 63975			•	400	HgMn
σ Gem			•	360	Solar-type
HD 98088	•	•	•	600/600/400	Ap
78 Vir	•	•	•	600/600/360	Ap
HD 144206			•	360	HgMn
			25/01/1999		
β Cep			•	300	Hot
II Peg			•	600	Solar-type
UX Ari			•	360	Solar-type
HR 1099			•	360	Solar-type
HD 32633	•	•	•	600/600/360	Ap
σ Gem			•	360	Solar-type
49 Cam	•	•	•	600/600/360	Ap
HD 71866	•	•	•	600/600/400	Ap
HD 108651			•	400	Am
			26-29/01/1999		
No observations because of weather					

Table B.1: Observations personally made by the author

Appendix C

LSD line mask abundance table

C.1 Chemical abundances used for the generation of LSD line masks

The chemical abundances in Table C.1 are in the sense $\log A - \log H$, where H is the abundance of hydrogen. "Hot Am" refers to $T_{\rm eff} = 9000 - 10000$K. "Cool Am" are those with $T_{\rm eff} \leq 8500$K. "Ap" refers to all magnetic Ap line masks. One is referred to Table 5.1 for more specifications on the individual line masks. Bibliographic references are those given in the dicussion of Section 5.2.1.

Table C.1: LSD line mask abundance table

Element	Solar	Hot Am	Cool Am	HgMn 10K	HgMn 11K	HgMn 12K	HgMn 13-14K	λ Boo	Ap
C	-3.5	-3.7	-3.5	-3.9	-4.0	-4.0	-4.0	-3.5	-3.5
Mg	-4.5	-4.5	-4.5	-4.7	-5.0	-5.1	-5.2	-5.5	-4.5
Al	-5.6	-5.6	-5.6	-5.6	-5.6	-5.6	-5.6	-5.6	-4.6
Si	-4.5	-4.5	-4.5	-4.7	-4.6	-4.7	-4.5	-5.3	-3.5
P	-6.6	-6.6	-6.6	-6.6	-5.7	-5.8	-4.7	-6.6	-6.6
S	-4.8	-4.2	-4.7	-5.0	-4.8	-5.3	-5.6	-4.8	-3.8
Ca	-5.7	-5.5	-6.3	-6.1	-5.1	-5.5	-5.7	-6.5	-5.7
Sc	-8.9	-9.3	-9.8	-8.2	-8.9	-9.2	-8.4	-9.7	-8.9
Ti	-7.0	-6.9	-6.9	-6.4	-6.7	-6.0	-6.8	-8.2	-6.0
V	-8.0	-7.4	-7.7	-8.2	-7.6	-8.0	-7.6	-8.0	-7.0
Cr	-6.4	-6.1	-6.0	-5.8	-6.0	-5.9	-6.4	-7.4	-4.4
Mn	-6.6	-6.3	-6.4	-6.0	-5.1	-4.7	-4.4	-6.6	-5.6
Fe	-4.4	-4.3	-4.3	-4.5	-4.4	-4.9	-4.5	-5.6	-3.4
Co	-7.1	-6.5	-6.2	-6.2	-5.9	-7.1	-7.1	-7.1	-6.1
Ni	-5.8	-5.2	-5.1	-5.6	-5.9	-6.7	-6.2	-6.8	-4.8
Ga	-9.2	-9.2	-9.2	-9.2	-9.2	-6.0	-4.7	-9.2	-9.2
Zn	-7.4	-6.2	-6.9	-7.4	-7.4	-7.4	-7.4	-7.4	-6.4
Sr	-9.1	-8.3	-8.4	-8.0	-7.2	-8.1	-8.5	-9.1	-8.1
Y	-9.8	-9.2	-8.8	-7.8	-7.4	-8.0	-8.3	-9.8	-8.8
Zr	-9.5	-8.5	-8.5	-7.6	-7.5	-9.5	-9.5	-9.5	-8.5
Ba	-9.9	-8.5	-8.9	-9.9	-9.9	-9.9	-9.9	-10.8	-8.9
La	-10.8	-10.0	-9.6	-10.8	-10.8	-10.8	-10.8	-10.8	-9.8
Ce	-10.5	-10.5	-10.5	-10.5	-10.5	-10.5	-10.5	-10.5	-9.5
Pr	-11.3	-11.3	-11.3	-11.3	-11.3	-11.3	-11.3	-11.3	-10.3
Nd	-10.5	-10.5	-10.5	-10.5	-10.5	-10.5	-10.5	-10.5	-9.5
Eu	-11.5	-11.5	-11.5	-11.5	-11.5	-11.5	-11.5	-11.5	-10.5
Gd	-10.9	-10.9	-10.9	-10.9	-10.9	-10.9	-10.9	-10.9	-9.9
Dy	-10.9	-10.9	-10.9	-10.9	-10.9	-10.9	-10.9	-10.9	-9.9
Hg	-11.0	-11.0	-11.0	-7.8	-6.0	-5.9	-6.0	-11.0	-11.0

Appendix D
An example of rotation and radial velocity determination

D.1 Introduction

The spectral line modelling program, ZEEMAN, was used to determine projected rotation velocities, $v \sin i$, and radial velocities, $v_{\rm rad}$ for the stars in the magnetic field survey found in Chapter 6. The use of this technique was briefly introduced in Section 6.3.3, and will be elaborated upon here using one star as an example. The chosen example, HD 95608, is an A3m chemically peculiar star. It has been found in our survey to be non-magnetic.

D.2 Stellar parameters

The stellar parameters necessary for the modelling of a spectral line are the star's effective temperature, surface gravity, rotation velocity, radial velocity, microturbulent velocity, and chemical abundance. The effective temperature and surface gravity ($T_{\rm eff}$ and $\log g$) used during the spectral line modelling are those adopted in Section 6.3.3. Strömgren photometry was used as compiled by Hauck & Mermilliod (1998) in order to calculate $T_{\rm eff}$ and $\log g$ using the calibration of Moon & Dworetsky (1985). Initial guesses for rotation velocity and radial velocity were taken from the SIMBAD database, and chemical abundances in this case were taken to be solar. Initial abundance values for other stars were taken from the appropriate literature.

D.3 Modelling

In modelling a single spectral line of a star, a series of modelling steps were performed with a single value of microturbulent velocity, ξ. A best-fitting radial velocity, rotation velocity and chemical abundance value were found at the single value of ξ. ξ was then changed, and the steps repeated. This entire procedure was then repeated for a number of spectral lines, and the set of line modelling results analyzed to determine the relevant stellar parameters.

At a single value of ξ and for a single line, the best fitting radial velocity, using the the initial guess values of $v \sin i$ and chemical abundance, was found by ZEEMAN as it varied $v_{\rm rad}$ and minimized the χ^2 of the fit to the observed line. At the newly determined $v_{\rm rad}$, line profiles were generated with rotation velocities in a small range above and below the initial guess of $v \sin i$. A best fitting value of $v \sin i$ was interpolated from that range, or estimated outside the range if the range was too small. Abundance was then varied to find a best-fitting abundance, again by minimizing χ^2, at constant rotation velocity. The determination of rotation velocity, then abundance, was repeated iteratively until a minimum improvement between steps was attained. The resulting $v_{\rm rad}$, $v \sin i$ and abundance were then used to tune the initial guesses and the procedure repeated. Examples of synthetic line profiles generated over a range in $v \sin i$ and compared to observed line Fe II profiles for HD 95608 are shown in Figs. D.1 to D.3

Each iterative determination of radial velocity, rotation velocity and abundance was performed at a single value of ξ. ξ was changed to a new single value and the three best-fitting parameters found again. In the case of HD 95608, ξ was varied from $1 \leq \xi$ $(\mathrm{km\,s^{-1}}) \leq 7$ in 1 $\mathrm{km\,s^{-1}}$ increments. This procedure was repeated for each of a small number of lines of Cr II and Fe II for each star. A plot of the determined chemical abundance value vs. ξ was generated for each line (see Fig. D.4 as an example for Fe in HD 95608) and the intersection of the curves examined to find where a common value of ξ and chemical abundance described the data. In this case, a value of $\xi \approx 3.5$, $\log A(\mathrm{Fe})/\log A(\mathrm{H}) \approx -4.3$ is appropriate. This corresponds to the best-fit rotation velocities determined simultaneously for each line at the values of ξ and abundance determined above. Those rotation velocity values were averaged (in this case over all modelled spectral lines and between the rotation velocities determined for $\xi = 3$ $\mathrm{km\,s^{-1}}$ and $\xi = 4$ $\mathrm{km\,s^{-1}}$) to be $v \sin i = 18.3 \pm 0.6$ for HD 95608.

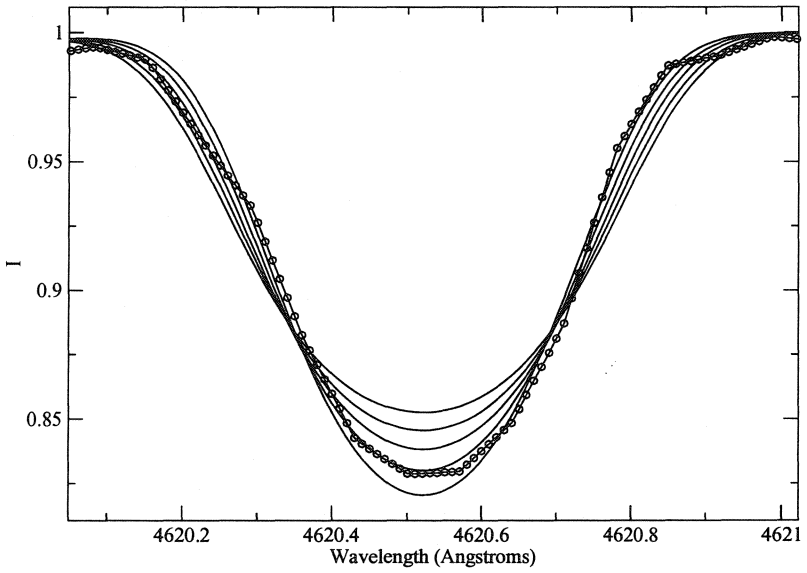

Figure D.1: Synthetic profiles with $v \sin i$ = 17, 18, 19, 20 and 21 $\mathrm{km\,s^{-1}}$(from top to bottom, solid lines) compared to the Fe II 4620 Å line of HD 95608 (solid line with circles) at $\xi = 3\ \mathrm{km\,s^{-1}}$.

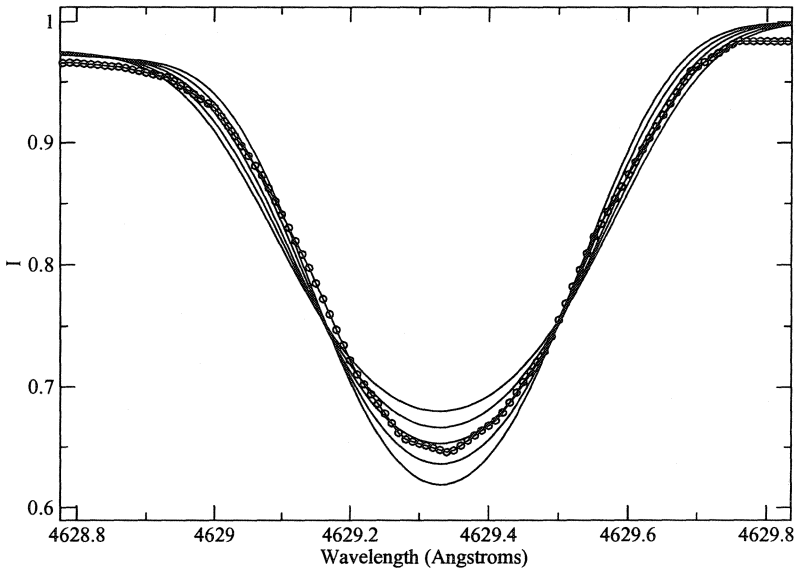

Figure D.2: Synthetic profiles with $v \sin i$ = 17, 18, 19, 20 and 21 $\mathrm{km\,s^{-1}}$(from top to bottom, solid lines) compared to the Fe II 4629 Å line of HD 95608 (solid line with circles) at $\xi = 3\ \mathrm{km\,s^{-1}}$.

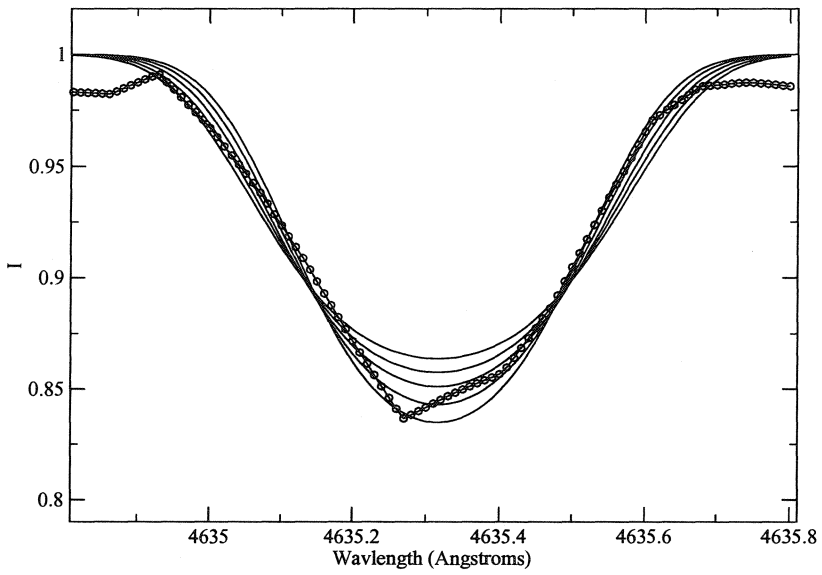

Figure D.3: Synthetic profiles with $v \sin i$ = 17, 18, 19, 20 and 21 $\mathrm{km\,s^{-1}}$(from top to bottom, solid lines) compared to the Fe II 4634 Å line of HD 145389 (solid line with circles) at $\xi = 3\ \mathrm{km\,s^{-1}}$.

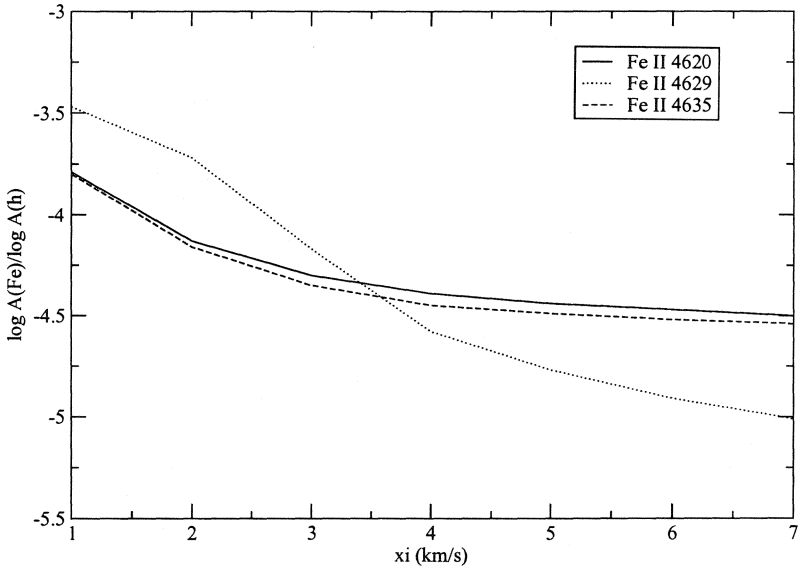

Figure D.4: Blackwell diagram of iron abundance vs. microturbulence velocity, ξ, in lines modelled for HD 95608. Solid line is for the Fe II 4620 Å spectral line, dotted line is for the Fe II 4629 Å spectral line, and dashed line is for the Fe II 4635 Å spectral line

References

Hauck, B., & Mermilliod, M. 1998, A&AS, 129, 431

Moon, T. T., & Dworetsky, M. M. 1985, MNRAS, 217, 305

Appendix E

Copyright Release

VITA

NAME:	Stephen Lawerence Short Shorlin
PLACE OF BIRTH:	Corner Brook, Newfoundland
YEAR OF BIRTH:	1973
POST-SECONDARY EDUCATION AND DEGREES:	Memorial University of Newfoundland St. John's, NL 1990-1995, B.Sc. (Hons.)
	Saint Mary's University Halifax, NS 1995-1999, M.Sc.
	The University of Western Ontario London, ON 1997-2004, Ph.D.
HONOURS AND AWARDS:	NSERC Undergraduate Summer Research Award Memorial University of Newfoundland 1993
	Father Burke-Gaffney Memorial Scholarship Saint Mary's Univeristy 1996-1997

HONOURS AND AWARDS, CON'D:

Prize for Best Student Oral Presentation
CASCA Annual General Meeting
1999

Ontario Graduate Scholarship in Science and Technology
The University of Western Ontario
1999-2001

RELATED WORK EXPERIENCE:

Research Assistant
Mmeorial University of Newfoundland
1992-1994

Research Assistant
Saint Mary's University
1995-1997

Research Assistant
The University of Western Ontario
1997-2004

Teaching Assistant
Saint Mary's University
1995-1997

Teaching Assistant
The University of Western Ontario
1997-2004

REFEREED PUBLICATIONS:

(1) Petit, P., Donati, J.-F., Wade, G. A., Landstreet, J. D., Bagnulo, S., Luftinger, T., Sigut, T. A. A., Shorlin, S. L. S., Strasser, S., Auriere, M., Oliveira, J. M., 2004, *Magnetic topology and surface differential rotation on the K1 subgiant of the RS CVn system HR 1099*, A&A, 348, 1175

(2) Shorlin, S. L. S., Turner, D. G., Pedreros, M. H., 2004, *A Newly Discovered Open Cluster Surrounding the Wolf-Rayet Stars WR 38 and WR 38a*, PASP, 116, 170

(3)Chadid, M., Wade, G. A., Shorlin, S. L. S., Landstreet, J. D, 2004, *No evidence of a strong magnetic field in the Blazhko star RR Lyrae*, A&A. 413, 1087

(4)Wade, G. A., Chadid, M., Shorlin, S. L. S., Bagnulo, S., Weiss, W. W., 2002, *No magnetic field variations with pulsation phase in the classical Cepheid star eta Aquilae*, A&A, 392, L17

(5)Shorlin, S. L. S., Wade, G. A., Donati, J.-F., Landstreet, J. D., Petit, P., Sigut, T. A. A., Strasser, S., 2002, *A highly sensitive search for magnetic fields in B, A and F stars*, A&A, 392, 637

(6) Wade, G. A., Donati, J.-F., Landstreet, J. D., Shorlin, S. L. S. 2000, *High-precision magnetic field measurements of Ap and Bp stars*, MNRAS 313, 851

REFEREED PUBLICATIONS CON'D:

(7) Wade, G. A., Donati, J.-F., Landstreet, J. D., Shorlin, S. L. S. 2000, *Spectropolarimetric measurements of magnetic Ap and Bp stars in all four Stokes parameters*, MNRAS 313, 823

(8) Sigut, T. A. A., Landstreet, J. D., Shorlin, S. L. S. 2000, *Emission Lines in the Spectrum of the 3HE Star 3 Centauri A*, ApJ 530, 89L

(9) Forbes, D., Short (Shorlin), S. 1996, *NGC 6204 and HOGG 22: The Odd Couple* , AJ, 111, 1609

(10) Forbes, D., Short (Shorlin), S. 1994, *PISMIS 6 and the F0 IA supergiant HD 74180* , AJ, 108, 594

NON-REFEREED PUBLICATIONS:

(1) Shorlin, S. L. S., Landstreet, J. D., Sigut, T. A. A., Strasser, S., Wade, G. A., Donati, J.-F., Petit, P., *Spectropolarimetric Measurements of Longitudinal Fields Using LSD*, 2001, in *Magnetic Fields Across the Hertzsprung-Russell Diagram*, ASP Conference Proceedings 248, 423

(2) Petit, P., Donati, J.-F., Wade, G. A., Landstreet, J. D., Oliveira, J. M., Shorlin, S. L. S., Sigut, T. A. A., Collier Cameron, A., *Differential Rotation of Close Binary Stars: Application to HR 1099* , 2001, in *Astrotomography, Indirect Imaging Methods in Observational Astronomy* , Lecture Notes in Physics, 573, 232

(3)Donati, J.-F., Wade, G. A., Landstreet, J. D., Shorlin, S. L. S., 2000, *Zeeman-Doppler imaging of active stars using the MuSiCoS spectropolarimeter*, in the proceedings of *Magnetic Fields of Chemically Peculiar and Related Stars*, SAO, Yu.V. Glagolevskij and I.I. Romanyuk eds., p. 129

(4) Henrichs, H. F., de Jong, J. A., Donati, J.-F, Wade, G. A.; Babel, J.; Shorlin, S. L. S., et al. 2000, *Detection of a weak magnetic field in the pulsating Be star beta; Cephei* , in the proceedings of *Magnetic Fields of Chemically Peculiar and Related Stars*, SAO, Yu.V. Glagolevskij and I.I. Romanyuk eds., p. 57

(5)Shorlin, S. L. S., Landstreet, J. D., Wade, G. A., Donati, J.-F. 2000, *Precise measurements of the longitudinal magnetic fields of chemically peculiar stars*, in the proceedings of *Magnetic Fields of Chemically Peculiar and Related Stars* , SAO, Yu.V. Glagolevskij and I.I. Romanyuk eds., p. 54